Improvements to the acoustic pulse reflectometry technique for measuring duct dimensions

Thesis

Improvements to the acoustic pulse reflectometry technique for measuring duct dimensions

Thesis submitted by

Aijun Li

for the Degree of Doctor of Philosophy

Department of Environmental and Mechanical Engineering

Faculty of Technology

The Open University

September 2004

Declaration

I declare that this thesis has been composed by me and the work is my own.

……

Abstract

In the study of tubular structures such as pipeline sections, musical wind instruments and human airways, acoustic pulse reflectometry has become established as a useful tool for non-invasively measuring the input impulse response, from which the internal duct dimensions can be calculated.

In this thesis, the theory describing wave propagation in a duct of varying cross-section is outlined, culminating in a discussion of the layer peeling algorithm used to reconstruct a duct's bore profile from its input impulse response. Experimental measurements of the input impulse responses of various test objects, together with the subsequent bore reconstructions, are then presented.

The problem of offset in input impulse response measurements is discussed and the effect on the bore reconstruction is shown. The offset is found to consist of both a DC component and a sinusoidal component. Methods for eliminating the two offset components are explored and the resultant improvement in the stability and reproducibility of the bore reconstructions is demonstrated.

Two adaptations to the reflectometry technique, designed to extend the bandwidth of input impulse response measurements, are described. The improved high frequency content brought about by these adaptations is shown to lead to bore reconstructions of high axial resolution, allowing rapid changes in cross-sectional area to be more accurately reproduced.

Finally, limitations of the acoustic pulse reflectometry technique (particularly those brought about by the bandwidth improvements) are discussed and potential future ways of overcoming the limitations are proposed.

Acknowledgements

My great and sincere thanks go to Dr. D. B. Sharp, my supervisor, for his generous help and enthusiastic support during the course of this research programme. As an expert on the acoustic pulse reflectometry technique, Dr. Sharp helped me greatly in deciding early on what directions of this research might be promising.

I am also grateful to Dr. T. J. Hill and Dr. M. van Walstijn for their invaluable discussions and help.

Thanks also to Dr. B. J. Forbes, who did some proof reading of my thesis.

Thanks to Peter Seabrook for his work on preparing test objects, etc. used in this research work.

I would also like to thank all members of acoustic research group in The Open University.

The greatest thanks go to my husband, my son and my mother for their continuous support and understanding during the course of this study.

Contents

List of Figures

List of tables

Chapter 1

Introduction

Determining the internal dimensions of ducts of varying cross-section is a problem common to many branches of science and industry. In certain situations the dimensions can be measured directly, and with a high degree of accuracy, using tools such as rulers and calipers. However, it is often not possible to access the whole length of a duct, either due to its geometry or to the surrounding environment. Buried pipelines and musical wind instruments containing a number of bends are just two examples of ducts whose dimensions cannot be completely determined through direct measurement. Another example can be found in the medical field where it is often desirable to be able to monitor changes in human airway geometry. For inaccessible ducts such as these, a means of determining the internal dimensions indirectly and non-invasively must be employed. One such approach involves measuring the acoustical properties of the duct under investigation and then using this information to carry out a bore reconstruction. Algorithms for bore reconstruction typically start from the input impulse response of the duct, which is most commonly measured in the time domain using the technique of acoustic pulse reflectomery that is central to this thesis. However, the bore may also be reconstructed from the duct's input impedance, which is usually measured in the frequency domain.

In the next section, the history of bore reconstruction from acoustical measurements is discussed. The description starts with an outline of the development of the acoustic pulse reflectometry technique for determining duct dimensions from input impulse response measurements. It then goes on to discuss methods which calculate duct geometries from measurements of input impedance.

1.1 History of bore reconstruction

1.1.1 Input impulse response approach

Acoustic pulse reflectometry is a non-invasive, time domain based technique for measuring the input impulse response of a duct. From this, with the application of a bore reconstruction algorithm, the duct's dimensions can be calculated.

Acoustic pulse reflectometry was originally developed as a technique for studying the earth's crust. The earth's crust is made up of layers of different types of rock. When an impulsive pressure wave is produced, for instance during oil exploration, it travels down into the earth where it is partially reflected at each of the changes in impedance that occur between rock layers of different densities. The reflections return to the surface where they are recorded and termed the input impulse response. [Ware and Aki 1969] were the first to calculate the reflection coefficients of the layer boundaries from the input impulse response. However, their algorithm does not compensate for any losses experienced by the input and reflected pressure waves while travelling through the rock layers.

In a largely theoretical paper published in 1971, [Sondhi and Gopinath 1971] suggested adaptations to the acoustic pulse reflectometry technique to enable the geometry of the vocal tract to be measured. They described how, by applying a sound pulse to an airway and recording the returning reflections, the airway dimensions could be calculated. This calculation was mathematically complex but, like the Ware-Aki algorithm, did not take into account any losses in the airway. An attempt to include the effect of losses was discussed in a later paper [Sondhi 1974] with some experimental results published in [Sondhi and Resnick 1983]. However, the treatment was not rigorous, with a number of simplifying approximations made in the modelling of the losses.

[Jackson et al. 1977, Jackson and Olsen 1980] reported an early design of pulse reflectometer which they used to measure the area profiles of the airways and lungs of dogs. A spark discharge was used to produce a sound pulse, which was then directed into the airway under investigation via a cylindrical tube referred to as the source tube. Reflections returning from the airway were recorded by a microphone in the source tube wall. Analysis of the reflections using the Ware-Aki algorithm then enabled Jackson et al. to reconstruct the profile of the airway. Similar measurements on human patients were carried out by [Fredberg et al. 1980] and later by [Marshall 1992] in a series of clinical trials.

The earliest reported attempt to apply the acoustic pulse reflectometry technique to the analysis of musical wind instruments was by [Benade and Smith 1981]. Using a spark source, a sound pulse was produced and injected into a tuba. The reflections, recorded by a microphone positioned at the tuba mouthpiece, were considered to be the input impulse response of the tuba. Similar work was reported by [Ayers et al. 1985a; Ayers et al. 1985b].

At the University of Surrey, [Goodwin 1981] and [Duffield 1984] carried out further research into the use of acoustic pulse reflectometry for measuring musical wind instruments. They developed a reflectometer with a source tube which used a loudspeaker rather than a spark source. The non-impulsive nature of the pulse produced by the loudspeaker required the recorded reflections returning from the instrument under test to be deconvolved with the pulse shape in order to determine the input impulse response of the instrument. This deconvolution procedure was initially unsuccessful with the first successful implementation achieved by [Deane 1986]

During the 1980s the work continued and reconstructions of brass instruments, calculated from input impulse response measurements made using acoustic pulse reflectometry, were presented by [Smith 1988] and Watson and Bowsher [Watson 1989; Watson and Bowsher 1987; Watson and Bowsher 1988]. The algorithms employed were

those developed by Sondhi and by Ware and Aki. As these algorithms do not take into account losses, the reconstructions of the instruments tended to increasingly underpredict the radius with the distance along the bore. Watson attempted to prevent this underprediction by manually adjusting the DC value of the input impulse response until the reconstructed radius matched with a measured radius at an arbitrary position towards the end of the measurement. However, this approach was not a rigorous method of compensating for the losses experienced by the input pulse and instrument reflections.

A reconstruction algorithm which takes into account losses precisely was developed by [Amir et al. 1995]. This ‘layer peeling’ algorithm was used by [Sharp and Campbell 1997] in their work on the development of acoustic pulse reflectometry. Also in this research, to ensure the DC value of the input impulse response was correctly calculated, Sharp proposed the insertion of a 50 cm long cylindrical tube between the reflectometer and the duct under test. Since there should be no signal reflected back from this cylindrical tube, the start of the input impulse response should be zero. By averaging over the first few milliseconds, any DC offset present in the input impulse response can be found and then removed. The combination of this calibration procedure with the use of the lossy layer peeling algorithm enabled Sharp to achieve accurate reconstructions with no underprediction.

The virtual DC tube method developed by [Kemp et al. 2001] is a variation of the DC tube method. By employing the virtual DC tube method, the need for insertion of the cylindrical tube is eliminated. Reconstructions obtained using this method were shown to be much the same as those using the standard DC tube method.

1.1.2 Input impedance approach

There is relatively little in the literature discussing bore reconstruction from frequency domain measurements of input impedance. The earliest reports of such work came in the medical research field with the papers of [Mermelstein 1967] and [Schroeder 1967]. Both of these researchers described how, by measuring the input impedance at the mouth, the cross-sectional area of an airway as a function of distance could be estimated from the resonance frequencies. Despite having to assume the overall vocal tract length and using only the first few resonances, [Schroeder 1967] in particular achieved good area profile reconstructions of several test objects.

More recently, [Kausel 2003] described how, by performing a bilinear transform and then an Inverse Fourier Transform, measured input impedance data could be used to determine the input impulse response of a tubular object. Subsequently, the area profile of the object could be found by applying a reconstruction algorithm. However, this method of bore reconstruction from input impedance data was shown to be very sensitive to the accuracy of the measurements at low frequencies and to using the correct value for the characteristic impedance.

In the same paper, Kausel proposed an alternative approach to bore reconstruction from measurements of input impedance. In this approach, the input impedance of a duct model made up of cylindrical sections of arbitrary initial radii is calculated theoretically. Using optimization techniques, the radii of the cylindrical sections are then adjusted until the calculated input impedance data matches a preciously measured impedance curve for the tubular object under investigation. Once this matching has been achieved, the theoretically modelled duct profile exhibits the same geometry as the tubular object whose input impedance was measured. This approach has been shown to provide bore reconstructions of good accuracy but is very computationally demanding.

1.2 Aims and outline of thesis

The main aims of this research project are:

1) to investigate causes of inconsistency and inaccuracy in measurements made using a standard pulse reflectometry system.
2) to find ways of improving the consistency and accuracy of the pulse reflectometry technique.
3) to increase the high frequency energy injected into the duct to be measured and thereby improve both the axial resolution of bore reconstructions and the accuracy with which regions of rapidly changing cross-sectional area are reconstructed.

The outline of thesis is as follows:

Chapter 2 describes the theory of plane wave propagation in a duct of varying cross-section. The duct is modelled using piecewise cylindrical sections and the reflection and transmission of plane waves between the sections is discussed. Finally, the input impulse response of a duct of known geometry is theoretically derived.

In chapter 3, the basic theory relating to the determination of the dimensions of a duct of varying cross-section from its input impulse response is discussed. The layer-peeling algorithm (in which losses are taken into account) that underpins the technique of acoustic pulse reflectometry is described. The success of the algorithm in reconstructing the bore profile of a stepped tube from a simulated input impulse response is then demonstrated.

A working acoustic pulse reflectometer is described in chapter 4, with the experimental procedure for operating it discussed in detail. A test object is measured on the reflectometer and its experimental input impulse response is presented.

In chapter 5, problems with the consistency and accuracy of the pulse reflectometry technique are investigated. The origin of the offset introduced into measurements of input impulse response is studied. Possible sources of the offset are then identified and methods

of preventing the offset are proposed. Finally, an accurate bore reconstruction of a test object, calculated from an improved input impulse response measurement where the offset has been eliminated, is presented.

In chapter 6, the improvements in bore reconstructions brought about by the elimination of offsets from input impulse response measurements are illustrated using both stepped tubes and musical instruments as test objects.

The finite bandwidth of an input impulse response measurement made using reflectometry limits the axial resolution of the calculated bore profile and is one of the reasons why regions of rapidly changing cross-section are poorly reconstructed. In chapter 7, the importance of the high frequency content of the input impulse response to the accuracy of the bore reconstruction is demonstrated. A method is proposed for increasing the acoustic energy entering the duct under investigation. The approach involves supplementing the standard sound pulse measurement by probing the duct further with bursts of high frequency sinusoidal pressure waves.

In chapter 8, an alternative means of improving the bandwidth of input impulse response measurements is discussed. This involves shortening the reflectometer's source tube. Whilst this reduces the losses incurred within the source tube, the reduction in length results in the input pulse and object reflections overlapping. A new calibration method for separating the signals of interest is described and results are presented.

In the last chapter, the effect of higher order modes of propagation on bore reconstructions made using acoustic pulse reflectometry is demonstrated and discussed. Some ideas for future work are also outlined.

Chapter 2

Wave propagation in a duct of varying cross-section—the direct problem

2.1 Introduction

In general, sound waves have non-planar wavefronts and propagate in a complex three-dimensional manner. Consequently, their motion can be difficult to model. However, there are conditions under which a simplified model is sufficient to describe acoustic wave propagation. This is the plane wave model, in which sound waves are assumed to have the same direction of propagation everywhere in space and their wavefronts are in planes perpendicular to that direction of propagation.

When a sound wave is travelling inside a tube and the wavelength is large compared with the diameter of the tube, wave propagation is very nearly one-dimensional. That is, waves inside the duct can be considered to be plane waves.

In this chapter, the plane wave model is discussed and the propagation of waves in ducts of both uniform and varying cross-section is considered.

2.2 One-dimensional wave equation

2.2.1 Waves travelling in air

Acoustic waves in air are longitudinal in nature, meaning that the motion of the air particles transmitting the wave is parallel to the direction of propagation of the wave. For one-dimensional propagation in the *x*-direction, the wave equation in terms of the pressure *p* is expressed as [Morse and Ingard 2000]

$$\frac{\partial^2 p}{\partial x^2} = \frac{1}{c^2}\frac{\partial^2 p}{\partial t^2} \tag{2.1}$$

where *c* is the acoustic wave velocity and *t* is the time. Note that $\frac{1}{c^2} = \rho\kappa$, where ρ and κ are respectively the equilibrium density of air and the compressibility of air.

It is necessary to point out that equation (2.1) is restricted to homogeneous, isotropic fluids and that small wave amplitude is also assumed. For this reason, equation (2.1) is often referred to as the linear, lossless wave equation.

A solution of equation (2.1) has the form

$$p(x,t) = p^+(x,t) + p^-(x,t) \tag{2.2}$$

where

$$p^+(x,t) = Ae^{i(\omega t - kx)} \tag{2.3a}$$

$$p^-(x,t) = Be^{i(\omega t + kx)} \tag{2.3b}$$

where ω is the angular frequency (given by $\omega = 2\pi f$, where f is the frequency in Hertz) and $k = \omega / c$ is the wave number. $p^+(x, t)$ in equation (2.3a) refers to waves travelling in the $+x$ direction and $p^-(x, t)$ in equation (2.3b) refers to waves travelling in the $-x$ direction. A and B therefore represent the amplitudes of the waves travelling in the $+x$ direction and the waves travelling in the $-x$ direction respectively.

The equation of wave motion written in terms of velocity u is

$$\frac{\partial u}{\partial t} = -\frac{1}{\rho}\frac{\partial p}{\partial x} \tag{2.4}$$

Solving equation (2.4), the particle velocity in the x-direction is given by

$$u(x,t) = \frac{1}{\rho c}[\, Ae^{\,i(\omega t - kx)} - Be^{\,i(\omega t + kx)}\,] \tag{2.5}$$

According to (2.3a) and (2.3b),

$$u^+(x,t) = \frac{p^+(x,t)}{\rho c} \tag{2.6a}$$

$$u^-(x,t) = -\frac{p^-(x,t)}{\rho c} \tag{2.6b}$$

The ratio of the acoustic pressure p to the velocity u is known as the specific acoustic impedance z. That is,

$$z = \frac{p}{u} \tag{2.7}$$

Combining equations (2.6) and (2.7), for plane wave propagation:

$$z = \frac{p}{u} = \pm \rho c \tag{2.8}$$

with the positive value applying to waves travelling in the $+x$ direction and the negative value applying to waves travelling in the $-x$ direction. The product ρc is defined as the characteristic impedance z_c of the medium (in this case, the medium is air).

2.2.2 Waves travelling in a duct

Acoustic waves of sufficiently large wavelength (low frequency) travelling in a cylindrical tube, to a good approximation, propagate as plane waves. This is because, in a cylindrical tube, higher order modes are evanescent at low frequencies. That is, they decay rapidly with distance along the duct and so do not propagate.

Each higher order mode has a cut off frequency ω_c associated with it. Below this cut off frequency, the corresponding higher order mode is non-propagating. The cut off frequency corresponding to the first nonplanar mode is $\omega_c = 1.84c/r$ for an air-filled cylindrical duct, where r is the radius of the tube. Expressed in Hertz, this is approximately $f_c = 100/r$ [Kinsler et al. 2000]. For example, in a cylindrical tube of radius $r = 8\times10^{-3}$ m, the first nonplanar mode has a cut off frequency $f_c = 12.5$ kHz. At frequencies lower than f_c, higher order modes do not propagate inside the duct. Consequently, waves with frequencies smaller than the cut off frequency can be considered to propagate as plane waves. One-dimensional wave propagation inside the tube can be conveniently described using equation (2.1) at such frequencies.

As the extent of the wavefronts is restricted by the dimensions of the cylindrical tube, it is convenient to introduce the volume velocity $U = Su$, where S is the cross-sectional

area of the tube. The acoustic impedance at any cross-section in the tube is defined as the ratio of the pressure and the volume velocity:

$$Z = \frac{p}{U} \tag{2.9}$$

Combining equations (2.8) and (2.9), the acoustic impedance at a cross section of area S is given by:

$$Z = \frac{p}{Su} = \pm\frac{\rho c}{S} \tag{2.10}$$

with the positive value applying to waves travelling in the $+x$ direction and the negative value applying to waves travelling in the $-x$ direction. The term $\frac{\rho c}{S}$ is defined as the characteristic impedance Z_c of the fluid-filled duct (in the current discussion, the fluid is air).

2.2.3 Reflection and transmission at a single discontinuity

If a planar acoustic wave propagating in an air-filled duct encounters a change in cross-sectional area, the associated change in characteristic impedance causes partial reflection and partial transmission of the incident wave.

Figure 2.1 shows the junction between two cylinders, one with cross-sectional area S_0 and one with cross-sectional area S_1. The incident and reflected waves in the first cylindrical tube are represented by $p_0^+(x,t)$ and $p_0^-(x,t)$ respectively while $p_1^+(x,t)$ is the transmitted wave in the second cylindrical tube. If it is assumed that the second cylinder is semi-infinite, there will be no backward travelling waves present.

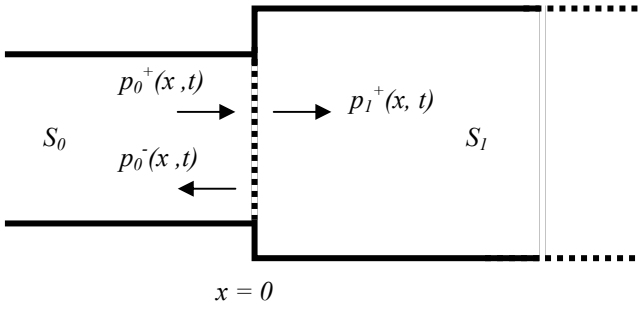

Figure 2.1: Scattering junction

The incident and reflected waves in the first cylinder take the form

$$p_0^+(x,t) = A_0 e^{i(\omega t - kx)} \tag{2.11a}$$

$$p_0^-(x,t) = B_0 e^{i(\omega t + kx)} \tag{2.11b}$$

While the transmitted wave in the second cylinder can be written as

$$p_1^+(x,t) = A_1 e^{i(\omega t - kx)} \tag{2.12}$$

The pressure and volume velocity at the junction are continuous. At $x = 0$, therefore

$$p_0^+(0,t) + p_0^-(0,t) = p_1^+(0,t) \tag{2.13}$$

$$\frac{p_0^+(0,t)}{Z_{c0}} - \frac{p_0^-(0,t)}{Z_{c0}} = \frac{p_1^+(0,t)}{Z_{c1}} \tag{2.14}$$

where $Z_{c0} = \frac{\rho c}{S_0}$ is the characteristic impedance of the first cylinder and $Z_{c1} = \frac{\rho c}{S_1}$ is the characteristic impedance of the second cylinder.

Combining equations (2.13) and (2.14),

$$\frac{p_0^-(0,t)}{p_0^+(0,t)} = \frac{Z_{c1} - Z_{c0}}{Z_{c1} + Z_{c0}} = \frac{S_0 - S_1}{S_0 + S_1} \tag{2.15}$$

Examination of equations (2.11a) and (2.11b) reveals that, at $x = 0$, the ratio of the instantaneous pressures of the reflected and incident waves is simply the ratio of their amplitudes.

$$\frac{p_0^-(0,t)}{p_0^+(0,t)} = \frac{B_0}{A_0} \tag{2.16}$$

Therefore, combining equations (2.15) and (2.16) yields the reflection coefficient $r_{0,1}$ (the ratio of the pressure amplitude of the reflected wave to that of the incident wave) for the boundary between first cylinder and second cylinder:

$$r_{0,1} = \frac{B_0}{A_0} = \frac{p_0^-(0,t)}{p_0^+(0,t)} = \frac{S_0 - S_1}{S_0 + S_1} \tag{2.17}$$

The reflection coefficient depends only on the change of cross-sectional area.

2.3 Plane wave propagation in a duct of varying cross-section

A duct whose cross-section varies along its length can be modelled as a series of short cylindrical segments, each of length L with corresponding two-way travel time $T = 2L/c$ [Marshall et al. 1991]. Figure 2.2 shows such a discretised tube consisting of segments

from *1* to *N*, terminated at the left end by a semi-infinite cylinder (defined as being the '*zeroth'* segment).

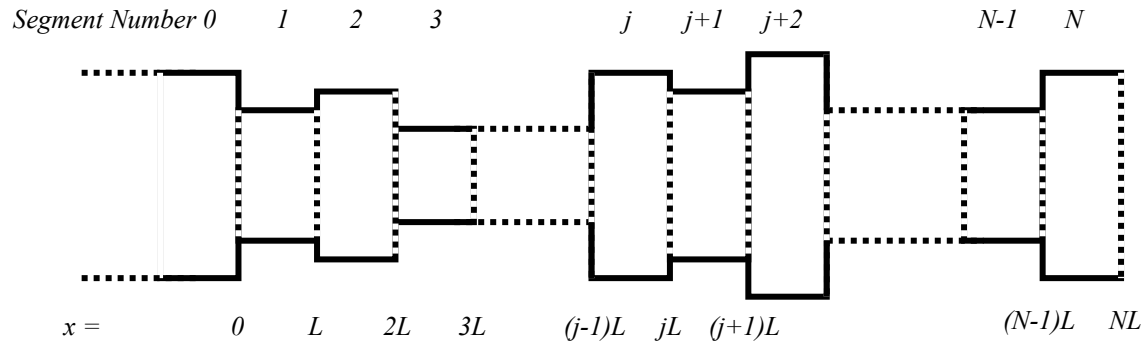

Figure 2.2: Cylindrically segmented duct

Consider the situation where both forward and backward travelling pressure waves propagate within each segment. *T* is defined as two-way travelling time within each segment. At the junctions between segments, each travelling wave experiences reflection and transmission. In Figure 2.3, the pressure signals around an arbitrary junction (between the *j*th and *(j+1)*th cylindrical segments) are shown. $p^{+}_{j,r}[nT]$ and $p^{-}_{j,r}[nT]$ represent the forward and backward travelling waves at the right side of the *j*th segment, $p^{+}_{j+1,l}[nT]$ and $p^{-}_{j+1,l}[nT]$ represent the forward and backward travelling pressure waves at the left side of the *(j+1)*th segment, and $p^{+}_{j+1,r}[nT]$ and $p^{-}_{j+1,r}[nT]$ represent the forward and backward travelling waves at the right side of the *(j+1)*th segment (all at time *nT*, where *n = 0, 1/2, 1, 3/2, 2…*). Note that the pressure signals are now only represented at discrete times (integer multiples of the time taken to propagate across one cylindrical segment).

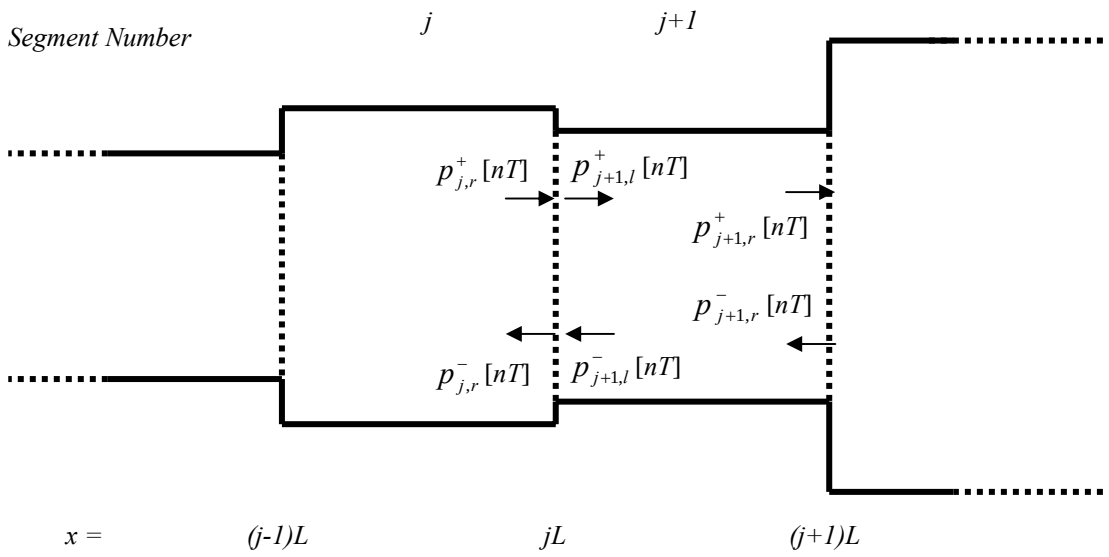

Figure 2.3: The jth and the(j+1)th cylindrical segments

Over the next two sections, wave scattering at a junction between two segments and wave propagation across a cylindrical segment are discussed. These discussions are then drawn together, resulting in a model that describes wave propagation in a duct of varying cross-section.

2.3.1 Plane wave scattering at a junction

The pressure and volume velocity across the junction between two cylindrical segments must both be continuous. These conditions can be used to derive an expression relating the pressure on either side of the boundary. Consider, for example, the junction between the *j*th and *(j+1)*th segments illustrated in Figure 2.3. The continuity conditions mean that:

$$p^{+}_{j,r}[nT] + p^{-}_{j,r}[nT] = p^{+}_{j+1,l}[nT] + p^{-}_{j+1,l}[nT] \tag{2.18}$$

$$\frac{p^{+}_{j,r}[nT]}{Z_{cj}} - \frac{p^{-}_{j,r}[nT]}{Z_{cj}} = \frac{p_{j+1,l}{}^{+}[nT]}{Z_{c(j+1)}} - \frac{p^{-}_{j+1,l}[nT]}{Z_{c(j+1)}} \tag{2.19}$$

where $Z_{cj} = \frac{\rho c}{S_j}$ is the characteristic impedance of *j*th cylindrical segment and $Z_{c(j+1)} = \frac{\rho c}{S_{j+1}}$ is the characteristic impedance of (*j+1*)th cylindrical segment.

Equations (2.18) and (2.19) can be rearranged and written in a matrix form as

$$\begin{bmatrix} p^{+}_{j,r}[nT] \\ p^{-}_{j,r}[nT] \end{bmatrix} = \begin{bmatrix} \frac{Z_{c(j+1)} + Z_{cj}}{2Z_{c(j+1)}} & \frac{Z_{c(j+1)} - Z_{cj}}{2Z_{c(j+1)}} \\ \frac{Z_{c(j+1)} - Z_{cj}}{2Z_{c(j+1)}} & \frac{Z_{c(j+1)} + Z_{cj}}{2Z_{c(j+1)}} \end{bmatrix} \begin{bmatrix} p^{+}_{j+1,l}[nT] \\ p^{-}_{j+1,l}[nT] \end{bmatrix} \tag{2.20}$$

which, in terms of cross-sectional area, can be written

$$\begin{bmatrix} p^{+}_{j,r}[nT] \\ p^{-}_{j,r}[nT] \end{bmatrix} = \begin{bmatrix} \frac{S_j + S_{j+1}}{2S_j} & \frac{S_j - S_{j+1}}{2S_j} \\ \frac{S_j - S_{j+1}}{2S_j} & \frac{S_j + S_{j+1}}{2S_j} \end{bmatrix} \begin{bmatrix} p^{+}_{j+1,l}[nT] \\ p^{-}_{j+1,l}[nT] \end{bmatrix} \tag{2.21}$$

If equation (2.17) is extended to the junction between the *j*th and *(j+1)*th segments, the reflection coefficient can be expressed as:

$$r_{j,j+1} = \frac{S_j - S_{j+1}}{S_j + S_{j+1}} \tag{2.22}$$

Consequently, by combining equations (2.21) and (2.22), the scattering equation can also be expressed in terms of the reflection coefficient.

$$\begin{bmatrix} p^{+}_{j,r}[nT] \\ p^{-}_{j,r}[nT] \end{bmatrix} = \frac{1}{1+r_{j,j+1}} \begin{bmatrix} 1 & r_{j,j+1} \\ r_{j,j+1} & 1 \end{bmatrix} \begin{bmatrix} p^{+}_{j+1,l}[nT] \\ p^{-}_{j+1,l}[nT] \end{bmatrix} \tag{2.23}$$

2.3.2 Plane wave propagation through a cylindrical segment

If it is assumed for the moment that waves propagating within a duct experience no attenuation then, referring again to Figure 2.3, the forward and backward travelling waves ($p^{+}_{j+1,l}[nT]$ and $p^{-}_{j+1,l}[nT]$) at the left end of the *(j+1)*th cylindrical segment can be expressed in terms of the forward and backward travelling waves ($p^{+}_{j+1,r}[nT]$ and $p^{-}_{j+1,r}[nT]$) at the right side of the segment by using two delay lines, each of duration *L/c = T/2* seconds (as shown in Figure 2.4).

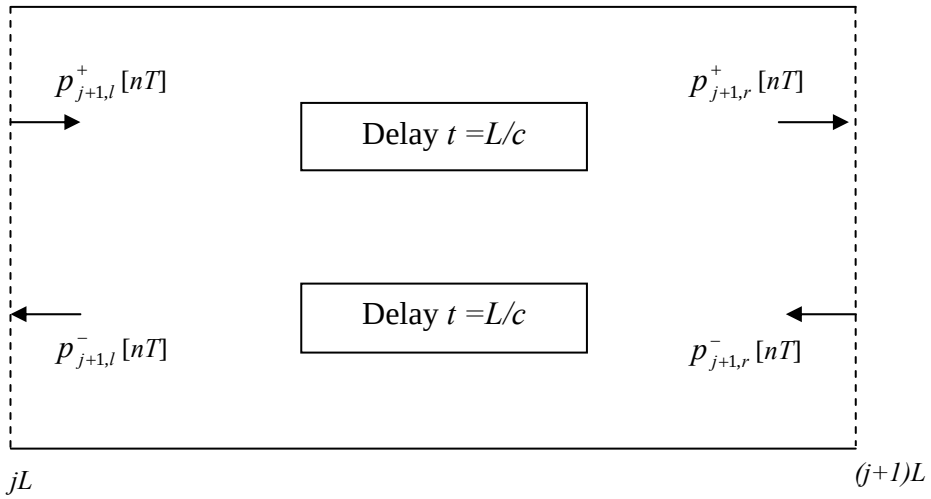

Figure 2.4: Cylindrical segment modelled as delay lines

The effect of these delay lines is to add a time of *L/c* seconds to the forward travelling waves and subtract *L/c* seconds from the backward travelling waves. That is,

$$p^{+}_{j+1,l}[nT] = p^{+}_{j+1,r}[nT + \frac{T}{2}] \tag{2.24a}$$

$$p^{-}_{j+1,l}[nT] = p^{-}_{j+1,r}[nT - \frac{T}{2}] \tag{2.24b}$$

The delay of *T/2* can be expressed in terms of a complex exponential term:

$$p^{+}_{j+1,l}[nT] = e^{ikL}\, p^{+}_{j+1,r}[nT] \tag{2.25a}$$

$$p^{-}_{j+1,l}[nT] = e^{-ikL}\, p^{-}_{j+1,r}[nT] \tag{2.25b}$$

Equations (2.25a) and (2.25b) can be written in a matrix form as

$$\begin{bmatrix} p^{+}_{j+1,l}[nT] \\ p^{-}_{j+1,l}[nT] \end{bmatrix} = \begin{bmatrix} e^{ikL} & 0 \\ 0 & e^{-ikl} \end{bmatrix} \begin{bmatrix} p^{+}_{j+1,r}[nT] \\ p^{-}_{j+1,r}[nT] \end{bmatrix} \tag{2.26}$$

Note that, so far in the discussions, it has been assumed that sound propagation is lossless. In fact, viscous losses and heat conduction losses are significant when sound waves propagate within tubular objects of the sizes used in this project. The effect of such losses should be therefore taken into account.

The term e^{-ikL} (where $k = \omega/c$) represents a delay of *T/2* in frequency domain. To include losses, this term is replaced by

$$H(\omega) = e^{-\Gamma L} \tag{2.27}$$

where Γ is a complex wavenumber. For losses in a cylinder of radius r and length L, an expression for Γ is given by [Keefe 1984],

$$\Gamma = \alpha(\omega) + i\,{\omega}/{v_p} \tag{2.28}$$

where $\alpha(\omega)$ is the frequency dependent attenuation due to boundary layer effects, ω is the angular frequency and v_p is the phase velocity. These parameters can be written as:

$$\alpha(\omega) = \frac{\omega}{c}\left(A r_v^{-1} + B r_v^{-2} + C r_v^{-3}\right) \tag{2.29}$$

$$\frac{\omega}{v_p} = \frac{\omega}{c}\left(1 + A r_v^{-1} - C r_v^{-3}\right) \tag{2.30}$$

where $r_v = \left({\omega\rho}/{\eta}\right)^{1/2} r$ is the ratio of the duct radius to the viscous boundary layer, ρ is the air density and η is the coefficient of shear viscosity of air. The coefficients A, B and C depend on the thermodynamic constants:

$$A = \frac{1}{\sqrt{2}}(1 + D) \tag{2.31}$$

$$B = \left[1 + D - \frac{D}{2v} - \frac{D^2}{2}\right] \tag{2.32}$$

$$C = \frac{1}{\sqrt{2}}\left[\frac{7}{8} + D - \frac{D}{2v} - \frac{D^2}{2} - \frac{D}{8v^2} + \frac{D^2}{2v} + \frac{D^3}{2}\right] \tag{2.33}$$

where $v = \sqrt{{\eta C_p}/{\kappa}}$, $D = {(\gamma - 1)}/{v}$, C_p is the specific heat of air at constant pressure, κ is the thermal conductivity of air, γ is the ratio of the principal specific heats of

air, $c = 331.6\sqrt{1+\tau/273}$ is the speed of sound in air in ms^{-1} and τ is the air temperature in Kelvin.

When losses are taken into consideration, the matrix representation of wave propagation in the *(j+1)*th segment becomes:

$$\begin{bmatrix} p^{+}_{j+1,l}[nT] \\ p^{-}_{j+1,l}[nT] \end{bmatrix} = \begin{bmatrix} e^{\Gamma L} & 0 \\ 0 & e^{-\Gamma L} \end{bmatrix} \begin{bmatrix} p^{+}_{j+1,r}[nT] \\ p^{-}_{j+1,r}[nT] \end{bmatrix} \tag{2.34}$$

2.3.3 Plane wave propagation through multiple segments

By combining equations (2.23) and (2.34), a single matrix equation describing plane wave propagation from one cylindrical segment to the next can be derived. The equation describes the pressure waves on the right side of the *j*th segment in terms of those on the right side of the *(j+1)*th segment.

$$\begin{bmatrix} p^{+}_{j,r}[nT] \\ p^{-}_{j,r}[nT] \end{bmatrix} = M_j \begin{bmatrix} p^{+}_{j+1,r}[nT] \\ p^{-}_{j+1,r}[nT] \end{bmatrix} \tag{2.35}$$

where

$$M_j = \frac{1}{1+r_{j,j+1}} \begin{bmatrix} 1 & r_{j,j+1} \\ r_{j,j+1} & 1 \end{bmatrix} \begin{bmatrix} e^{\Gamma L} & 0 \\ 0 & e^{-\Gamma L} \end{bmatrix} \tag{2.36}$$

For a duct like that of Figure 2.2, which is modelled as *N* cylindrical segments and is coupled at the left end to a semi-infinite tube (the ‘zeroth’ segment), each of the segments has a matrix of the same form as equation (2.36). The forward and backward travelling

waves at the junction between the semi-infinite tube and the first segment can be expressed in terms of those in the final *N*th segment through the multiple application of equation (2.35).

$$\begin{bmatrix} p_{0,r}^{+}[nT] \\ p_{0,r}^{-}[nT] \end{bmatrix} = M_0 M_1 M_2 \cdots\cdots M_{N-1} \begin{bmatrix} p_{N,r}^{+}[nT] \\ p_{N,r}^{-}[nT] \end{bmatrix} \tag{2.37}$$

The product of this group of matrices can be written simply as

$$M = M_0 M_1 M_2 \cdots M_{N-1} = \begin{bmatrix} M_{aa} & M_{ab} \\ M_{ba} & M_{bb} \end{bmatrix} \tag{2.38}$$

The ratio of the backward travelling waves and the forward travelling waves at the entry of the duct is defined as the reflectance *IIR(ω)*. The reflectance of the duct can therefore be found by combining equations (2.37) and (2.38),

$$IIR(\omega) = \frac{p_{0,r}^{-}[nT]}{p_{0,r}^{+}[nT]} = \frac{M_{ba} + M_{bb} \dfrac{p_{N,r}^{-}[nT]}{p_{N,r}^{+}[nT]}}{M_{aa} + M_{ab} \dfrac{p_{N,r}^{-}[nT]}{p_{N,r}^{+}[nT]}} \tag{2.39}$$

Providing that the dimensions of the duct (and hence the elements of matrix M) are known, the reflectance can be determined from the ratio of the forward and backward travelling waves at the right end of the duct. This ratio depends on how the duct is terminated at the far end. Two termination conditions are considered here:

1. If a semi-infinite tube is coupled to the right end of the duct, there are no backward propagating pressure waves; i.e. $p_{N,r}^{-}[nT] = 0$. Therefore, the ratio $\frac{p_{N,r}^{-}[nT]}{p_{N,r}^{+}[nT]} = 0$ and

$$IIR(\omega) = \frac{M_{ba}}{M_{aa}} \tag{2.40}$$

2. If the duct terminates in an open end, some of the sound energy is radiated out into free space but most is reflected to produce backward waves. In this case, the load impedance Z_L at the end of the duct is the radiation impedance. For an unflanged cylindrical duct, the radiation impedance is given by [Kinsler et al. P274].

$$Z_L = Z_{cN}\left[\frac{1}{4}(kr)^2 + i0.6kr\right] \tag{2.41}$$

where k is wave number and r is the radius at the end of the duct. Again, Z_{cN} is the characteristic impedance of the Nth cylindrical segment.

As a result of the pressure and volume velocity continuity conditions, the load impedance Z_L can also be expressed in terms of the pressure and the characteristic impedance Z_{cN}. It is given by

$$Z_L = Z_{cN}\frac{p_{N,r}^{+}[nT] + p_{N,r}^{-}[nT]}{p_{N,r}^{+}[nT] - p_{N,r}^{-}[nT]} \tag{2.42}$$

Rearranging this equation yields an expression for the ratio of backward travelling wave and forward travelling waves at the right end of the duct.

$$\frac{p_{N,r}^{-}[nT]}{p_{N,r}^{+}[nT]} = \frac{Z_L / Z_{cN} - 1}{Z_L / Z_{cN} + 1} \tag{2.43}$$

From equations (2.39), (2.41) and (2.43), the reflectance of the duct becomes

$$IIR(\omega) = \frac{p_{0,r}^{-}[nT]}{p_{0,r}^{+}[nT]} = \frac{M_{ba} + M_{bb}\left[\frac{1}{4}(kr)^2 - 1 + i0.6kr\right]}{M_{aa} + M_{ab}\left[\frac{1}{4}(kr)^2 + 1 + i0.6kr\right]} \tag{2.44}$$

2.3.4 Simulated input impulse response

Figure 2.5 shows the reflectance of a 310 mm long stepped tube (comprising two cylindrical sections of length 0.13 m and radii 6.2 mm and length 0.18 m and radii 9.45 mm respectively) calculated using the theory outlined in this chapter. The stepped tube is discretised into 45 cylindrical segments each of approximate length L = 6.9 mm. It is clear that, at very long wavelengths, little energy is radiated out of the open end. However, at high frequencies, more and more energy radiates out of the open end and the reflectance is decreased.

As mentioned previously, the reflectance is the ratio of the reflected waves to the incident waves at the input of the duct in the frequency domain. In the time domain, this ratio is known as the input impulse response (*iir*) of the duct. This is simply the response that would be measured if the duct were probed with an acoustic impulse. That is, when the incident wave is an impulse, the reflected wave is the input impulse response

$$p_{0,r}^{+}[nT] = \delta[nT] = \begin{cases} 1 & n = 0 \\ 0 & n \neq 0 \end{cases} \tag{2.45}$$

$$p_{0,r}^{-}[nT] = iir[nT] \tag{2.46}$$

where $iir[nT]$ represents the discrete form of the input impulse response.

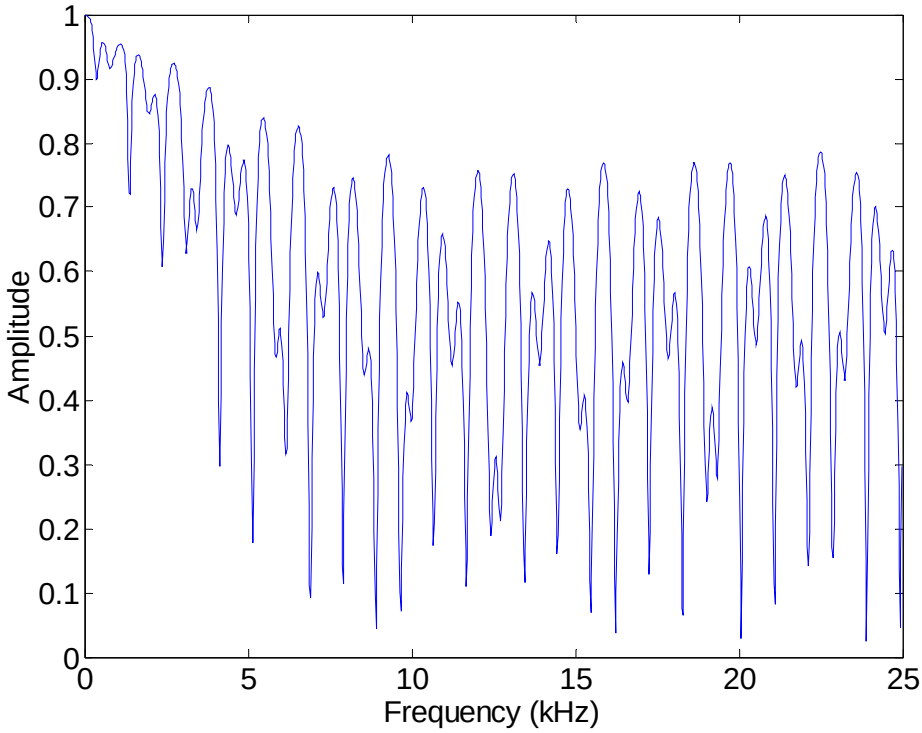

Figure 2.5: Reflectance of a stepped tube

Figure 2.6 shows the input impulse response of the stepped tube obtained by performing an inverse FFT on the reflectance shown in Figure 2.5. Each of the reflections in the input impulse response can be identified. The first negative peak is the reflection from the first expansion in the stepped tube (from a radius of 6.2 mm to a radius of 9.45

mm). The second negative peak is the reflection from the open end. Subsequent peaks are multiple reflections which have taken place within the stepped tube.

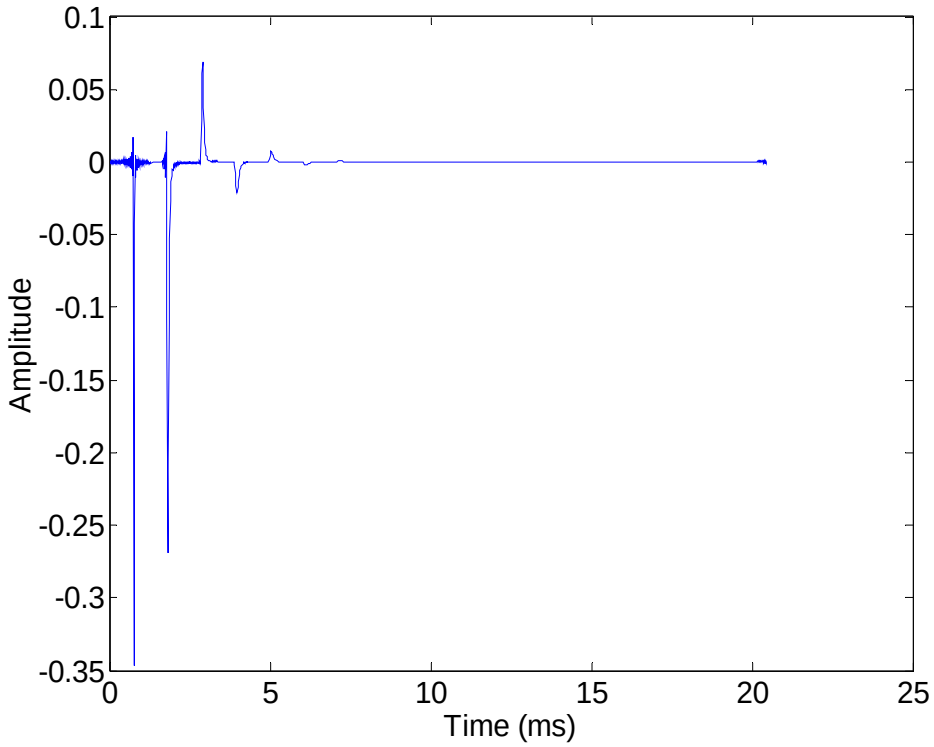

Figure 2.6: Input impulse response of a stepped tube

2.4 Concluding remarks

In this chapter, the reflection and transmission of plane waves within varying cross-section ducts of known dimensions has been discussed. This type of problem is referred to as the 'Direct Problem'. Solving the 'Direct Problem' is in essence predicting the reflectance, and hence the input impulse response of a duct, given knowledge of its dimensions. In the following chapter, we will discuss the 'Inverse Problem'. As the name suggests, solving the 'Inverse Problem' involves calculating the dimensions of a duct given its input impulse response. As will become clear, this is the basic theory that underpins acoustic pulse reflectomery.

Chapter 3

Wave propagation in a duct of varying cross-section—the inverse problem

3.1 Introduction

In this chapter, the inverse problem of determining the dimensions of a duct from its input impulse response is discussed. The algorithm used to calculate duct dimensions is first introduced with no account taken of viscous thermal losses. However, such losses are significant when sound waves propagate in tubular objects of the sizes examined in this study. Consequently, the algorithm is then extended to incorporate the effect of visco-thermal losses.

3.2 The reconstruction algorithm

The first means of solving the inverse problem was provided by [Ware and Aki 1969]. However, as the Ware-Aki algorithm does not compensate for the effect of losses, the bore reconstructions it produces tend to underpredict the duct's radial dimensions. An alternative layer peeling approach, developed by Amir et al. [Amir et al. 1995], allows losses to be taken into account. It is this solution to the inverse problem that was used by [Sharp and Campbell 1998] in their development work on the acoustic pulse reflectometry technique and which has been adopted in this present study.

3.2.1 Lossless method

Consider a duct of varying cross-section that is modelled as a series of short cylindrical segments, each of length *L*, and terminated at one end by a semi-infinite cylinder (such as the duct shown previously in figure 2.2). An incident wave injected into the duct via the 'zeroth segment' (the semi-infinite tube) will experience partial reflection and partial transmission at each segment boundary within the duct. The wave propagation in the zeroth and first segments in such a case is shown in Figure 3.1.

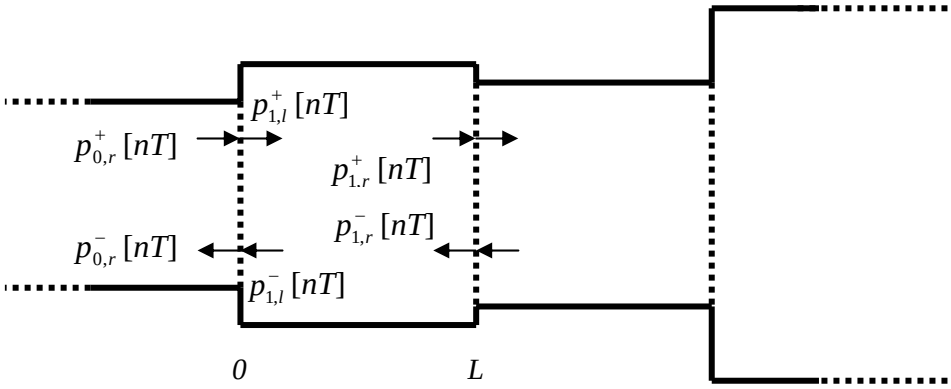

Figure 3.1: Forward and backward travelling waves in a duct.

If the incident wave injected into the duct is an acoustic impulse ($p^{+}_{0,r}[nT] = \delta[nT]$), then the reflected wave is the input impulse response ($p^{-}_{0,r}[nT] = iir[nT]$). At time $t = 0$ (defined as being the instant that the incident wave arrives at the entrance to the duct—the boundary between the zeroth and first segments), there are no backward travelling waves in the first cylindrical segment. That is, $p^{-}_{1,l}[nT]$ and $p^{-}_{1,r}[nT]$ are both zero. Consequently, the backward travelling wave in the zeroth segment is simply the reflection

of the forward travelling wave in that segment. The reflection coefficient at the boundary between the segment 0 and segment 1 is therefore:

$$r_{0,1} = \frac{p^{-}_{0,r}[0T]}{p^{+}_{0,r}[0T]} = iir[0T] \tag{3.1}$$

where $p^{+}_{0,r}[0T]$ and $p^{-}_{0,r}[0T]$ are the incident and reflected waves and $iir[0T]$ is the input impulse response, all at $t = 0$.

In equation (2.22), the reflection coefficient for the boundary between two arbitrary segments (the jth and the $(j+1)$th) was expressed in terms of the cross-sectional areas of those segments. Rearranging equation (2.22) therefore allows the cross-sectional area of the $(j+1)$th segment to be expressed in terms of the area of the jth segment and the reflection coefficient $r_{j,j+1}$:

$$S_{j+1} = S_j \left(\frac{1 - r_{j,j+1}}{1 + r_{j,j+1}} \right) \tag{3.2}$$

Therefore, assuming that the cross-sectional area S_0 of the zeroth segment (the semi-infinite cylinder) is known, the area S_1 of the first segment can be found from the reflection coefficient $r_{0,1}$ using equation (3.2).

The forward and backward travelling pressure waves at the left side of the first segment, $p^{+}_{1,l}[nT]$ and $p^{-}_{1,l}[nT]$, can be obtained from the forward and backward waves in the zeroth segment by rearranging the scattering equation (2.23), to give:

$$\begin{bmatrix} p_{1,l}{}^{+}[nT] \\ p_{1,l}{}^{-}[nT] \end{bmatrix} = \frac{1}{1 - r_{0,1}} \begin{bmatrix} 1 & -r_{0,1} \\ -r_{0,1} & 1 \end{bmatrix} \begin{bmatrix} p_{0,r}{}^{+}[nT] \\ p_{0,r}{}^{-}[nT] \end{bmatrix} \tag{3.3}$$

Next the pressure waves at the right side of the first segment must be found. To determine the forward and backward travelling pressure waves, $p^{+}_{1,r}[nT]$ and $p^{-}_{1,r}[nT]$, at the right side of the first segment, a delay of *T/2* is added to $p^{+}_{1,l}[nT]$ and subtracted from $p^{-}_{1,l}[nT]$ using the delay equation (2.24).

At the boundary between the first and second segments, when *t = T/2*, there is no backward travelling wave in the second segment. Therefore, the reflection coefficient at the junction between the first and second cylindrical segments is given by:

$$r_{1,2} = \frac{p^{-}_{1,r}[T/2]}{p^{+}_{1,r}[T/2]} \tag{3.4}$$

It should be noted that, when implementing the algorithm in practice, it is more convenient and entirely equivalent to subtract a delay of T from $p^{-}_{1,l}[nT]$ and leave $p^{+}_{1,l}[nT]$ unchanged. The time origin shift then requires the reflection coefficient $r_{1,2}$ to be calculated at $t = 0$ rather than at $t = T/2$.

Again, using equation (3.2), the cross-sectional area S_2 can be obtained from the previously calculated cross-sectional area S_1 and the reflection coefficient $r_{1,2}$.

The layer peeling procedure is carried out recursively until the reflection coefficient at each junction is determined and the entire area profile of the duct is calculated.

3.2.2 Incorporating the effect of losses

In the previous section, it was assumed that waves propagating from one side of a cylindrical segment to the other experienced a time delay of *T/2* but experienced no viscous and thermal (heat conduction) losses in doing so. In order to calculate the duct

profile accurately, however, such visco-themal losses must be taken into account. A digital filter representing the losses in a cylindrical segment has been developed by [Amir et al. 1996]. This filter depends on the length and radius of the segment. To compensate for the effect of losses, in addition to the *T/2* delay, such a digital filter is applied to each segment in the layer peeling algorithm. (Note that at each stage of the algorithm, the radius of the following segment is calculated, so the appropriate lossy filter can also be calculated).

Referring back to equations (2.27) and (2.28), the continuous frequency domain lossy filter for waves propagating through a cylindrical segment is given by

$$H(\omega) = e^{-\Gamma l} = e^{-\alpha(\omega) l} e^{-i\omega l / v_p} \tag{3.5}$$

The numerical computation of the equivalent digital frequency domain lossy filter is detailed in [Amir et al. 1995 and 1996]. By inverse Fourier Transforming the discretized lossy filter, the digital filter $h_j[nT]$ is found.

Moving from the left side to the right side of a cylindrical segment, the forward travelling wave $p^+_{j,l}[nT]$, is simply passed through the filter $h_j[nT]$. Meanwhile the backward travelling wave $p^-_{j,l}[nT]$, is passed through the inverse filter of $h_j[nT]$. Therefore, to include losses in the reconstruction procedure, the following equations are applied before adding and subtracting the delays of *T/2* from $p^+_{j,l}[nT]$ and $p^-_{j,l}[nT]$:

$$p_{j,l}{}^{+}[nT] = p_{j,l}{}^{+}[nT] \otimes h_j[nT] \tag{3.6a}$$

$$p_{j,l}{}^{-}[nT] = p_{j,l}{}^{-}[nT] \otimes^{-1} h_j[nT] \tag{3.6b}$$

where the operators $\otimes$ and $\otimes^{-1}$ represent convolution and deconvolution, and $h_j[nT]$ is the digital lossy filter in the *j*th segment.

3.3 Bore reconstruction using simulated data

Figure 3.2 shows the bore reconstruction of a 310 mm long stepped tube (comprising cylindrical sections of radius 6.2 mm and 9.45 mm respectively). The reconstruction was calculated by applying the layer peeling algorithm to the simulated input impulse response of Figure 2.6. The cylindrical sections of radius 6.2 mm and 9.45 mm are reconstructed accurately.

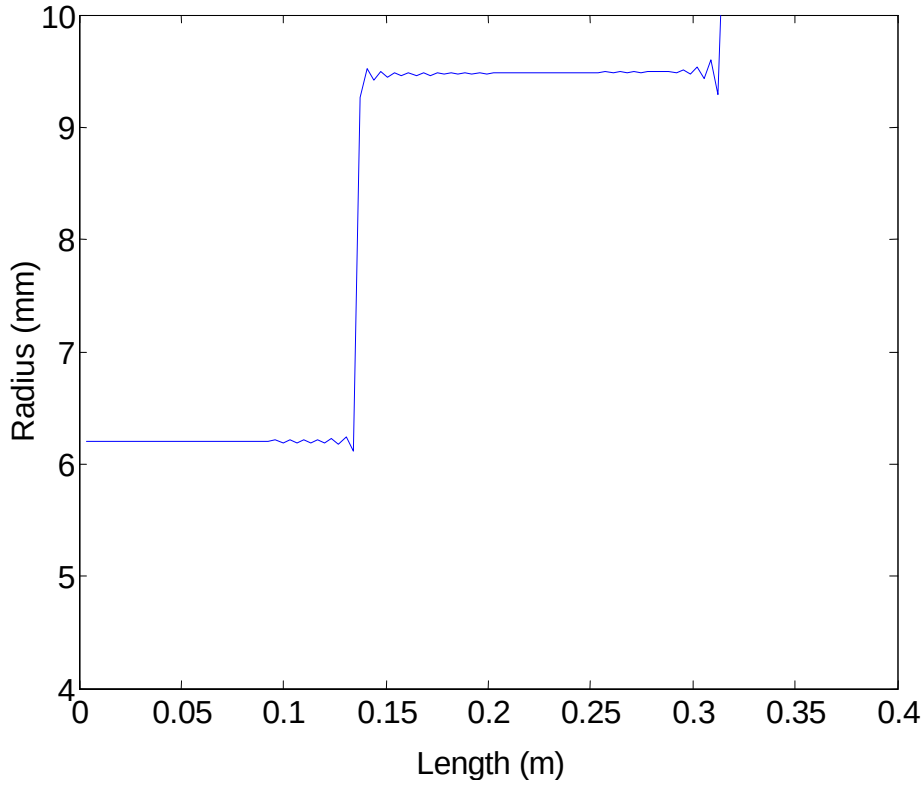

Figure 3.2: The reconstruction resulting from the application of layer-peeling algorithm to simulated data

3.4 Concluding remarks

In this chapter, the basic theory of solving the inverse problem of determining the dimensions of a duct of varying cross-section from its input impose response was

discussed. The layer-peeling algorithm that underpins the technique of acoustic pulse reflectometry has been described and successfully applied to the bore reconstruction of a stepped tube from simulated input impulse response data. In the next chapter, the technique of acoustic pulse reflectometry is introduced, detailing how it is used for measuring the input impulse response of ducts (from which the geometry can then be deduced using the layer peeling algorithm).

Chapter 4

Experimental measurement of input impulse response

4.1 Introduction

The acoustic pulse reflectometry technique for measuring various different duct properties was first introduced in chapter 1. It involves injecting a sound pulse via a source tube into the duct under investigation. The reflections returning from the duct are recorded by a microphone embedded in the source tube wall and then analyzed to find the input impulse response of the duct, from which its internal dimensions and input impedance can be deduced. The technique is particularly useful in cases, such as human airways and certain musical wind instruments, where parts of the duct are inaccessible to tools such as measuring calipers and rulers.

In this chapter, the acoustic pulse reflectometry experimental apparatus developed by Sharp [Sharp 1996] is described and input impulse response measurements are presented.

4.2 Experimental Procedure

Figure 4.1 shows a schematic diagram of the reflectometer used in the present study. A photograph of the apparatus is shown in Figure 4.2.

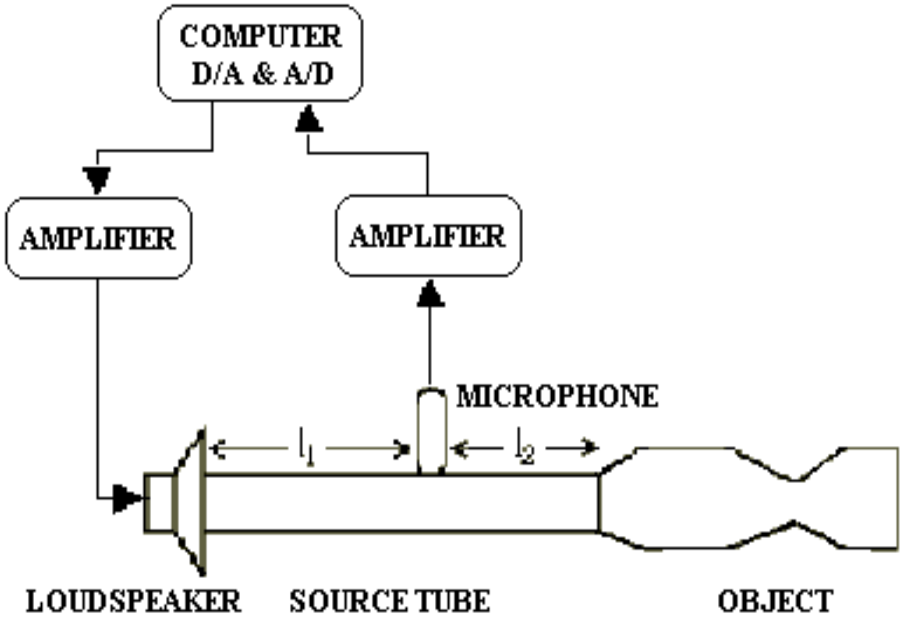

Figure 4.1: Schematic diagram of acoustic pulse reflectometer

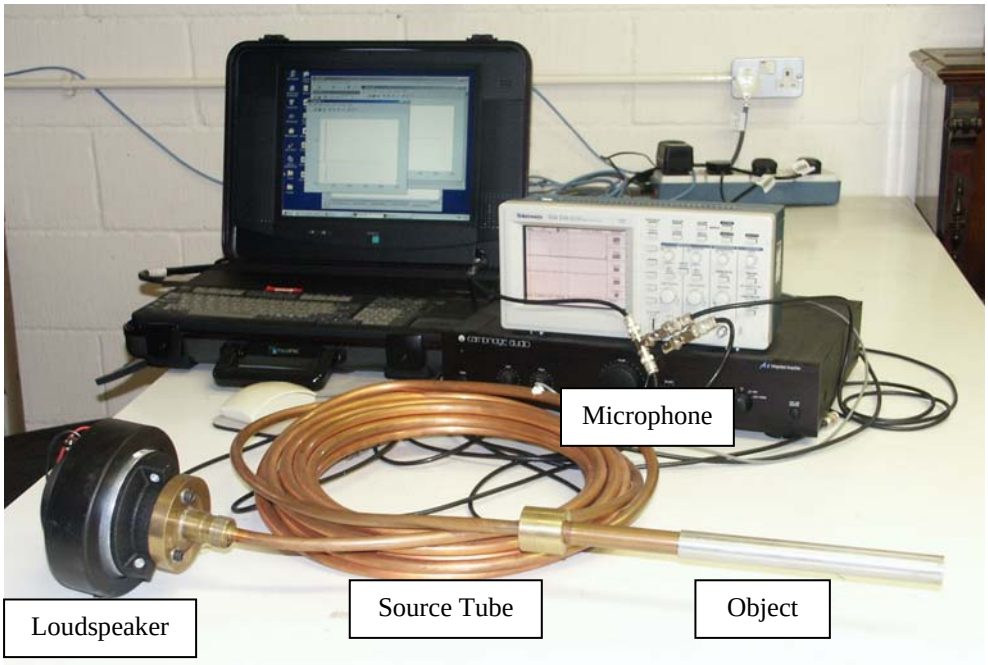

Figure 4.2: Photo of reflectometer

A 5V electrical pulse of 40 μs duration is produced by a computer with data acquisition facilities, sent to an amplifier and then used to drive a loudspeaker. The resultant sound pressure pulse travels down a 10 m long coiled source tube of internal radius 5 mm and is injected into the duct under test. The duct reflections are recorded by a microphone embedded in the wall of the source tube and are sampled by the computer's data acquisition card using a sampling rate of F_s= 50 kHz. The sampled duct reflections are stored on the PC. This experimental procedure is repeated 1000 times and the sampled reflections are averaged to improve the signal-to-noise ratio.

The source tube is necessary to separate forward and backward travelling signals. The section l_2 = 3 m ensures that input pulse has fully passed the microphone before the first of the reflections returning from the duct reaches it. The section l_1 = 7 m ensures that the duct reflections are separated from any further reflections from the loudspeaker. Once the duct reflections reach the microphone, they can be recorded for up to $2l_1/c$ seconds (the time taken to travel the distance from the microphone to the loudspeaker and back, where c is the speed of sound) before the loudspeaker reflections return and contaminate the received signal.

4.3 Deconvolution

If the incident sound pressure pulse were an ideal delta function then the reflections recorded by the microphone would be the input impulse response of the duct. In practice, though, it is impossible to produce a delta function sound pressure pulse. However, making use of signal processing techniques, the deconvolution of the duct reflections with the incident wave enables the input impulse response of the duct to be determined.

The incident wave $p^{+}_{0,r}[nT]$ produced by the experimental reflectometer is a pulse of finite width. Therefore, to obtain the input impulse response of the duct, the measured reflections are deconvolved with the input pulse. By rigidly terminating the source tube using a cap with a flat face, the backward reflected pulse is recorded and used as the input pulse. This ensures that both the duct reflections and the input pulse travel up and down the same length l_2 of source tube and hence experience the same source tube losses. It also ensures that the deconvolution yields just the input impulse response of the duct under test, without the section l_2 of source tube included. The deconvolution is carried out by performing a FFT on both the duct reflections and the input pulse. A complex division is then carried out in the frequency domain:

$$IIR\ (\omega) = \frac{R(\omega)}{I(\omega)} \tag{4.1a}$$

where ω is the discretized angle frequency, $I(\omega)$ is the Fourier Transform of the input pulse and $R(\omega)$ is the Fourier Transform of the duct reflections. $IIR(\omega)$ is the Fourier transform of the input impulse response, which is then inverse FFTed to give the input impulse response in the time domain, $iir[nT]$.

In practice, a constrained deconvolution is used:

$$IIR\ (\omega) = \frac{R(\omega)I^{*}(\omega)}{I(\omega)I^{*}(\omega) + q} \tag{4.1b}$$

where $I^{*}(\omega)$ denotes the complex conjugate of $I(\omega)$ and q is a constraining factor, used to prevent division by zero at higher frequencies where the input pulse drops below the background noise level [Marshall 1990]. It therefore acts like a low-pass filter. Again, the input impulse response $iir[nT]$ is found by inverse FFTing $IIR(\omega)$.

The frequency domain division of the duct reflections $R(\omega)$ by the input pulse $I(\omega)$ is considered to be an ill-posed problem [Sondhi 1981; Sondhi and Resnick 1983]. The introduction of the constraining factor q in the deconvolution, as shown in equation (4.1b), is one means of resolving the problem. Another means of overcoming the problem is provided by the method of Singular Value Decomposition (SVD), as described in detail in [Forbes et al. 2003]. By truncating the singular value decomposition of the convolution matrix of the input pulse, the input impulse response is obtained.

4.4 Optimising the reflectometer

When recording the input pulse (reflected from the rigid termination provided by the source tube end cap) and the duct reflections, it is important to ensure that the signal-to-noise ratio is as high as possible. This is achieved through adjustment of the two amplifiers present in the reflectometer set-up (see Figure 4.1). However, there are upper limits on the amount of amplification that can be used. To avoid damage to the loudspeaker, the amplification of the initial electrical pulse must not be too great. In addition, the output of the microphone amplifier must remain within the -6V to +6V range over which the amplifier behaves linearly. In fact, both the recorded input pulse and the duct reflections actually need to be within a -5V to +5V range as this is the maximum input range of the data acquisition card.

Taking these limits into consideration, it might be considered optimal to adjust the amplifiers so that the input pulse (returning to the microphone after reflection from the end cap) has an amplitude of approximately +5V. However, when this is done, distortion is still introduced into the input pulse. This can be seen clearly in Figure 4.3. The solid line shows the reflected input pulse recorded when the amplifiers were adjusted to give it an amplitude of just less than +5V. This pulse is plotted together with a second reflected pulse (plotted

as a dashed line), this time recorded when the amplifiers were adjusted to give it an amplitude of just under +1V (on the graph, the pulse has been scaled up by ×5 for comparison purposes). If the reflectometer were behaving linearly, the two curves should coincide. However, close examination reveals that this is not the case.

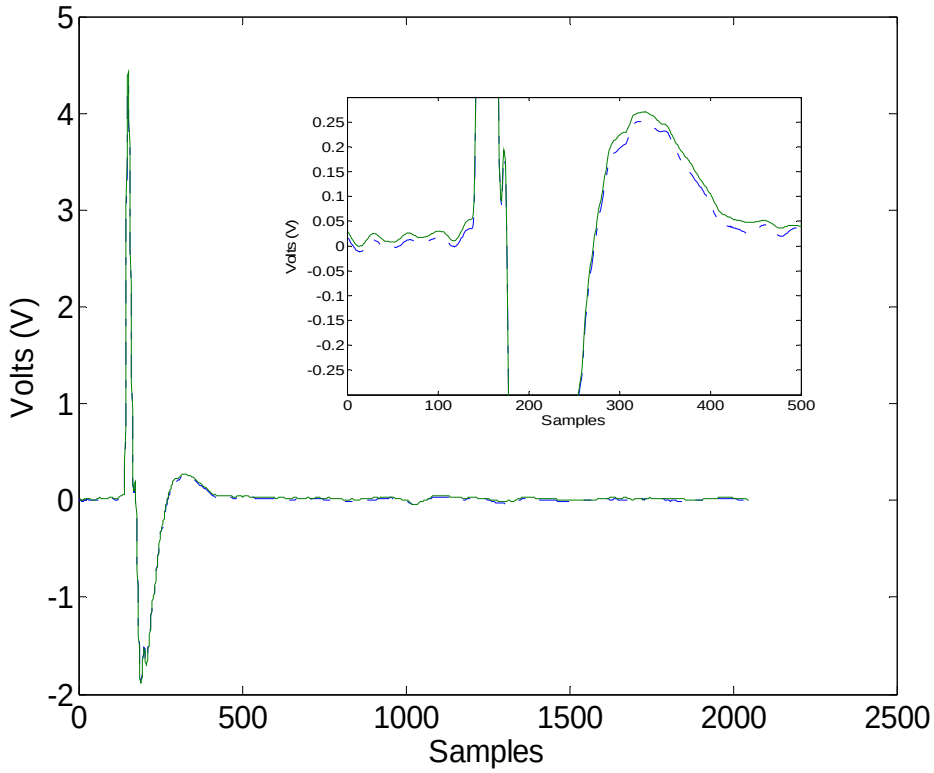

Figure 4.3: Comparison of measured input pulses (amplifier behaving non-linearly)

The reason for this is that the effect of the initial forward travelling pulse has not been considered. When the amplification is adjusted to ensure that the reflected input pulse has an amplitude of +5V, safely within the -6V to +6V range of the amplifier, the initial forward travelling pulse has an amplitude of +15V, which is clearly outside the amplifier's linear range. This is highlighted in Figure 4.4 which shows both the +15V initial forward travelling pulse as it passes the microphone (the signal data outside of the -6V to +6V range of the amplifier is cut off and not shown) and the returning +5V reflected pulse.

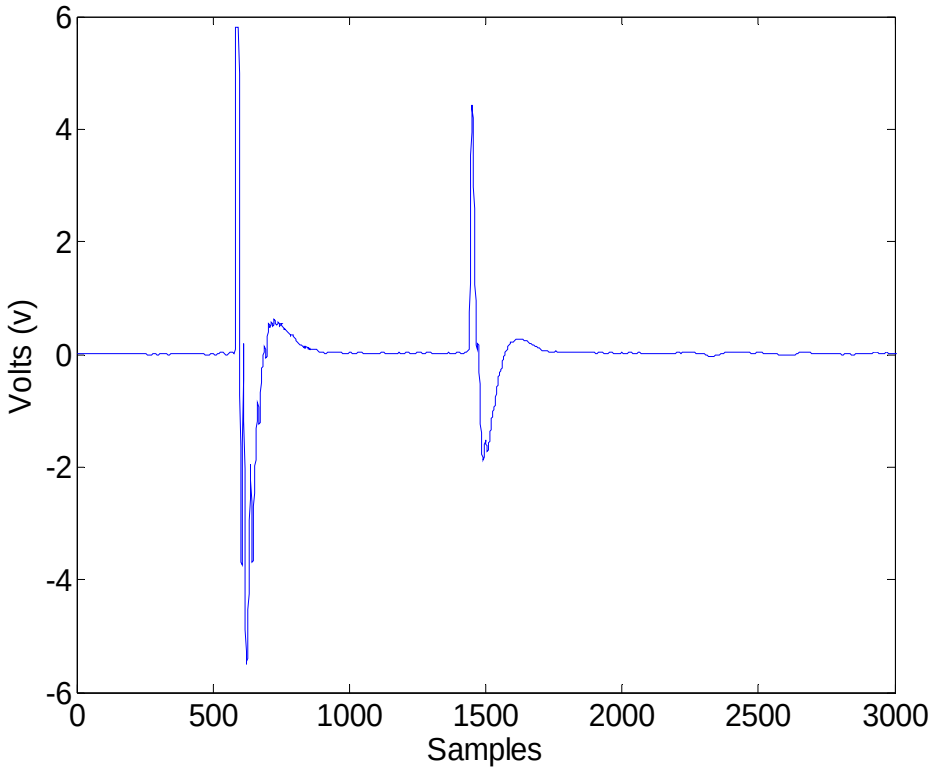

Figure 4.4: The initial forward travelling and reflected pulses

Consequently, to avoid distortion, it is actually necessary to adjust the amplifiers so that the initial forward travelling pulse has an amplitude of approximately +5V. Figure 4.5 demonstrates this. The solid line shows the reflected input pulse of approximately +1.5 V amplitude, recorded when the amplifiers were adjusted to give an initial forward travelling pulse of +5 V amplitude. Also shown is the reflected input pulse recorded when the initial forward travelling pulse has an amplitude of +1 V (on the graph, as before, the pulse has been scaled up by ×5 for comparison purpose and is shown as a dashed line). The two curves coincide, indicating that with these levels of amplification the reflectometer behaves linearly.

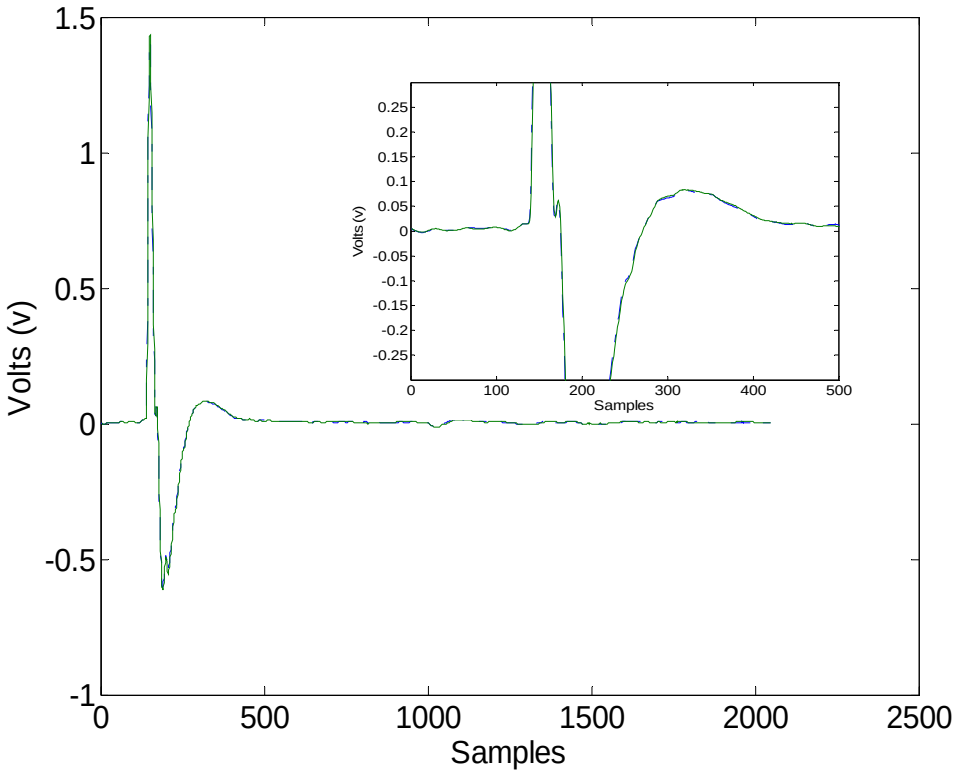

Figure 4.5: Comparison of measured input pulses (amplifier behaving linearly)

4.5 Input impulse response measurements of a stepped tube

In this section, measurements made using the reflectometer shown in Figure 4.2, of a stepped tube consisting of a 0.13 m long cylinder of 6.2 mm radius and a 0.18 m long cylinder of 9.45 mm radius (shown in Figure 4.6), are presented. Figure 4.7 shows the input pulse (the signal reflected from a rigid termination at the end of the source tube) recorded by the microphone in the source tube wall. Figure 4.8 shows the reflections from the stepped tube. The input impulse response of the stepped tube is obtained by deconvolving the reflections in Figure 4.8 with the input pulse in Figure 4.7. The result is shown in Figure 4.9. The first reflection shown in the graph is from the expansion of the source tube up to the 6.2 mm radius section of the stepped tube. The second reflection is from the expansion between the 6.2 mm radius section and the 9.4 mm radius section. The

third reflection is from the open end of the stepped tube. The following small positive and negative reflections are multiple reflections at changes of the stepped tube.

The application of the layer peeling algorithm described in chapter 3 to the measured input impulse response of the test object (in this case, the stepped tube) should enable the bore profile of the test object to be reconstructed accurately. However, in practice, the presence of a DC offset, together with the lack of low frequency content in the test object's experimentally determined input impulse response, causes the reconstructed bore profile either to expand or contract spuriously. In the following chapter, the problem of DC offset and the lack of low frequency content are discussed in detail.

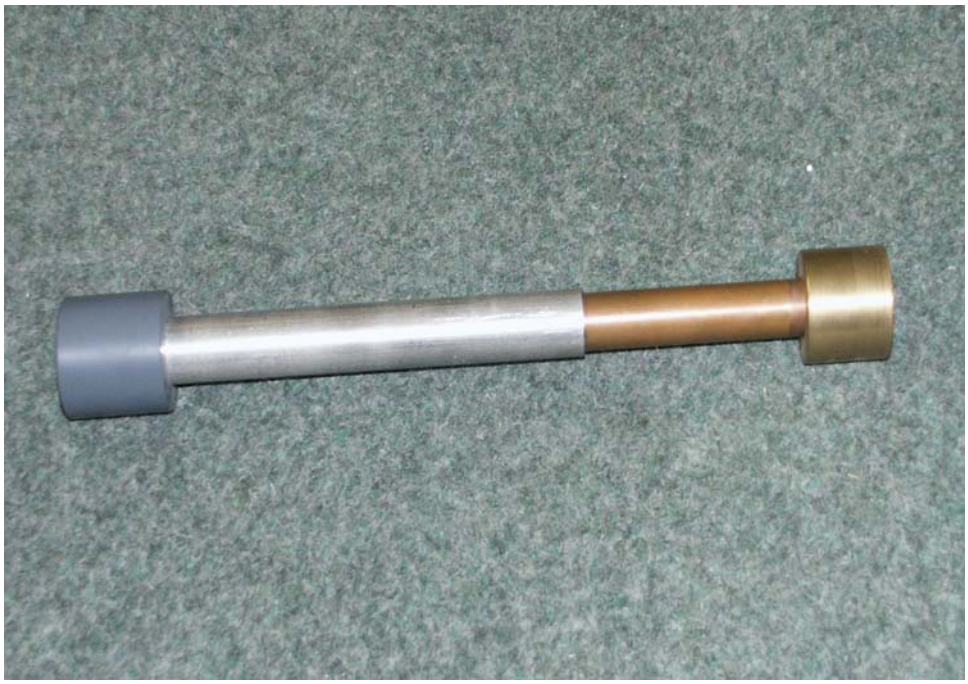

Figure 4.6: Test object and couplers

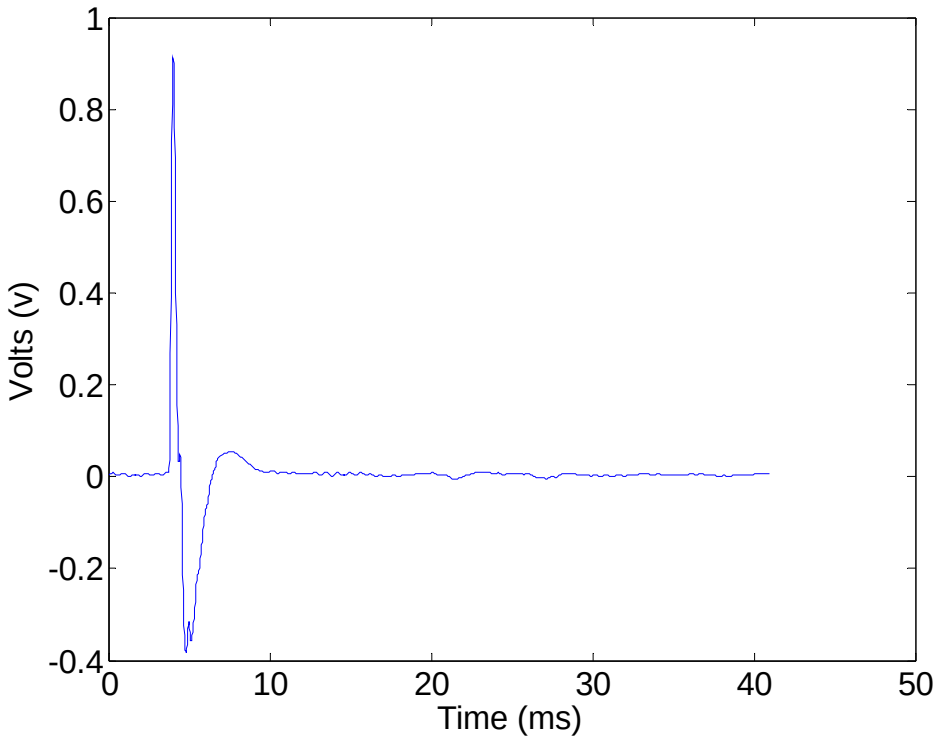

Figure 4.7: Input pulse

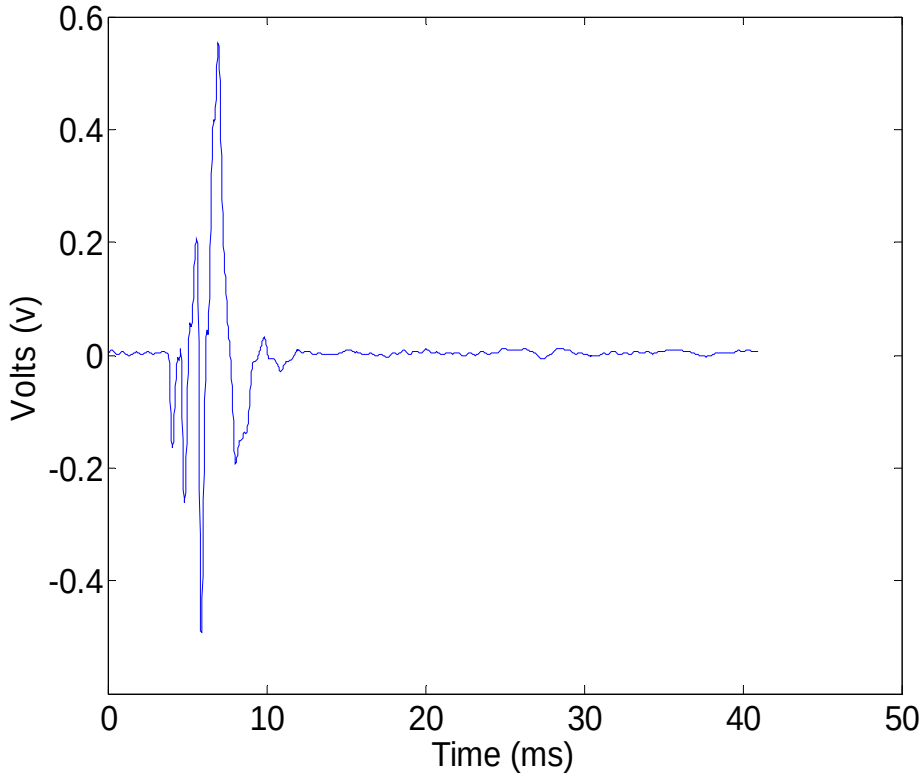

Figure 4.8: Reflections of the stepped tube

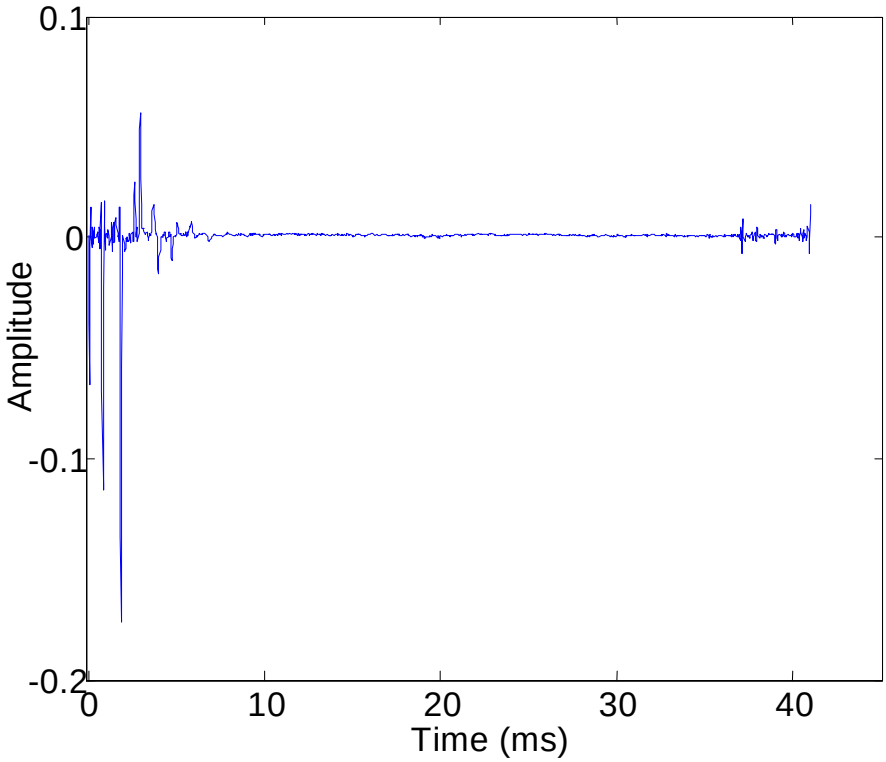

Figure 4.9: Input impulse response of the stepped tube

Chapter 5

The problem of offset in acoustic pulse reflectometry measurements

5.1 Introduction

In this chapter, the nature of the offset introduced into reflectometry measurements is studied. Possible sources of the offset are then identified and methods of preventing the offset are investigated. Finally, accurate bore reconstructions of a test object, calculated from input impulse response measurements where the offset has been eliminated, are presented.

5.2 Demonstration of the offset problem

A measurement of the input impulse response of a duct made using acoustic pulse reflectometry generally contains an offset. The presence of this offset causes the calculated duct profile to expand or contract spuriously. Figure 5.1 shows the input impulse response of the stepped tube measured in chapter 4 and previously shown in Figure 4.8. The expansion of the y-scale in Figure 5.1 makes the offset in the input impulse response clearly visible.

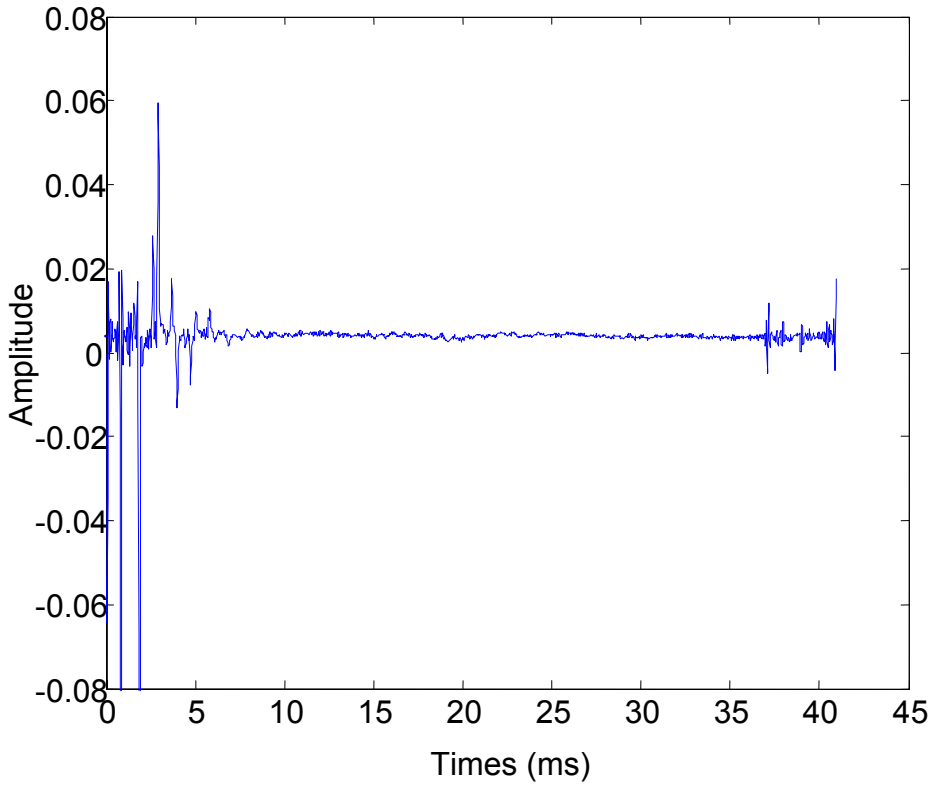

Figure 5.1: Input impulse response of stepped tube with offset from x = 0 line

Figure 5.2 shows the duct profile calculated when the layer peeling algorithm described in chapter 3 is applied to the input impulse response of Figure 5.1. The dotted line shows direct measurements of the radii of the cylindrical sections made using calipers. It can be clearly seen that, in the reconstruction, the radius of each section of the stepped tube decreases with distance along the tube rather than remaining constant. To obtain an accurate reconstruction, the offset must be prevented from occurring or removed from the input impulse response before application of the reconstruction algorithm.

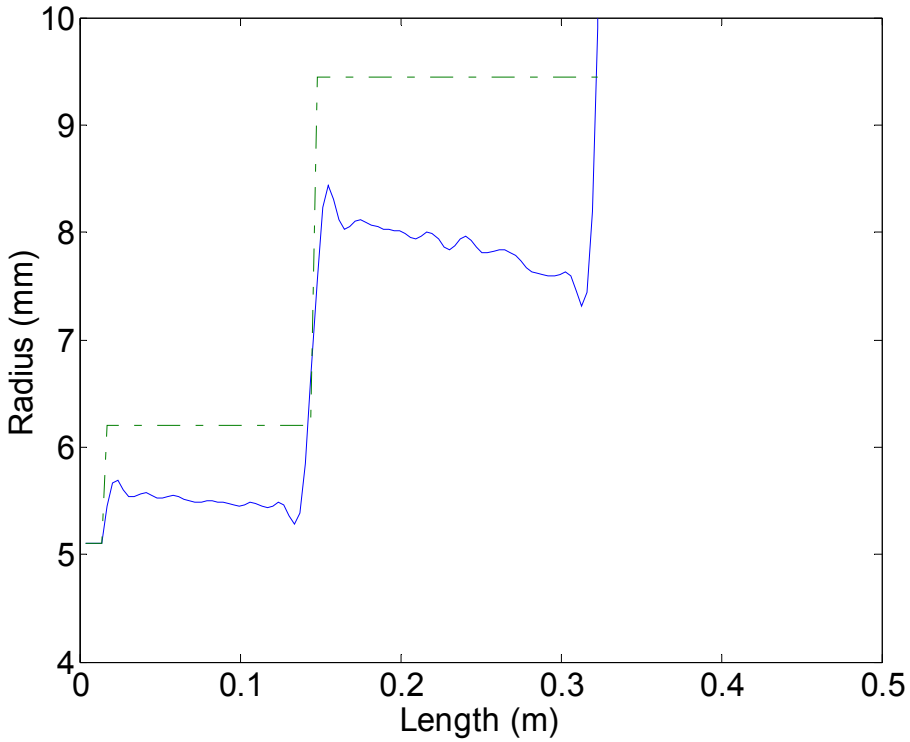

Figure 5.2: Reconstruction of stepped tube

Ideally, the introduction of offset into the input impulse response should be prevented in the first place. In order to be able to do this it is first necessary to establish the origin of the offset.

5.3 Theoretical analysis of the nature of the offset

In pulse reflectometry analysis, the input impulse response *iir'*(n) of a duct is obtained by performing an Inverse Discrete Fourier Transform of *IIR'*(ω), calculated from the input pulse and reflection measurements. This experimental input impulse response can be expressed as

$$
\begin{aligned}
iir'(n) &= \frac{1}{N}\sum_{k=0}^{N-1} IIR'(k)e^{j(2\pi/N)kn} \\
&= \frac{IIR'(0)}{N} + \frac{1}{N}\sum_{k=1}^{N-1} IIR'(k)e^{j(2\pi/N)kn}
\end{aligned}
\tag{5.1}
$$

where *IIR'*(*k*), is the *k*th element of the discrete form of *IIR'*(ω), and *IIR'*(0) is the first element (0 Hz value) of the input impulse response in frequency domain. From equation (5.1), it can be seen that *iir'*(*n*), the *n*th element of the experimental impulse response in the time domain, consists of both a constant component and a number of sinusoidal components.

If the true input impulse response is defined as being *iir*(*n*) in the time domain and *IIR*(*k*) in the frequency domain, it can be expressed as

$$
iir(n) = \frac{IIR(0)}{N} + \frac{1}{N}\sum_{k=1}^{N-1} IIR(k)e^{j(2\pi/N)kn} \tag{5.2}
$$

The offset Δ in the experimental input impulse response is the difference between the experimental input impulse response *iir'*(*n*) and the true input impulse response *iir*(*n*). It can be written as:

$$
\Delta = iir'(n) - iir(n) \tag{5.3}
$$

Substituting equations (5.1) and (5.2) into equation (5.3) yields:

$$\Delta = \left[\frac{IIR'(0)}{N} - \frac{IIR(0)}{N} \right] + \left[\frac{1}{N} \sum_{k=1}^{N-1} IIR'(k) * e^{j(2\pi/N)/kn} - \frac{1}{N} \sum_{k=1}^{N-1} IIR(k) e^{j(2\pi/N)kn} \right] = \Delta_1 + \Delta_2 \quad (5.4)$$

where $\Delta_1 = \frac{IIR'(0)}{N} - \frac{IIR(0)}{N}$ and

$$\Delta_2 = \frac{1}{N} \sum_{k=1}^{N-1} IIR'(k) e^{j(2\pi/N)kn} - \frac{1}{N} \sum_{k=1}^{N-1} IIR(k) e^{j(2\pi/N)kn}$$

Examination of equation 5.4 reveals that the offset in the experimental input impulse response is a result of the incorrect measurement of both constant and sinusoidal components. That is, the total offset Δ is made up of a DC offset Δ_1 and a sinusoidal offset Δ_2.

In the following section, the causes of the DC offset are discussed and possible methods of eliminating them are presented. Then, in section 5.5, the cause of the sinusoidal offset is investigated and a means of preventing the offset is implemented.

5.4 Eliminating the DC offset in the input impulse response

5.4.1 Origin of DC offset

According to Discrete Fourier transform (DFT) theory, for an input vector *x* of length *N*, the DFT is a vector *X* also of length *N* defined by

$$X(k) = \sum_{n=0}^{N-1} x(n) * e^{-j(2\pi/N)kn} \qquad 0 \le k \le N\text{-}1 \qquad (5.5)$$

Therefore, the first elements of the input pulse and the duct reflections in the frequency domain are given respectively by

$$I(0) = \sum_{n=0}^{N-1} i(n) \qquad (5.6)$$

$$R(0) = \sum_{n=0}^{N-1} r(n) \qquad (5.7)$$

where $i(n)$ represents the input pulse and $r(n)$ represents the duct reflections in the time domain. That is, the first element of the input pulse in the frequency domain is the sum over all sample points of the input pulse in the time domain. Similarly, the first element of the duct reflections in the frequency domain is the sum over all sample points of the duct reflections in the time domain.

From equations (4.1a), (5.6) and (5.7)

$$IIR'(0) = \frac{R(0)}{I(0)} = \frac{\sum_{n=0}^{N-1} r(n)}{\sum_{n=0}^{N-1} i(n)} \qquad (5.8)$$

Examination of equation (5.1) reveals that the DC level in the experimental input impulse response depends on *IIR'*(0) which, according to equation (5.8), in turn depends on the sum of over all sample points of the input pulse and reflections in the time domain. To eliminate DC offset from the experimentally measured input impulse response, any DC offset in the input pulse and duct reflections must be prevented from occurring.

5.4.2 Eliminating the DC offset in the input pulse and reflections

Figure 5.3 shows a typical input pulse measured on a pulse reflectometer. The inset shows the first 6 milliseconds of the pulse in detail. A small DC offset of approximately 5 mV is clearly visible. The most likely cause of this offset is a slight inaccuracy in the calibration of the data acquisition card, which contains the D/A and A/D converters[Fincham 1985]. Any DC offset introduced by the data acquisition card can be removed by performing two reflectometry measurements. In the first measurement, a positive electrical pulse is used to drive the loudspeaker. The resultant positive pressure pulse (Figure 5.3) is recorded by the microphone. In the second measurement, a negative electrical pulse is used to drive the loudspeaker. This time a negative pressure pulse (Figure 5.4) is produced and is recorded by the microphone. Again a systematic DC offset of approximately 5 mV is visible. The negative pressure pulse is then inverted (Figure 5.5) and the DC offset becomes –5 mV. Averaging the inverted pulse of Figure 5.5 with the pulse of Figure 5.3 gives a pulse with no DC offset (Figure 5.6).

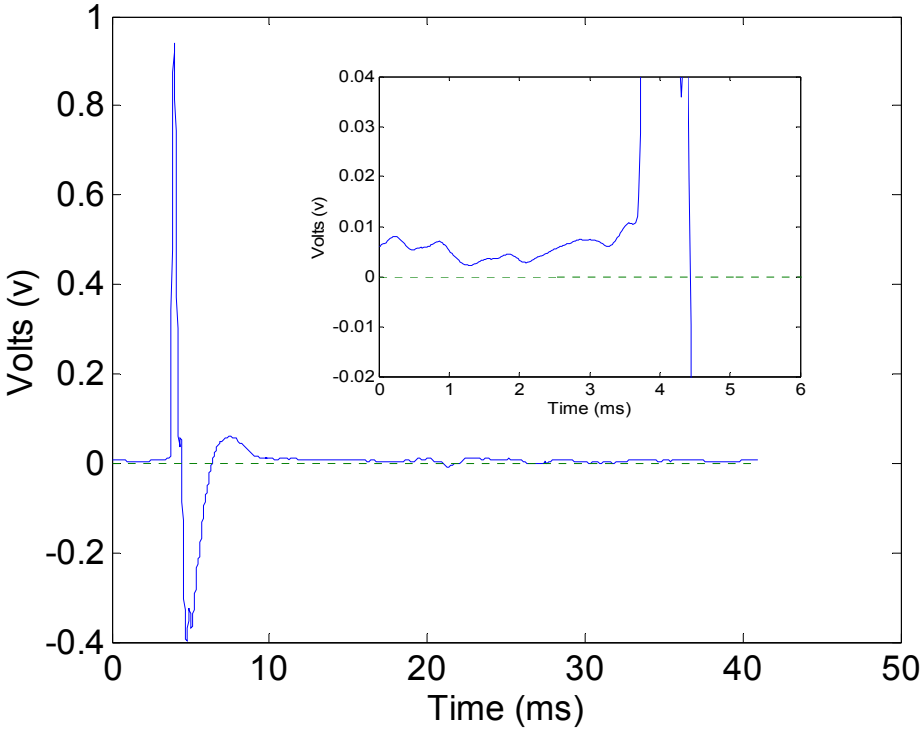

Figure 5.3: The positive input pulse

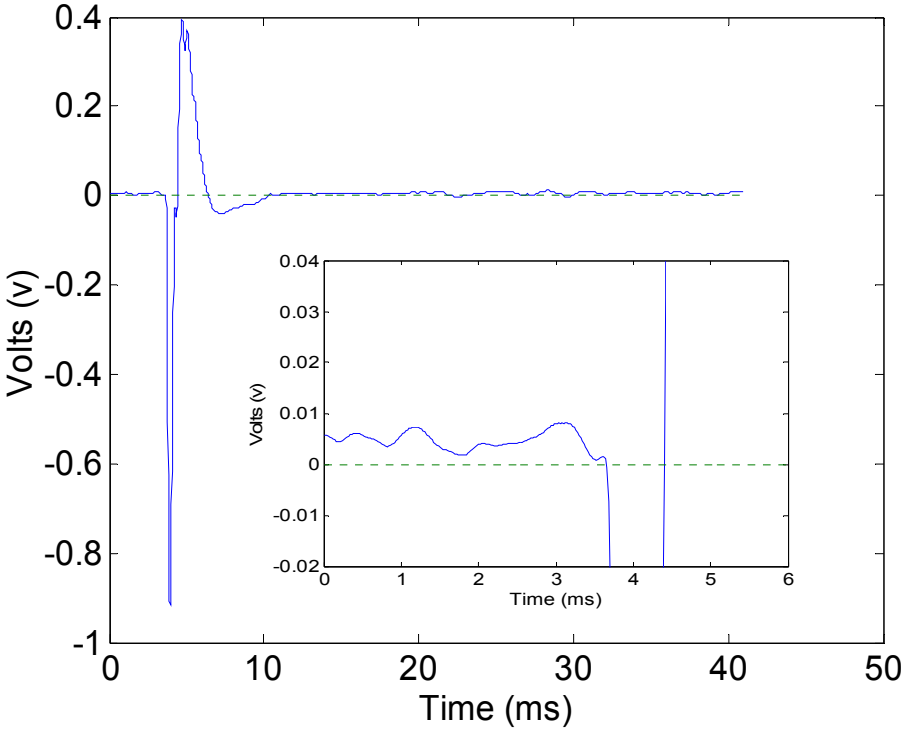

Figure 5.4: The negative pulse

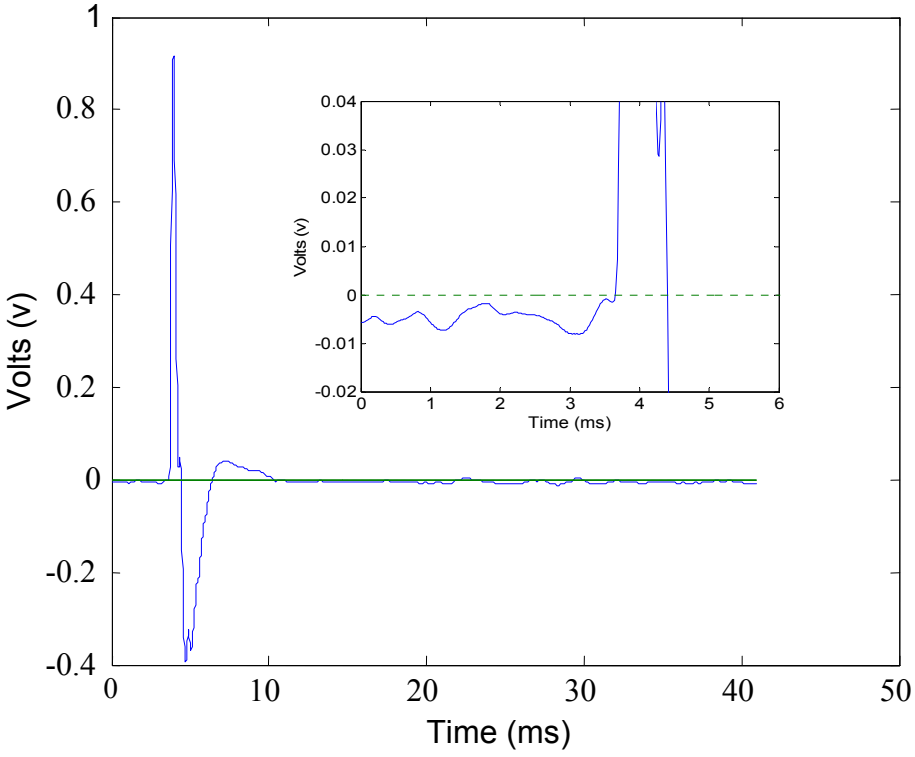

Figure 5.5: Inverted input pulse

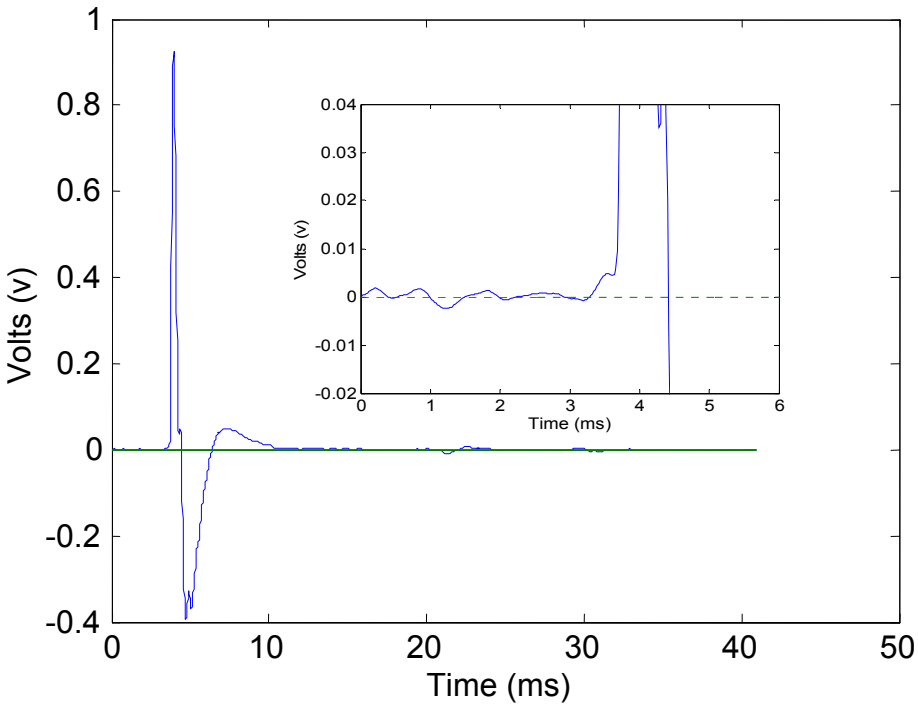

Figure 5.6: Input pulse without DC offset

Figures 5.7 and 5.8 show the reflections, which return from the 310 mm long stepped tube described in chapter 4 when positive and negative electrical pulses are used to drive the loudspeaker. Figure 5.9 shows the result of averaging the signals of Figures 5.7 and 5.8. Again, the averaged reflections have no DC offset.

By alternating the pulse polarity in this way, it is possible to obtain measurements of both the input pulse and the duct reflections with no DC offset. However, when such measurements are used to calculate an impulse response, the response generally still contains a DC offset. Figure 5.10 shows the impulse response calculated from the input pulse and stepped tube reflections of Figures 5.7 and 5.9. The impulse response can be seen to contain a DC offset. The cause of the DC offset in the calculated input impulse response is investigated in the next section.

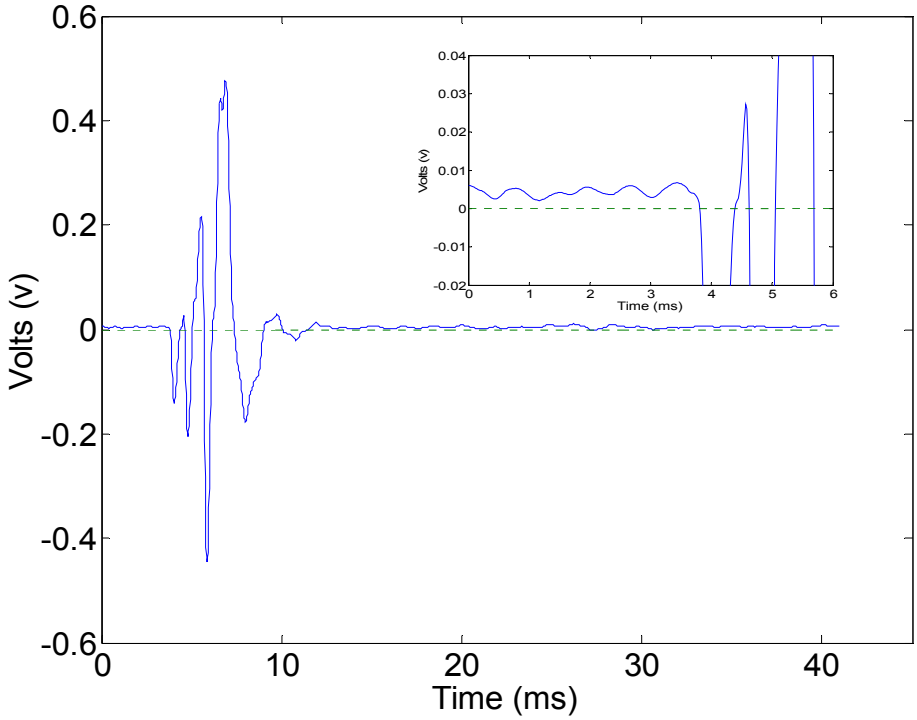

Figure 5.7: Reflections from stepped tube

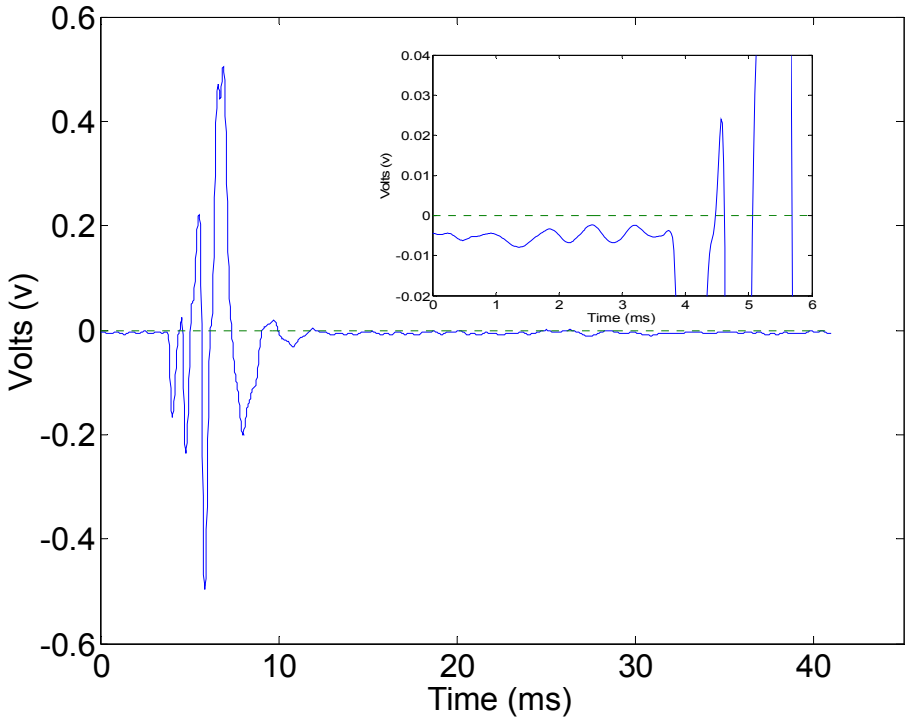

Figure 5.8: Inverted reflections from stepped tube

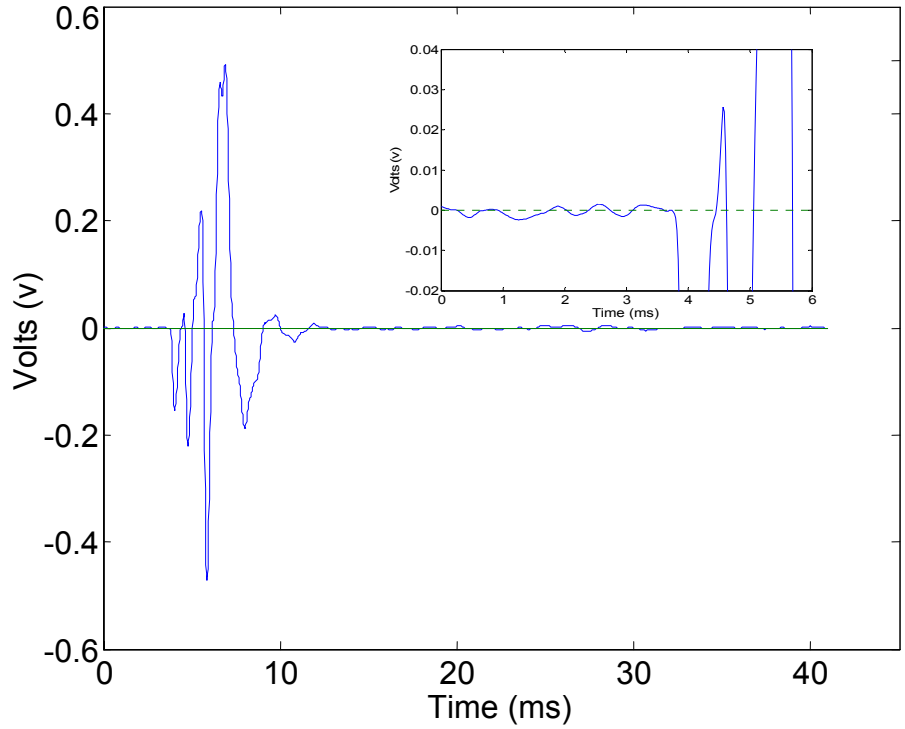

Figure 5.9: Stepped tube reflections without DC offset

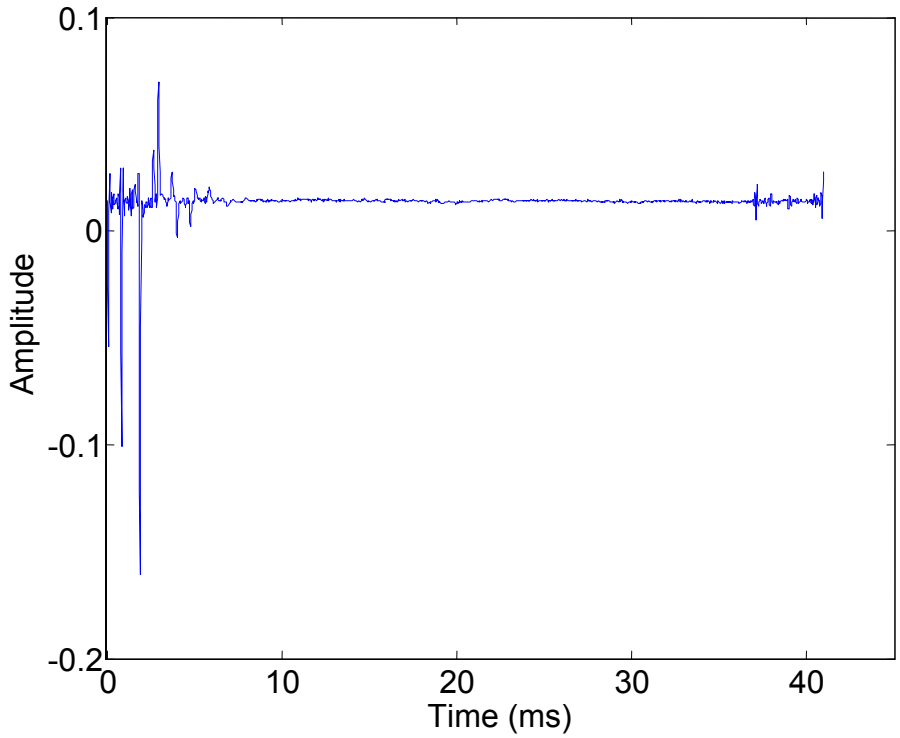

Figure 5.10: Stepped tube input impulse response

5.4.3 Generating a pulse with greater polarity

From equation (5.4) it can be seen that the offset Δ_1 depends on *IIR'*(0) which, according to equation (5.8), is equal to the sum of all the sample points which make up the duct reflections divided by the sum of all the sample points which make up the input pulse (all in the time domain). Close examination of Figures 5.6 and 5.9 reveals that neither the input pulse nor the duct reflections exhibit strong polarity. That is, the sum of the sample points which make up the input pulse and the sum of the sample points which make up the duct reflections are both close to zero. Consequently, the calculation of *IIR'*(0*)* can result in a division by zero or near-zero causing numerical instability[Marshall 1990]. The incorrect evaluation of *IIR'*(0), is the cause of the DC offset in the input impulse response.

If an input pulse of greater polarity could be produced, the duct reflections resulting from using such an input pulse would also show a greater degree of polarity. Thus division by zero problems would be removed allowing the DC level, *IIR'*(0), to be accurately determined and input impulse responses to be measured with no DC offset [Li et al. 2002].

5.4.3.1 The 'step method'

Various methods have been used to produce impulse-like pressure pulses. For example, [Jackson et al. 1977] used spark discharges while [Watson and Bowsher 1988], [Sondhi and Resnick 1983] and others used a loudspeaker driven by short delta-like electrical pulses. Another method of producing short duration polar pressure pulses, named the 'step method', is described by Marshall [Marshall 1992]. As name suggests, the excitation sent to the loudspeaker is a step voltage. The motivation for Marshall's work was to remove the deconvolution stage required to determine the impulse response. In a similar manner,

[Fredberg et al. 1980] used a ‘ double pulse ’ excitation of a loudspeaker, consisting of equal-amplitude 200 μs and 150 μs pulses, separated by 150 μs.

In this section, Marshall’s method is adopted in an attempt to produce a more polarised input pulse. For a square electrical driving signal, the response of a loudspeaker takes the form of a damped sinusoid $P(t) = Ae^{-\alpha t}\sin\omega t$, where A is the amplitude, ω is the angular frequency and α is the damping coefficient. If, for instance, A = 0.78, α = 250, and ω = 200 rad s^{-1} (giving a period of $T = 2\pi/\omega = 0.0314$ s), the damped sinusoid will take the form shown in Figure 5.11. This is very similar to the input pulse shape in the present study (Figure 4.5). To create a more polarised pulse, it is necessary to isolate the first cycle of the damped sinusoid. Suppose that at time $t = T/2$ an additional step of relative amplitude $\exp^{-\alpha t}$ is applied. Assuming that the loudspeaker behaves linearly, the response to the additional step will be exactly out of phase with the response to the original step. From time t, the two responses will cancel out, leaving only the first half cycle of the response to the first step. The stepped electrical driving signal is shown in Figure 5.12, the two responses to the two steps of the driving signal are shown in Figure 5.13 and the ideal polar pressure pulse remaining after the cancellation of the two responses is shown in Figure 5.14.

In the present study, a number of different combinations of stepped electrical signals (with different amplitudes of electrical (square) pulses and different time intervals between the electrical pulses) were used to drive the compression driver. The most polar acoustic pressure pulse achieved is shown in Figure 5.15. Partial cancellation has resulted in the negative part being reduced from -0.4 V to -0.2 V. Only a partial cancellation was achieved as the step response of the transducer is not an ideal damped sinusoid. It does not have a simple exponential decay. Therefore, although a complete cancellation is theoretically possible, it proved impossible to achieve in practice.

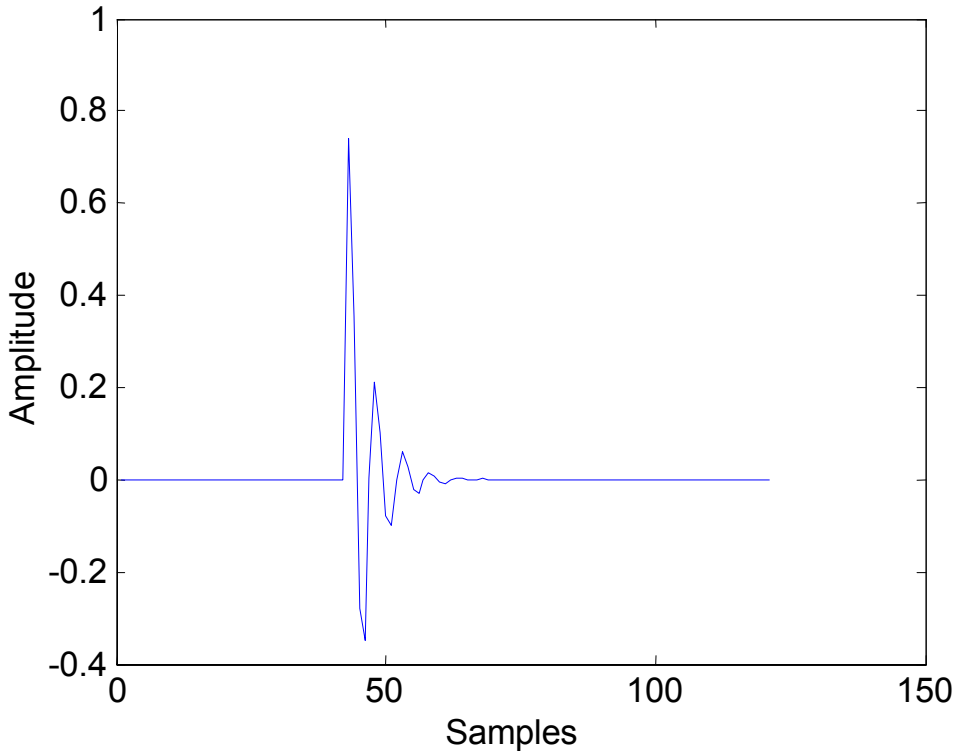

Figure 5.11: Damped Sinusoidal

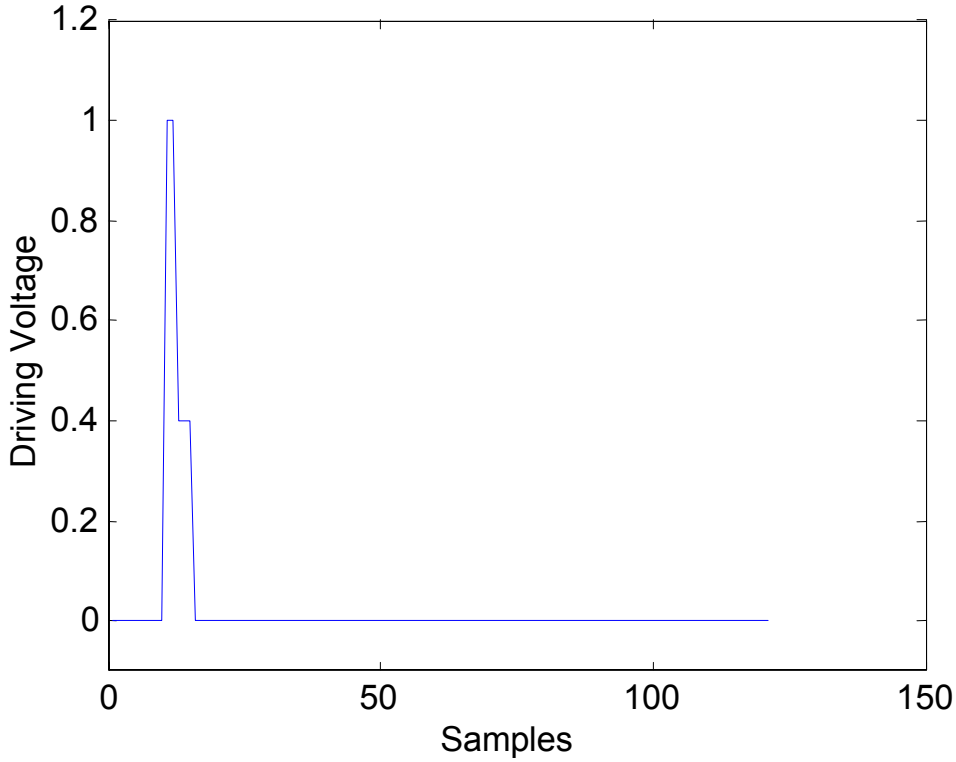

Figure 5.12: Stepped electrical driving signal

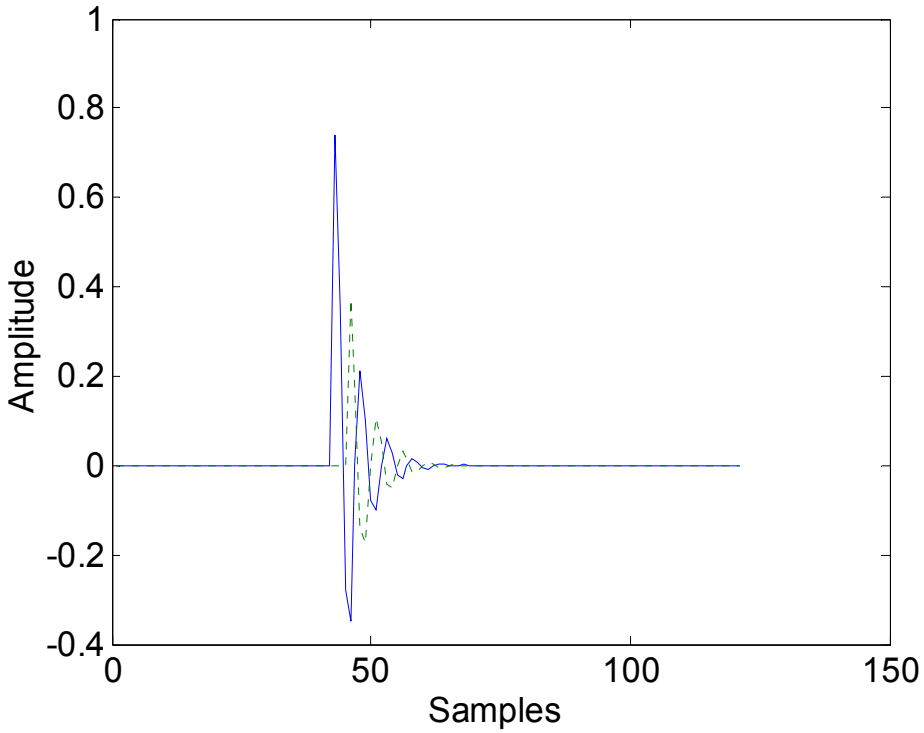

Figure 5.13: Theoretical responses to two steps of electrical driving signal

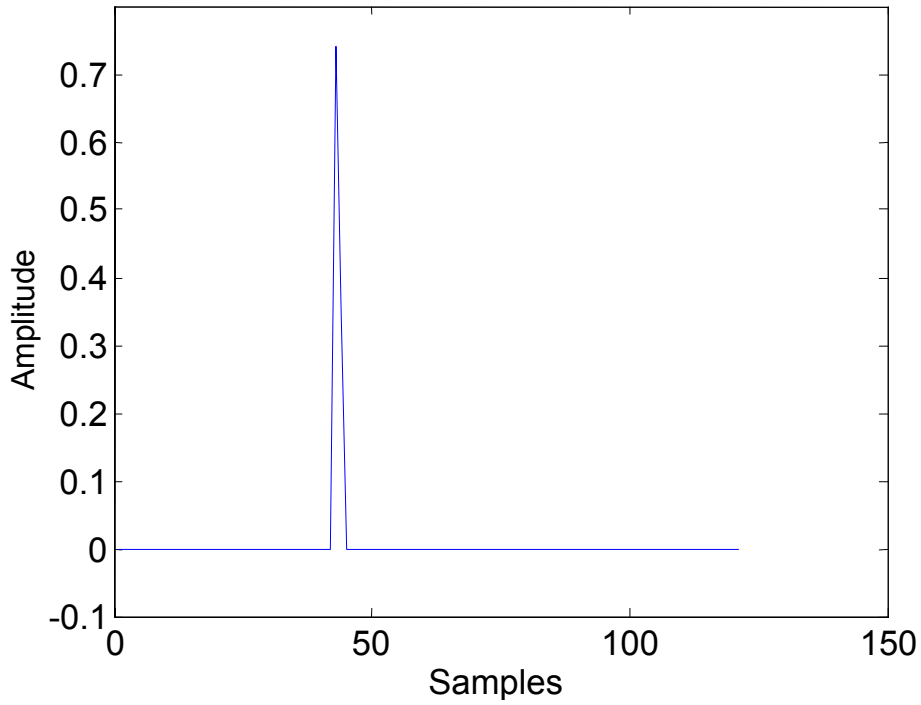

Figure 5.14: Ideal polarised pressure pulse

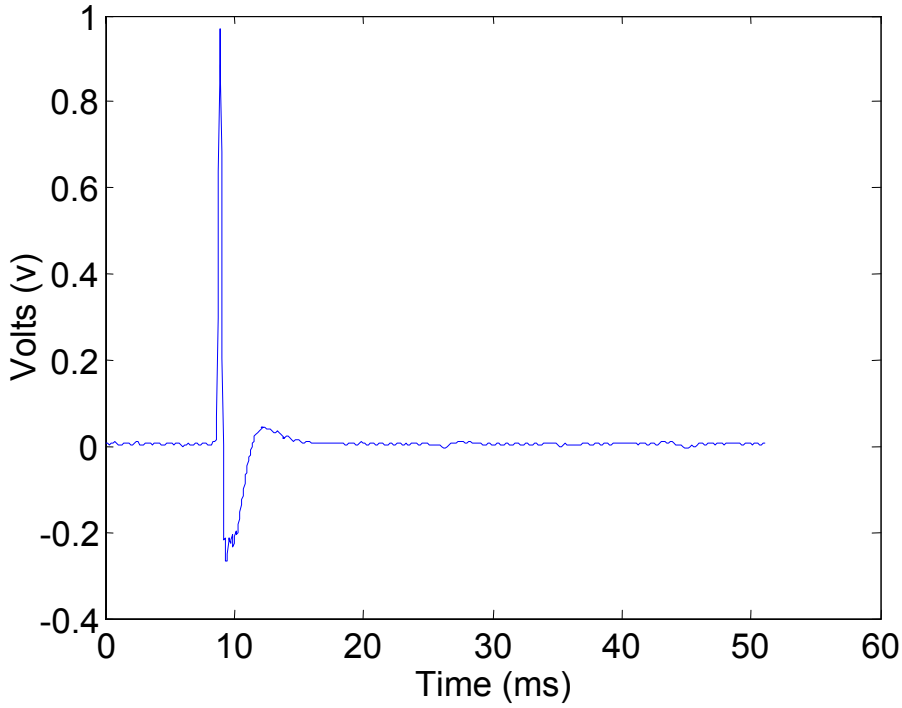

Figure 5.15: Input pulse using step method

5.4.3.2 Inverse filter method

In principle, the reflectometer (loudspeaker, coupler, source tube, microphone etc.) can be treated as a linear system. Therefore, a filter $h(t)$, representing the impulse response of this system, can be defined which describes the relationship between the electrical pulse $v(t)$ sent to the speaker and the pressure pulse $p(t)$ measured by the microphone. This relationship is shown schematically in Figure 5.16.

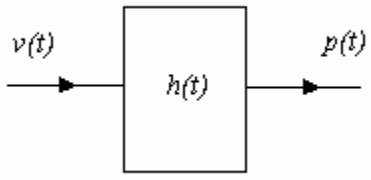

Figure 5.16: Schematic describing relationship between electrical pulse v(t) and pressure pulse p(t)

The relationship can be expressed using equation

$$p(t) = v(t) \otimes h(t) \tag{5.9}$$

where the symbol $\otimes$ denotes convolution.

In theory, this relationship can be used to determine the electrical driving signal necessary to produce a more polarised pressure pulse.

First of all the filter $h(t)$ of the system is calculated. A 100 μs square electrical pulse is sent to the loudspeaker and the resultant pressure pulse (Figure 5.17) is recorded by the microphone and stored on the computer (1024 sample points are captured). A sampling frequency of 20 kHz is used because the maximum bandwidth of signal encountered in this study is approximately 10 kHz. According to equation (5.9), the filter $h(t)$, representing the impulse response of the system (i.e. coupler, speaker, source tube and microphone), is obtained by deconvolving the recorded pulse with the electrical signal. The calculation is carried out by performing a division in the frequency domain. Then, the desired polarised pulse (the initial positive part of Figure 5.17) is selected by setting the typical pulse to zeros after the main peak. To avoid discontinuity, the desired polarised pulse is convolved with a Gaussian window function of the same 1024 point sample length. It is shown in Figure 5.18. The electrical driving waveform needed to produce this more polarised pulse is determined by deconvolving the desired pressure pulse with the filter $h(t)$. The required driving electrical waveform (with DC level removed) is shown in Figure 5.19.

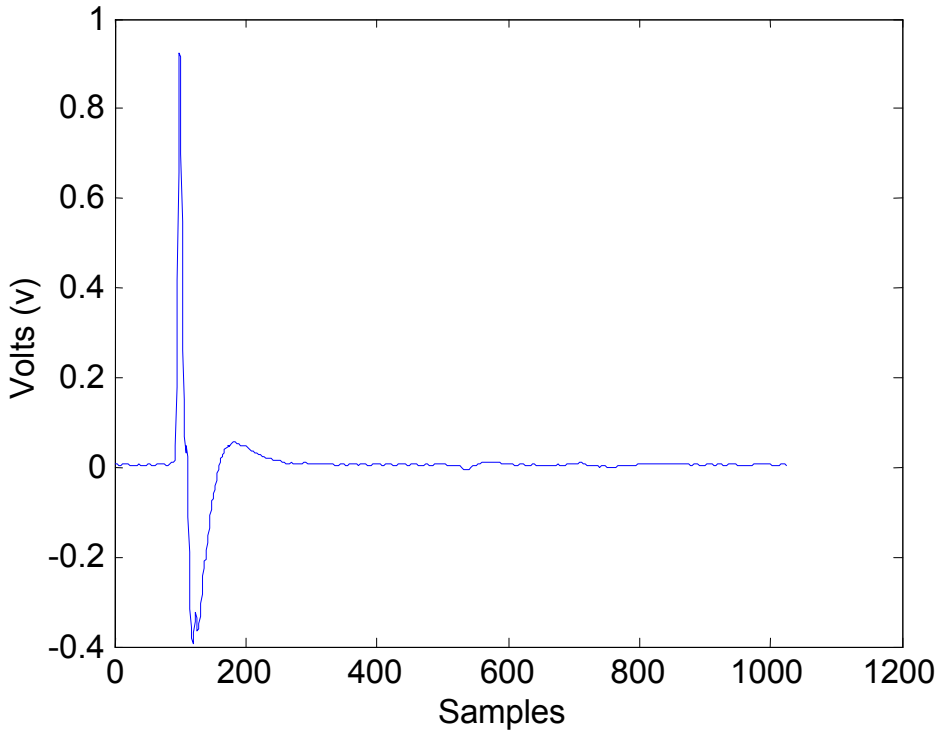

Figure 5.17: Pressure pulse generated by 100µs square electrical pulse

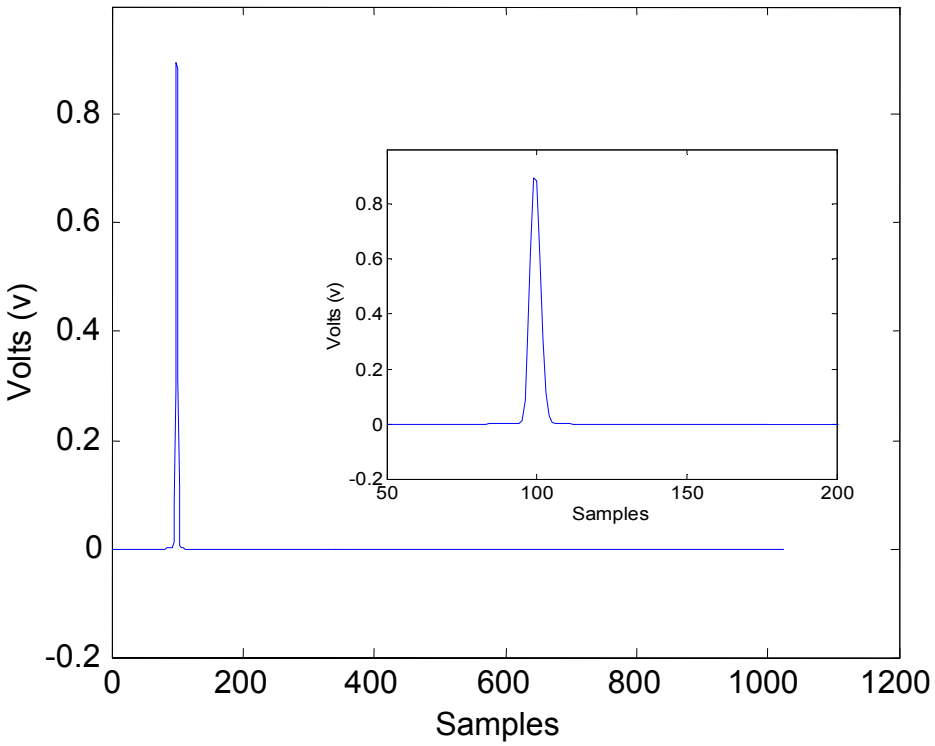

Figure 5.18: Desired polar pulse

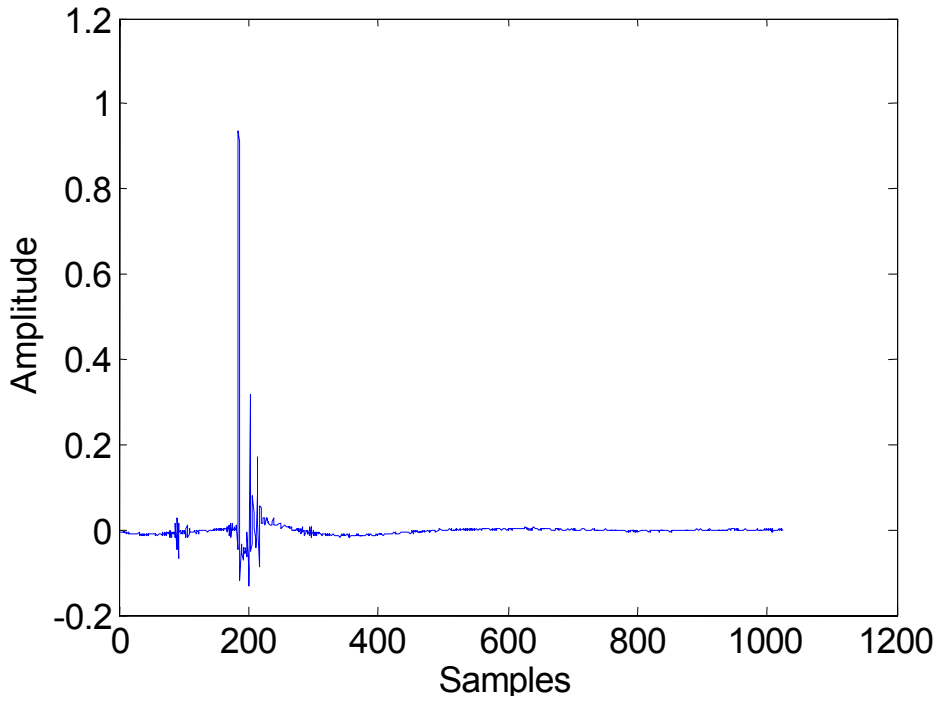

Figure 5.19: Calculated electrical driving signal

Figure 5.20 shows the pressure pulse produced when the electrical signal of Figure 5.19 is used to drive the loudspeaker. The input pulse looks similar to the pulse shown in Figure 5.15 with again the negative part being only partly reduced in amplitude. Like the step method, the 'inverse filter' is only partly successful in producing a more polarised pulse.

Neither of the methods has been successful in producing a polar pressure pulse. It is impossible using the present set-up to provide a significant frequency response down to DC. Therefore, instead of preventing the DC offset from occurring in the input impulse response it must be removed by calibration.

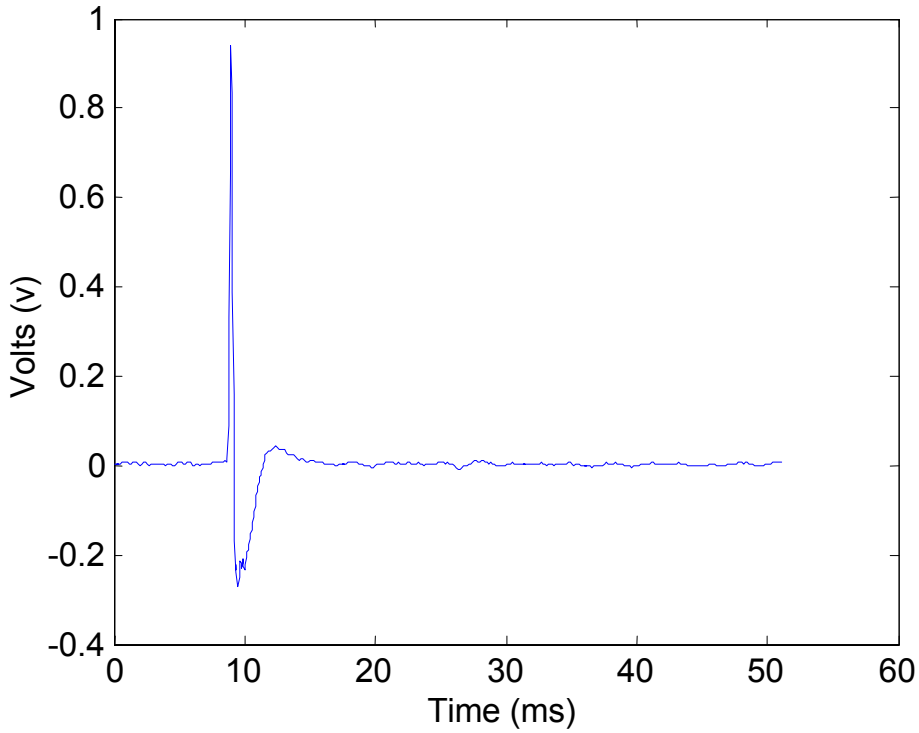

Figure 5.20: Input pulse using filter method

5.4.4 DC tube method

The methods reported in sections 5.42 and 5.43 proved unsuccessful in preventing a DC offset from occurring in the experimentally measured input impulse response. In this section and in section 5.4.5, two methods of removing the DC offset are outlined. Assuming the sinusoidal components of the input impulse response have been accurately measured (i.e. Δ_2 of equation 5.4 is zero), these two methods should enable accurate reconstructions to be calculated.

The DC offset present in an experimentally measured input impulse response can be determined and removed by inserting a 50 cm long cylindrical tube between the source tube and the duct under test prior to the measurement (Figure 5.21). The internal diameter of the DC tube should be similar to that of the source tube. In the present study, a DC tube

of diameter 9.5 mm was used whilst the source tube had a diameter of 10.2 mm. The reflectometer measurement is then carried out in the same way as described previously (chapter 4). However, since there should be no signal reflected back from the DC tube, it can be deduced that approximately the first three milliseconds of the input impulse response should be zero. In principle, therefore, finding the average value over the first three milliseconds of the measured input impulse response should give the DC offset. This value can then be subtracted from the whole input impulse response. In practice, however, there is always a small discontinuity at the start of the DC tube due to the coupling of the source tube to the DC tube. To overcome this, the DC value is actually calculated by finding the average value over the second millisecond of the input impulse response and then the first millisecond of the input impulse response is set to zero [Sharp and Campbell 1997]. Figure 5.22 shows the input impulse response of the stepped tube and the DC tube after the DC offset has been removed using the 'DC tube' method.

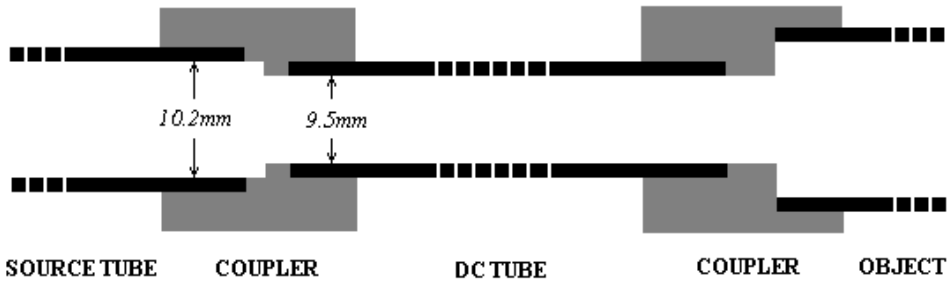

Figure 5.21: DC tube method

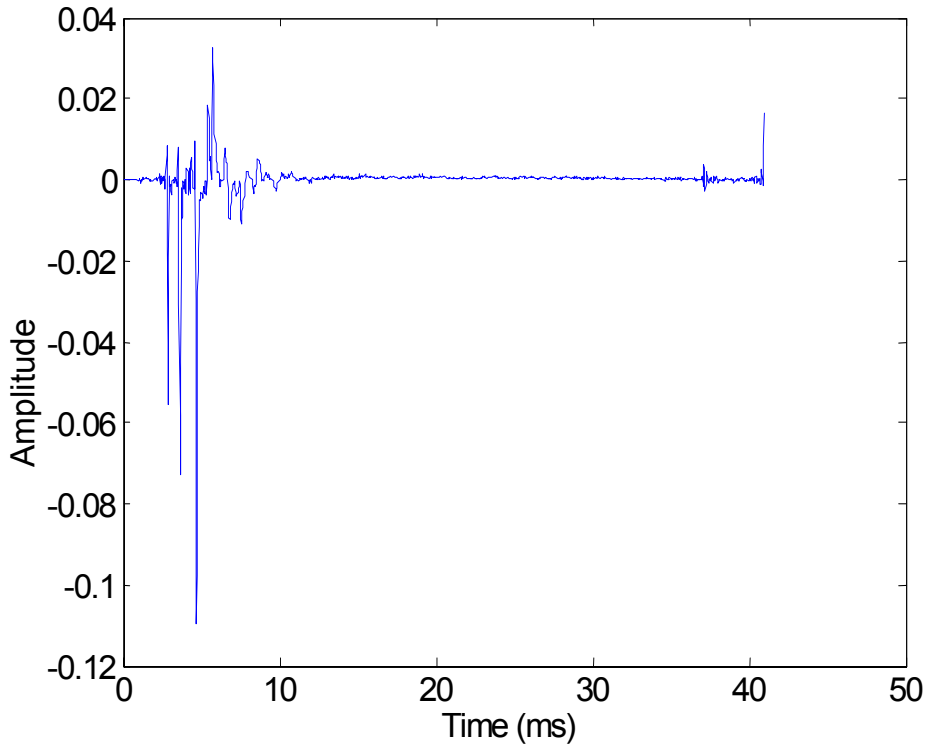

Figure 5.22: Stepped tube input impulse response with DC offset removed

Figure 5.23 shows the calculated stepped tube and the DC tube profile resulting from applying the reconstruction algorithm to the input impulse response of Figure 5.22. The first 0.5 m of the reconstruction is the 'DC tube'. It can be seen that, although the first section of the stepped tube has been accurately reconstructed, the radius of the second section decreases with distance when compared with the direct measurement shown by the dotted line. The reason for this is that although the DC offset Δ_1 has been removed, there is still a sinusoidal error Δ_2 present in the input impulse response.

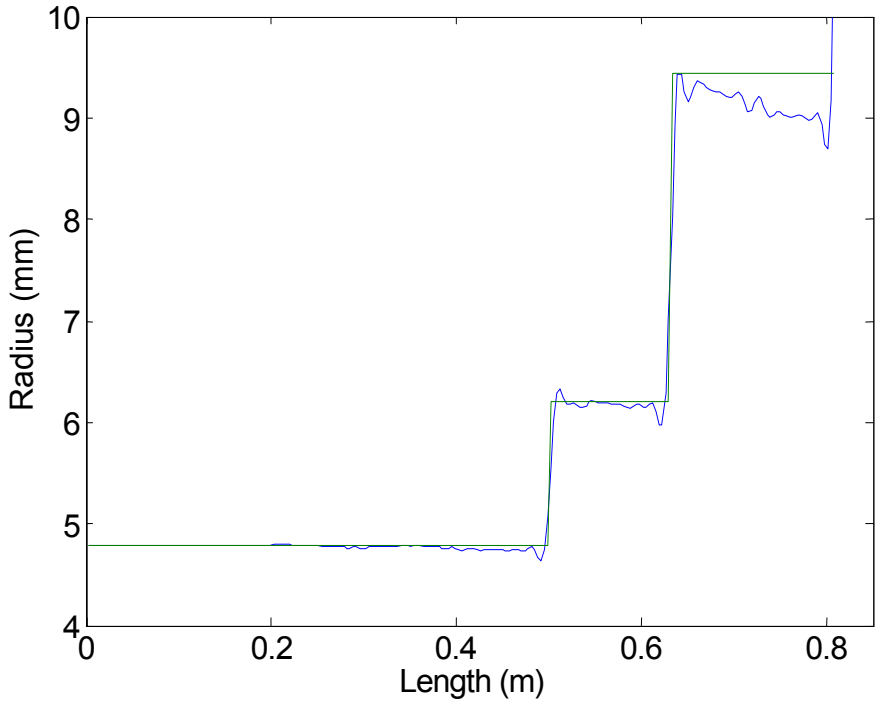

Figure 5.23: Reconstruction of stepped tube and DC tube

5.4.5 Virtual DC tube

The virtual DC tube method [Kemp et al. 2001] is a variation of the DC tube method. Signal processing methods are employed which enable part of the source tube to be used as the 'DC tube'. In this method, the reflections of the test object are recorded 3 ms earlier than the input pulse. The input pulse is then deconvolved with a filter representing the losses that would be experienced by the signal if it had travelled for an extra 3 ms within the source tube. Therefore, the input pulse and reflections of the test object experience the same losses travelling inside the source tube. The reconstruction obtained using this method is the much the same as that using DC tube method (shown in Figure 5.23). However, it has the advantage of eliminating the small discontinuity at the join between the DC tube and the source tube.

5.4.6 Known termination of test object

If the termination of the tubular object under investigation is known (e.g. the object has an open end or it is closed by a rigid termination), the value of *IIR'*(0*)* in the experimental input impulse response can be replaced by the true value *IIR*(0*)*. For instance, *IIR*(0) = -1 for an open end termination. If this value is used to replace *IIR'*(0) in the experimental input impulse response, there should no longer be a DC offset Δ_1. Figure 5.24 shows the reconstruction of the stepped tube (with an open ended termination) when *IIR'*(0) has been set to –1 in the input impulse response. Clearly the radius of the reconstructed stepped tube is still lacking in accuracy. Although the DC offset has been removed from the input impulse response there is still a sinusoidal offset present. To obtain an accurate reconstruction, this sinusoidal offset Δ_2 must be eliminated. A method to eliminate the sinusoidal error is described in following section[Li et al. 2002].

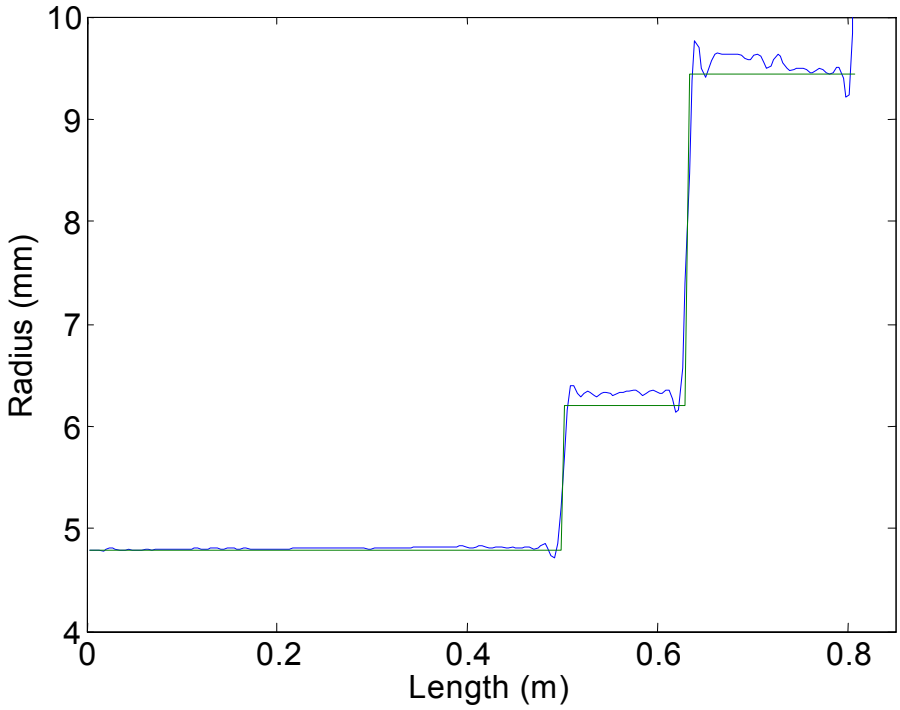

Figure 5.24: The reconstruction of stepped tube with known termination

5.5 Eliminating sinusoidal error in the input impulse response

The 'DC tube' method of DC offset removal works on the assumption that all the sinusoidal components that make up the input impulse response are calculated correctly. This is not always the case. For example, Figure 5.25 shows an experimentally measured input impulse response spectrum for the stepped tube at frequencies between 0 Hz and 1000 Hz, when a sampling frequency of 50 kHz is used. Since $IIR'(\omega)$ is a reflection coefficient, its amplitude should not exceed 1 at any frequency. However, examination of Figure 5.25 reveals that the amplitude of measured $IIR'(\omega)$ is greater than 1 at frequencies of 25 Hz and 50 Hz. This incorrect evaluation is due to the poor response of the compression driver loudspeaker at low frequencies.

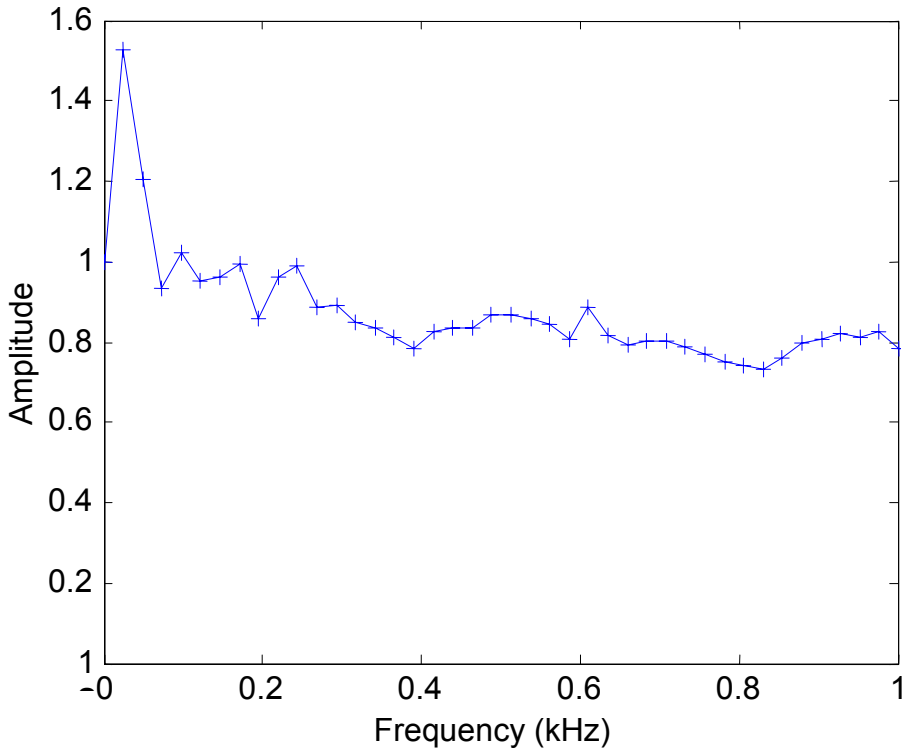

Figure 5.25: Spectrum of input impulse response of stepped tube

To improve the low frequency content of the input impulse response spectrum, a second set of reflectometry measurements are made, this time using a bass loudspeaker with a good response at low frequencies. Again, a sampling frequency of 50 kHz is used. Figure 5.26 shows the experimental input impulse response spectrum of the stepped tube at frequencies between 0 Hz and 1000 Hz measured using the bass loudspeaker. It is clear that below 200 Hz (excluding 0 Hz), $IIR'(\omega)$ remains less than 1. By combining the components of $IIR'(\omega)$ between 0 Hz and 170 Hz measured using the bass loudspeaker with the components between 170 Hz and 25 kHz measured using the compression driver, a combined input impulse response spectrum of the stepped tube can be constructed (see Figure 5.27).

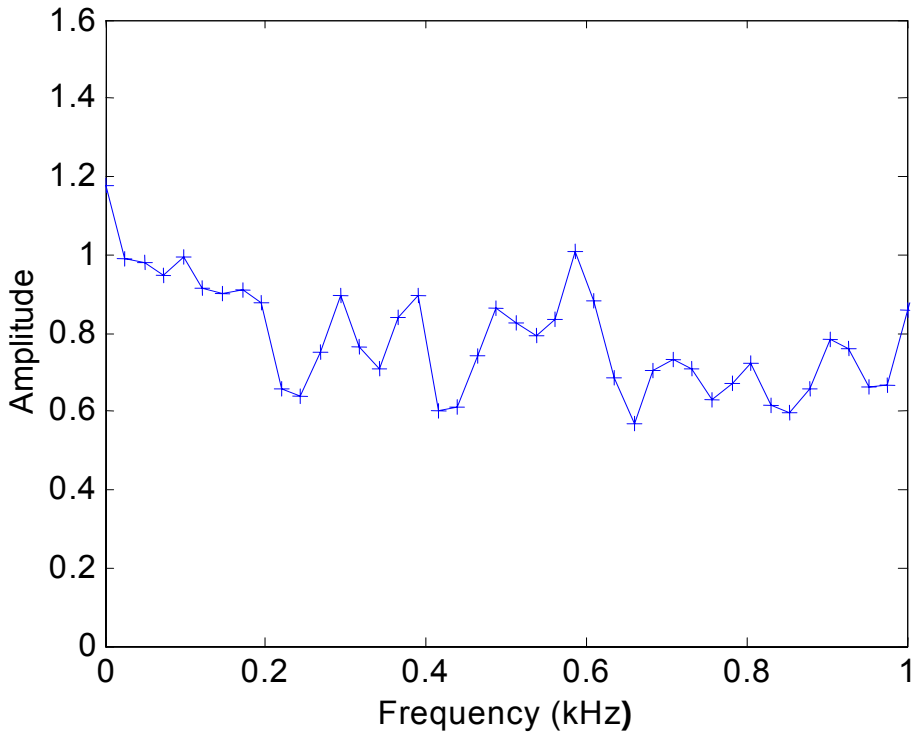

Figure 5.26: Input impulse response spectrum using bass speaker

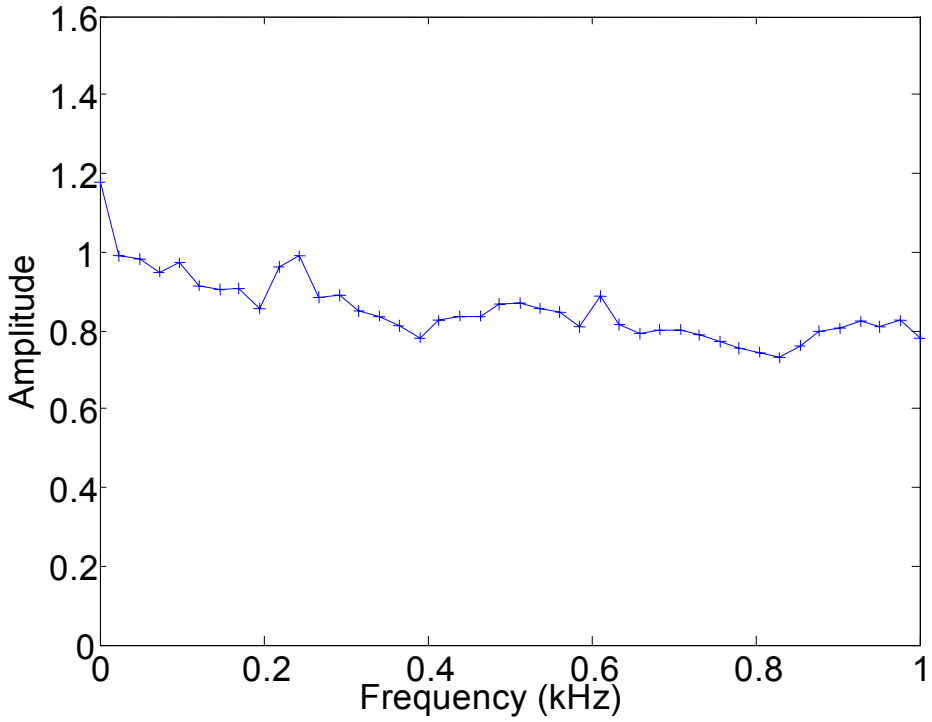

Figure 5.27: Combined spectrum of input impulse response of stepped tube

Figure 5.28 shows the calculated duct profile resulting from applying the reconstruction algorithm to the combined input impulse response of Figure 5.27 (again, after implementing the 'DC tube' method). The radii of each of the cylindrical sections of the stepped tube now remain constant with distance and show a good agreement with the values measured directly with calipers.

After the low frequency content has been improved, there is only a DC offset Δ_1 present in the input impulse response. If the end conditions of the test object are known, this DC offset can be eliminated by setting *IIR'*(0) (the 0 Hz value of the experimental input impulse response) to the true value *IIR*(0). This has the effect of removing the DC offset from the experimental input impulse response obtained using the reflectometer. For example, Figure 5.29 shows the reconstruction of the open-ended stepped tube calculated from the combined input impulse response of Figure 5.27 when *IIR'*(0) is set to –1.

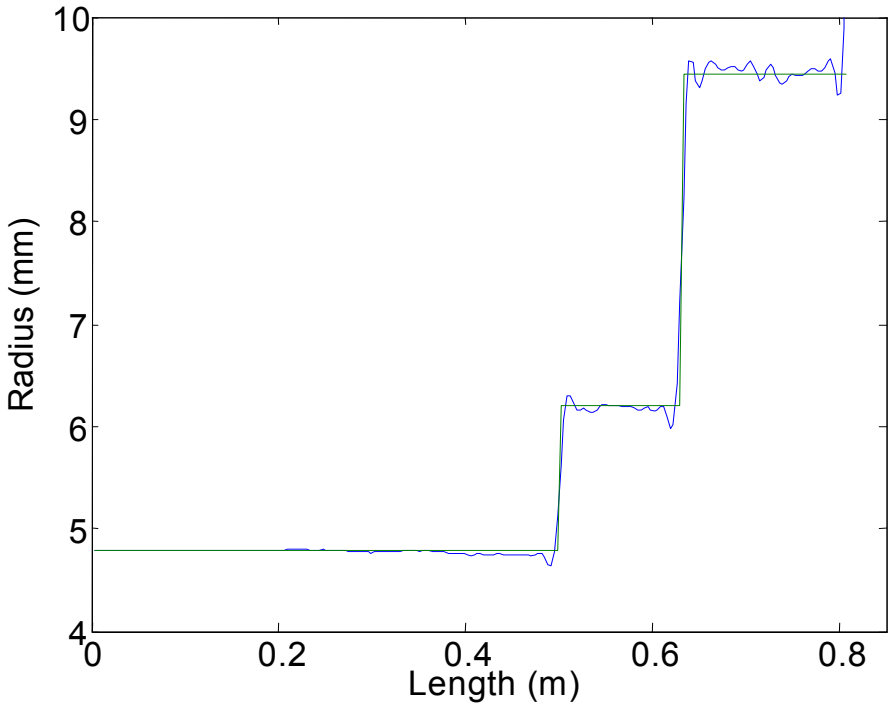

Figure 5.28: Reconstruction using combined input impulse response (using DC tube method)

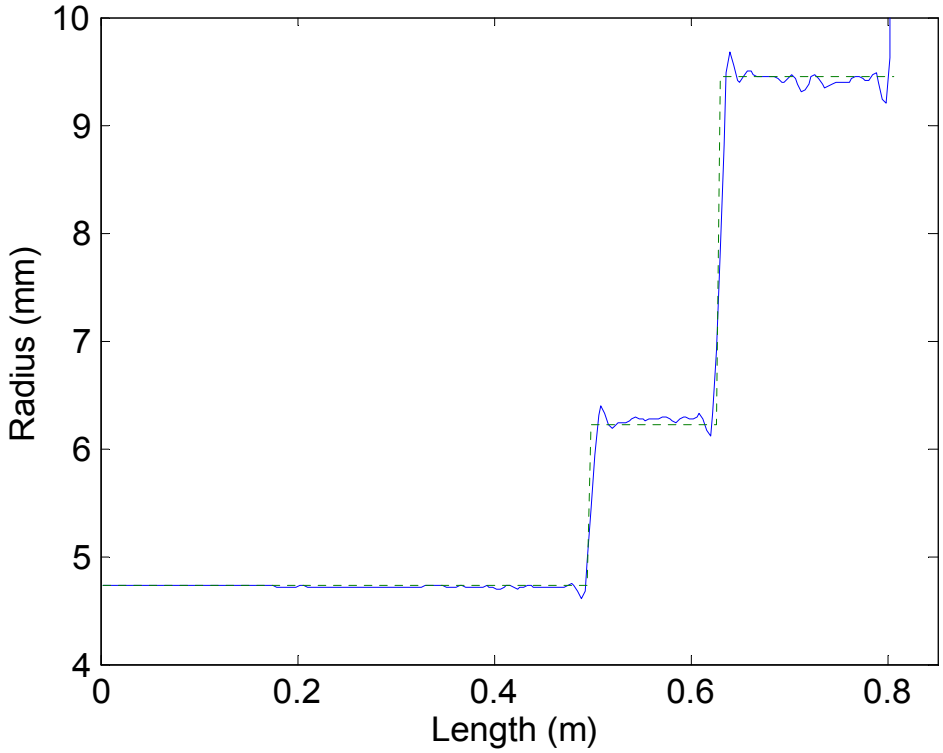

Figure 5.29: Reconstruction using combined input impulse response (using theoretical DC level)

5.6 Conclusions

In conclusion, the offset in acoustic pulse reflectometry measurements of input impulse response is made up of two elements; a DC component and sinusoidal components. After improving the low frequency content of the input pulse, the offset caused by sinusoidal components is eliminated. Then the 'DC tube' method can be used to remove the DC offset from the input impulse response measurements. The input impulse response with improved low frequency content yields an accurate bore reconstruction. Alternatively, for an object whose end conditions are known, the DC offset can be prevented by simply replacing the DC level of the experimental input impulse response with a known theoretical value. In the following chapter, a number of stepped tubes are measured and analysed. The bore profiles of the stepped tubes calculated from input impulse response measurements with improved low frequency content are presented.

Chapter 6

Bore reconstruction after low frequency improvement of the input impulse response

6.1 Introduction

In the previous chapter it was shown that improving the low frequency content (including the DC component) of input impulse response measurements results in more accurate bore reconstructions. In this chapter, the accuracy and consistency of such bore reconstructions are explored through measurements on a number of stepped tubes.

6.2 Test object measurements

Three stepped tubes, each consisting of two cylindrical sections, were used to investigate the improved accuracy of the reflectometry bore reconstructions. Details of the geometries of the three stepped tubes are given in Table 6.1, where the quoted radii were measured using calipers to a precision of 0.02 mm. Six couplers were produced so that each stepped tube could be coupled to the source tube (or, to be more precisely, to the DC tube) in two different ways; either with section I connected or with section II connected. The three stepped tubes and the six couplers are shown in Figure 6.1.

Test object	Section I		Section II	
	Radius (mm)	Length (m)	Radius (mm)	Length (m)
stepped tube A	2.25	0.15	3.55	0.15
stepped tube B	3.55	0.15	5.58	0.15
stepped tube C	5.58	0.15	8.78	0.15

Table 6.1: Dimensions of the stepped tubes

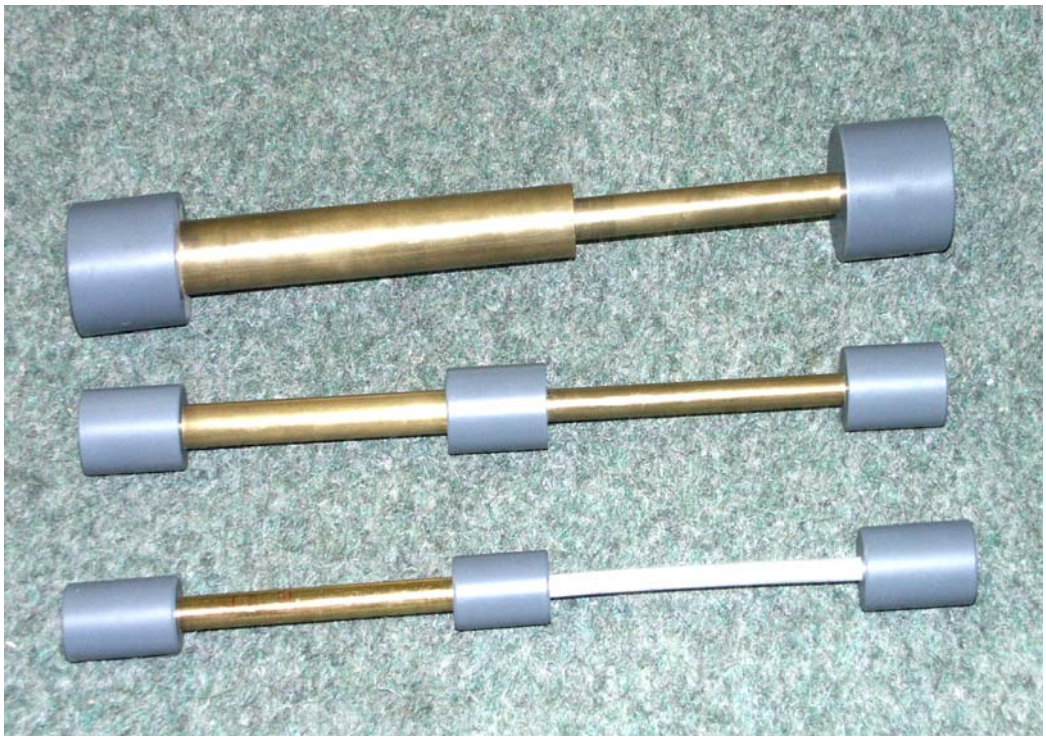

Figure 6.1: Stepped tubes and couplers

Using the reflectometer and the technique described in chapter 4 (referred to from now on as the standard reflectometry technique), the input impulse responses of the stepped tubes in both orientations were measured. The layer peeling algorithm was then applied to each input impulse response to yield six bore reconstructions (two for each stepped tube). The low frequency content of the six stepped tube input impulse responses was then improved by carrying out further measurements in the manner described in section 5.5. Following this, the layer peeling algorithm was reapplied to each of the input impulse responses to yield six improved bore reconstructions.

Figures 6.2 to 6.7 show bore reconstructions for the three stepped tubes in each of their orientations (the first 0.5 m of each reconstruction is the DC tube). In each figure, the dashed line is the reconstruction made using the standard reflectometry technique while the solid line is the reconstruction produced once the low frequency content of the input impulse response had been improved. The horizontal dotted lines show the actual radii of sections I and II of the stepped tubes as detailed in Table 6.1.

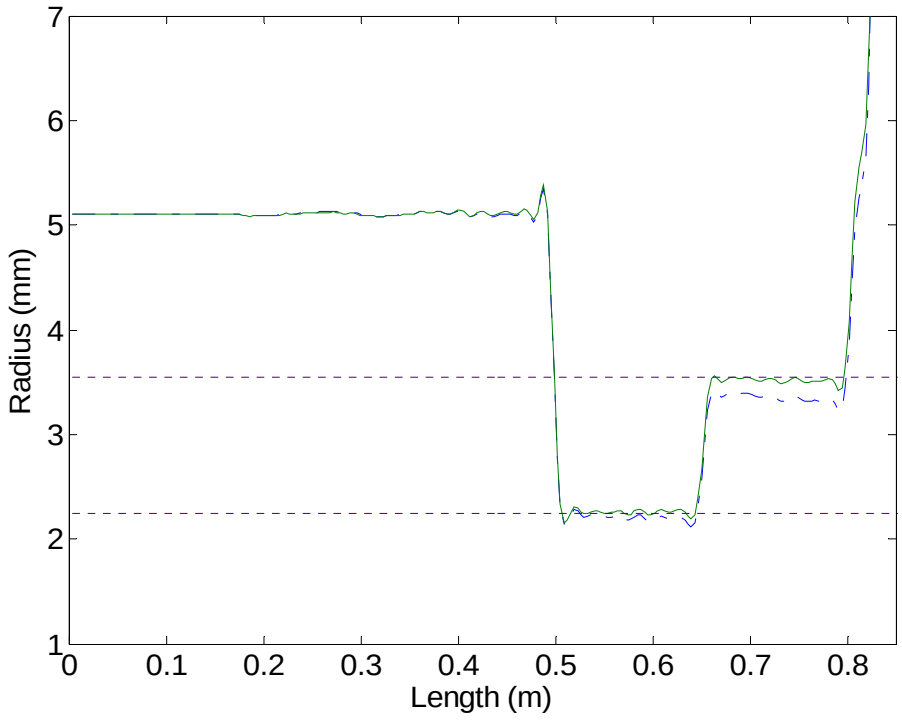

Figure 6.2: Bore reconstructions of stepped tube A (Section I coupled)

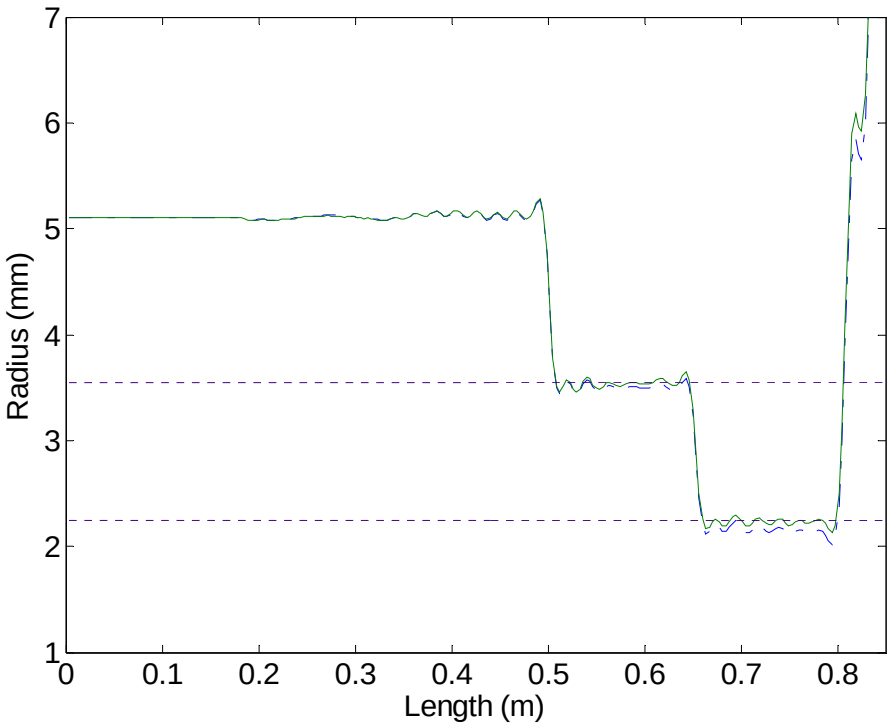

Figure 6.3: Bore reconstructions of stepped tube A (Section II coupled)

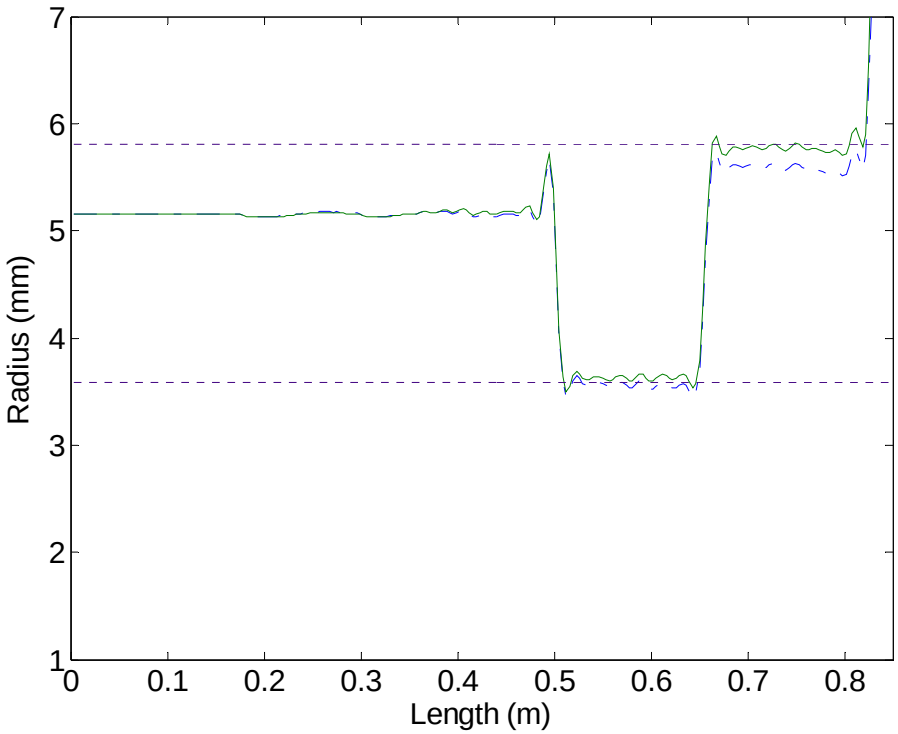

Figure 6.4: Bore reconstructions of stepped tube B (Section I coupled)

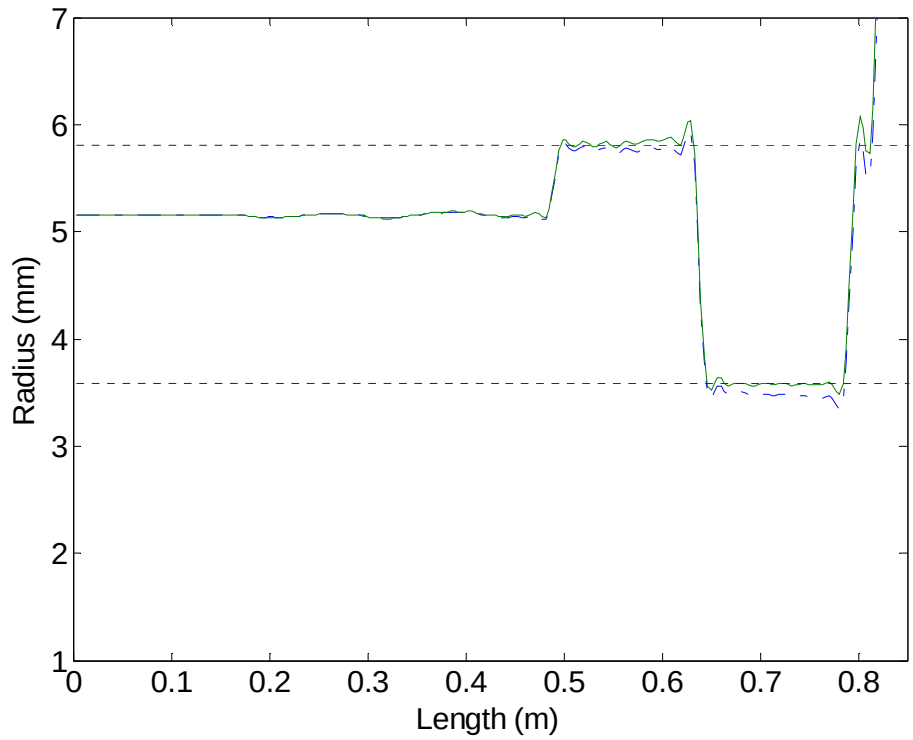

Figure 6.5: Bore reconstructions of stepped tube B (Section II coupled)

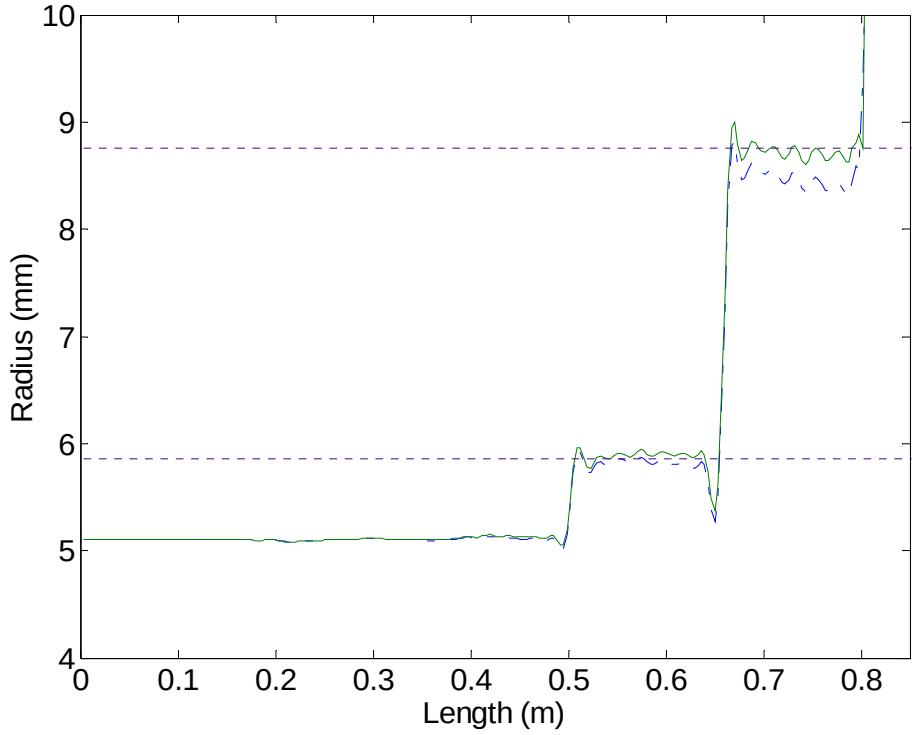

Figure 6.6: Bore reconstructions of stepped tube C (Section I coupled)

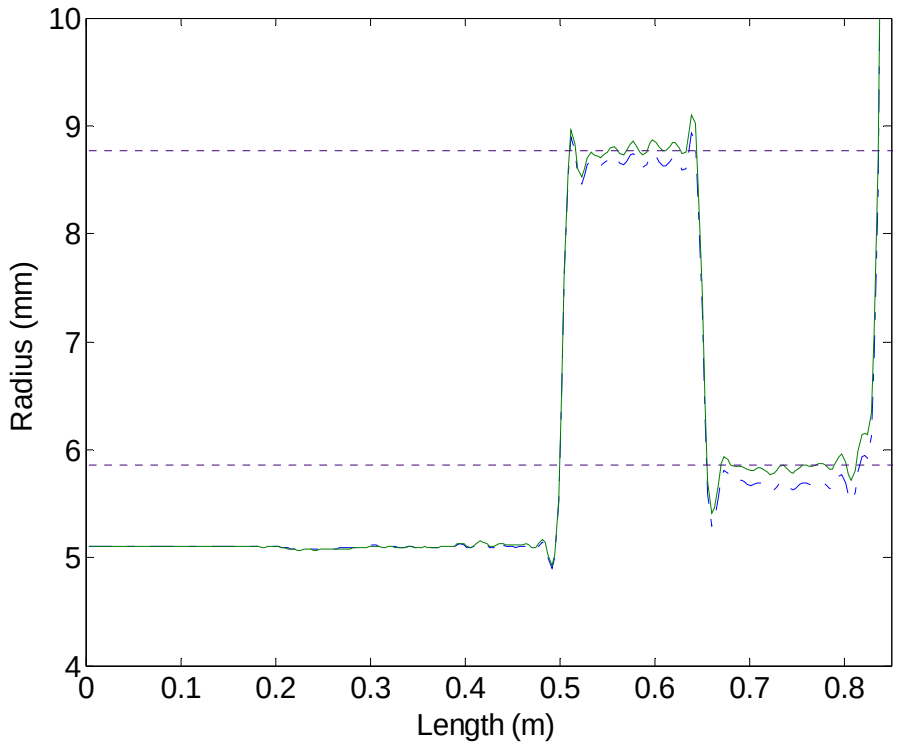

Figure 6.7: Bore reconstructions of stepped tube C (Section II coupled)

Examination of the reconstructions made using the standard reflectometry technique reveals, in all cases, an underprediction in radius. The error increases with distance along the stepped tube so that the degree of underprediction is always greater for the section of the stepped tube which is not coupled to the DC tube. This is most likely a consequence of the layer peeling algorithm where any small error in the predicted radius towards the start of a reconstruction accumulates as the reconstruction progresses.

The stepped tube reconstructions calculated from the improved low frequency content input impulse response measurements all show a much better agreement with the directly measured radii. In each case, this is particularly apparent for the section of stepped tube which is not coupled to the DC tube. By improving the measurement of the input impulse response at low frequencies, when the layer peeling algorithm is applied, any error in the predicted radius at the start of the reconstruction is significantly reduced. Consequently,

although the error must still accumulate as the reconstruction progresses, it remains small over the length of the test object.

6.3 Measurements on musical instruments

6.3.1 Renaissance cornett

Improving the low frequency content of the input impulse response measurements has led to a significant improvement in the accuracy and consistency of the bore reconstructions. Further evidence of this is provided in this section through measurements of a Renaissance cornett by Jeremy West.

Figure 6.8 shows a bore reconstruction of the cornett made using the standard reflectometry technique (dashed line) together with a reconstruction calculated when a supplementary measurement using a bass loudspeaker was made to improve the low frequency content of the input impulse response (solid line). The first few centimetres of the reconstructed profiles show the coupler used to connect the cornett to the DC tube with the arrow indicating the start of the cornett bore. Both reconstructions show a good agreement with the radius of 3.94 mm directly measured at the mouthpiece end of the cornett using calipers. However, at the far end of the cornett, the reconstruction made using the standard reflectometry technique predicts a radius of approximately 11 mm when in fact the actual radius is measured as being 12.87 mm. This underprediction is not seen in the reconstruction calculated from the input impulse response with improved low frequency content where the radius at the end of the cornett closely matches the directly measured value.

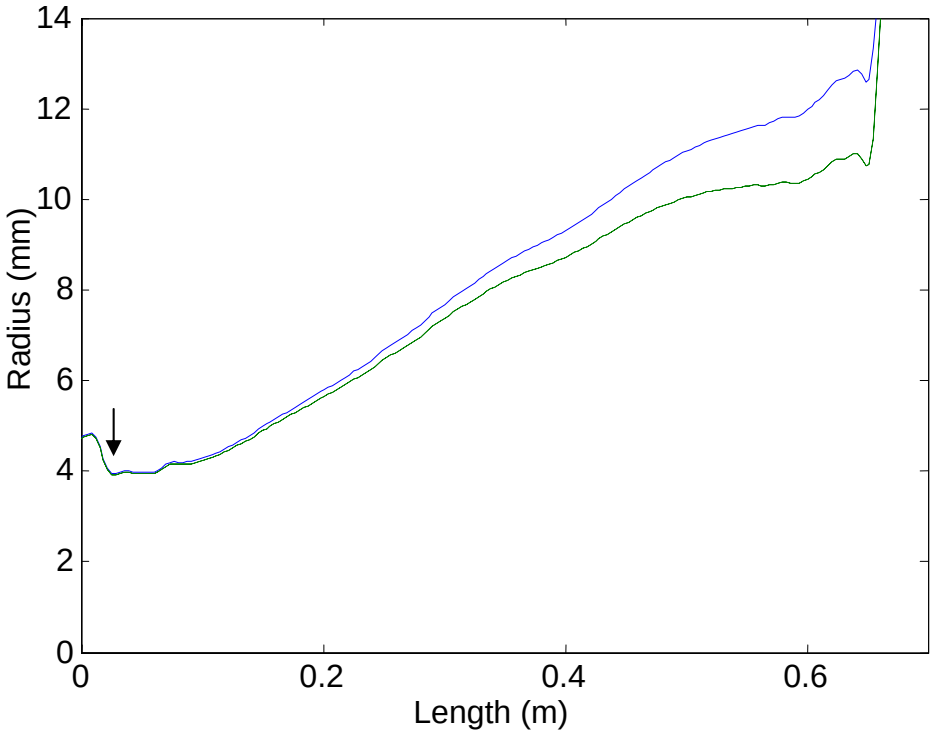

Figure 6. 8: Bore reconstructions of a Renaissance Cornett

6.3.2 Bugle horn

The improvements in the accuracy of the bore reconstructions have enhanced the usefulness of the reflectometry technique as a tool for measuring the bore profiles of instruments non-invasively. As a demonstration of this, non-invasive measurements of an 18th century bugle horn which is kept in the Royal College of Music Historical Instrument Collection, and for preservation reasons can no longer be played, are presented here. Figure 6.9 is a photo of the bugle horn coupled to the pulse reflectometer and Figure 6.10 shows a 3D representation of the internal bore profile of the bugle horn obtained using acoustic pulse reflectometry.

Figure 6.9: 18th century Bugle Horn coupled to pulse reflectometer

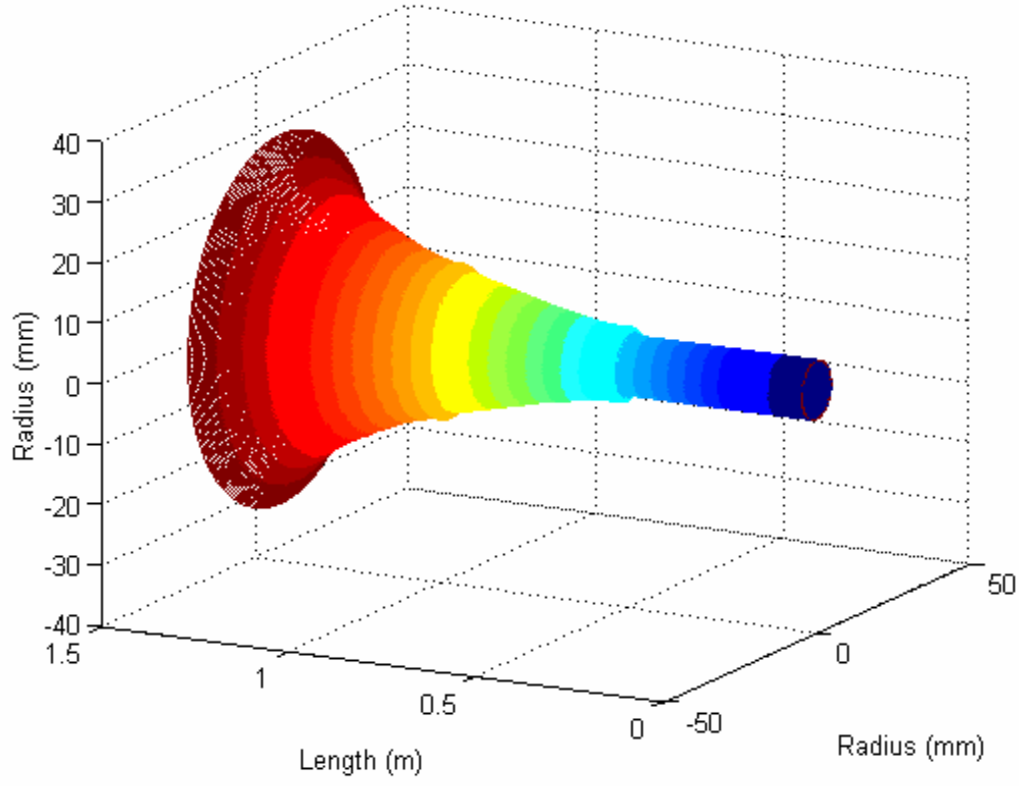

Figure 6.10: 3-D reconstruction of internal profile of Bugle Horn

6.4 Summary

In this chapter, the improvement in the accuracy of bore reconstructions that is brought about by performing a second reflectometer measurement, using a bass loudspeaker to increase the low frequency content of the measured input impulse response, has been demonstrated. The improvement was shown through a series of measurements made on both stepped tubes and musical instruments. In the next two chapters, attention is turned to the effect on the bore reconstruction of increasing the high frequency content of the input impulse response.

Chapter 7

Additional high frequency probing to improve bandwidth of input impulse response

7.1 Introduction

It was shown in the previous two chapters that the low frequency content of the input impulse response is vital to the stability and accuracy of the reconstructed bore profile. However, the fine detail in the bore reconstruction depends on a good high frequency content. The finite bandwidth of an input impulse response measurement made using reflectometry limits the axial resolution of the calculated bore profile and is one of the reasons why regions of rapidly changing cross-section are poorly reconstructed.

In this chapter, the importance of the high frequency content of the input impulse response to the accuracy of the bore reconstruction is demonstrated. The chapter consists of three main sections. In the first section, by applying the layer peeling algorithm to theoretically calculated input impulse responses of different bandwidths, the effect of the higher frequencies on the bore reconstruction is shown. In the second section, the lack of high frequency content in the input impulse generated by a typical pulse reflectometer is described and the error introduced into the measured input impulse response as a result is discussed. In the third and final section, a method for increasing the amount of high frequency energy injected into the duct under investigation is presented. The method involves supplementing the standard sound pulse measurement by probing the duct further with bursts of high frequency sinusoidal pressure waves. Results obtained using this

method are presented and compared with those measured using the standard reflectometry technique [Li et al. 2001].

7.2 Simulated data

To demonstrate the importance of the high frequency signal content to the bore reconstruction, two theoretical input impulse response spectra for the stepped tube (which is 310 mm long and whose radius expands from 6.2 mm to 9.45 mm) previously described in chapter 4 were calculated using equation (2.39). Different sampling frequencies were used for the two spectra. For the first input impulse response spectrum, a sampling frequency of 16 kHz was employed, defining a Nyquist frequency of 8 kHz. For the second spectrum, a sampling frequency of 22.05 kHz was used with an associated Nyquist frequency of 11.025 kHz. By inverse Fourier Transforming the spectra, two input impulse responses were obtained. Application of the layer peeling algorithm described in chapter 3 to these calculated input impulse responses provided two bore reconstructions of the stepped tube. The axial resolutions of the bore reconstructions have the following dependence on the sampling frequency:

$$\mathrm{Re} = \frac{c}{2F_s} \tag{7.1}$$

where Re is the axial resolution, c is the speed of sound and F_s is sampling frequency.

Figure 7.1 shows the simulated input impulse response spectrum of the stepped tube with frequency content up to 8 kHz and Figure 7.2 shows the stepped tube reconstruction obtained from that input impulse response. According to equation (7.1), the axial resolution in Figure 7.2 is about 11 mm. The oscillations along the axis are caused by the limited high frequency content. In addition, it is seen that the regions of rapidly changing

cross-section are poorly reconstructed. Figure 7.3 shows the simulated input impulse response spectrum of the stepped tube with frequency content up to 11.025 kHz and Figure 7.4 shows the reconstructed stepped tube calculated from that input impulse response. The axial resolution is now approximately 8 mm according to equation (7.1). The reconstruction of regions of rapidly varying cross-section is improved due to the increased high frequency content. These results show that the greater the high frequency content of the input impulse response, the more accurate the profile of the stepped tube, especially in regions of rapid cross-sectional change. The remaining ripple in Figure 7.4 is caused by the Gibbs phenomenon [Wylie and Barrett 1982]

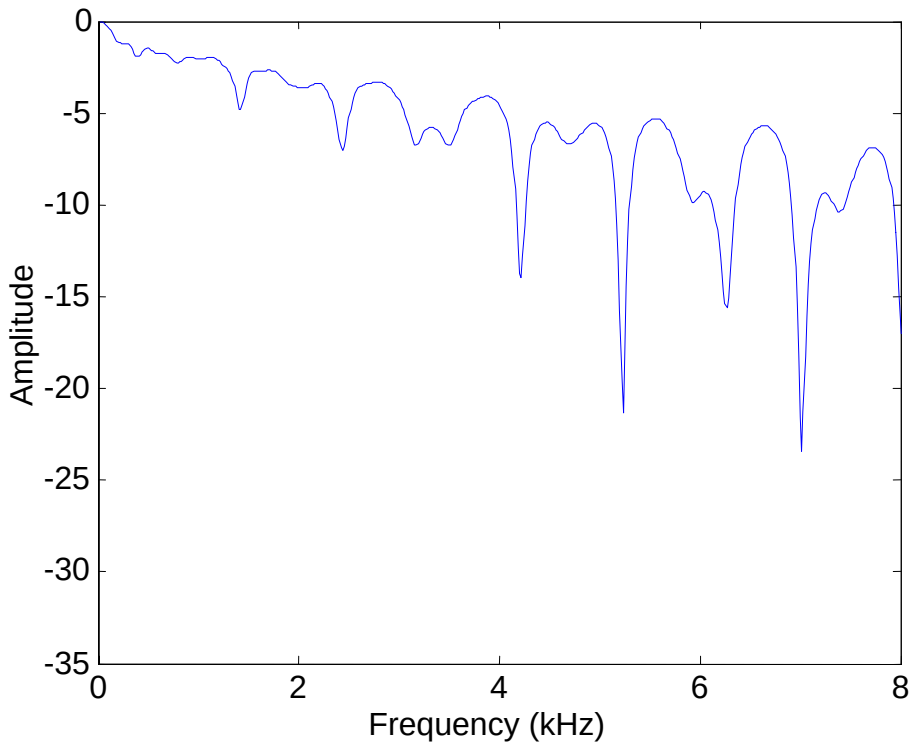

Figure 7.1: Simulated 8 kHz spectrum of stepped tube input impulse response

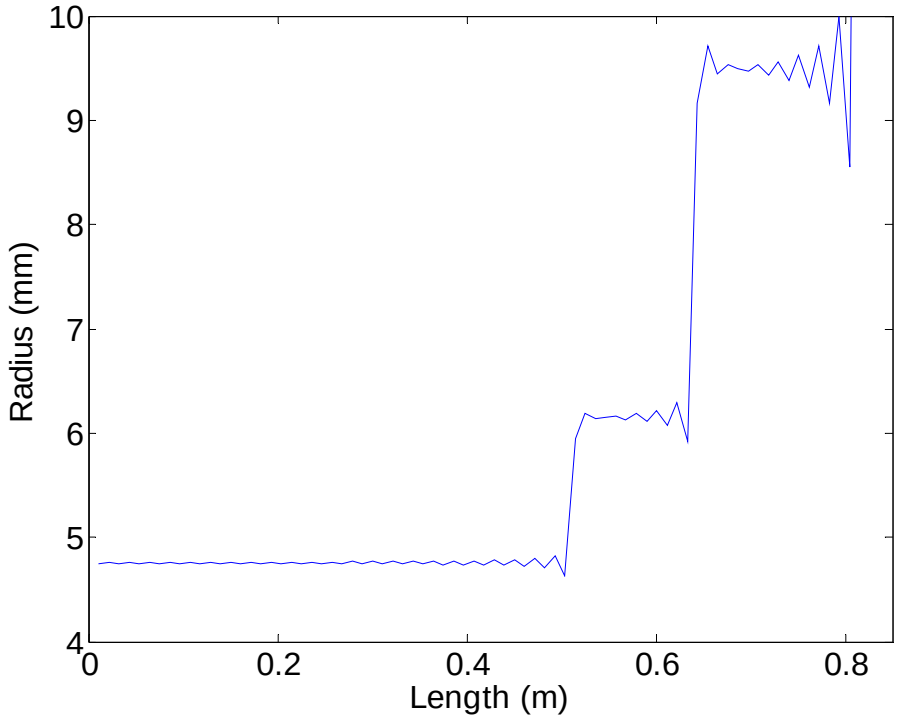

Figure 7. 2: Stepped tube bore reconstruction from simulated 8 kHz input impulse response

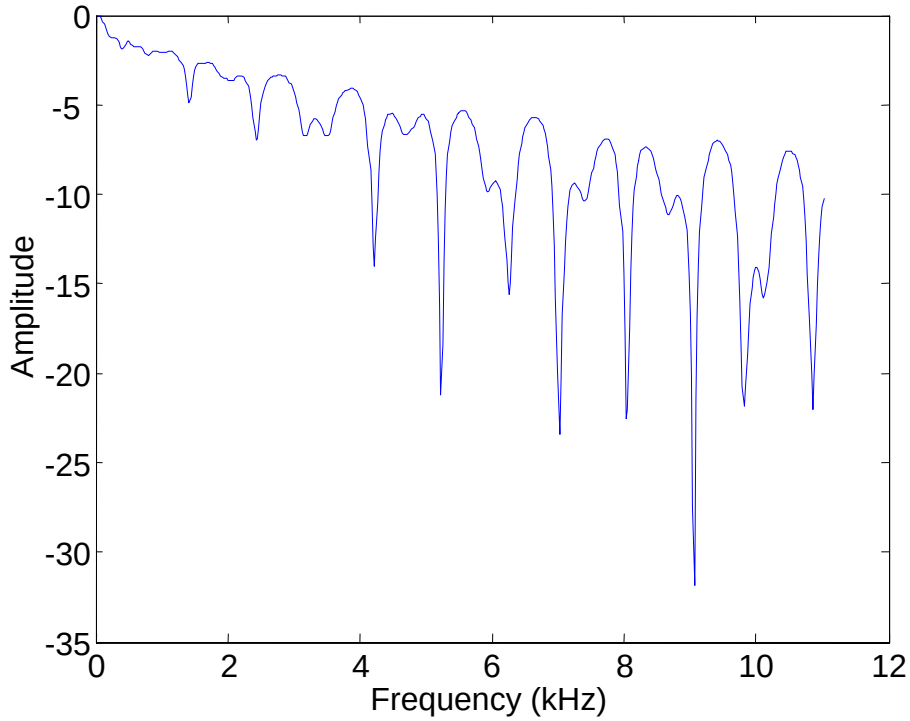

Figure 7.3: Simulated 11.025 kHz spectrum of stepped tube input impulse response

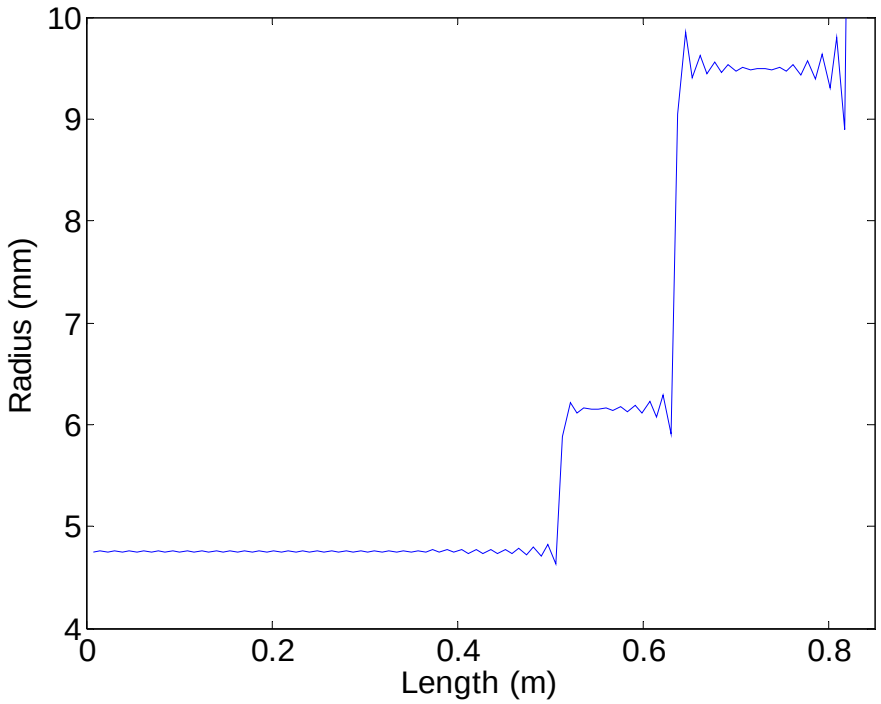

Figure 7.4: Stepped tube bore reconstruction from simulated 11.025 kHz input impulse response

7.3 The problem of the lack of high frequency content in the standard reflectometry technique

An input pulse produced by a reflectometer typically has little energy at high frequencies. Figure 7.5 shows the frequency spectrum of an input pulse, $I(\omega)$, measured on the reflectometer described in chapter 4 using a sampling frequency of 22.05 kHz (so the Nyquist frequency is 11.025 kHz). Above about 8 kHz the signal becomes comparable in amplitude to the background noise level. The lack of energy at high frequencies in the input signal consequentially leads to any reflections measured by the reflectometer also having a limited bandwidth. For example, Figure 7.6 shows the frequency spectrum of the reflections, $R(\omega)$,which return from the stepped tube. Again, above approximately 8 kHz the signal becomes comparable in amplitude to the background noise level. The consequence of this is that, in the standard reflectometry procedure, the deconvolution of

the reflected and input signals, as described by equation (4.1a), can lead to a "division by noise" error. This can be seen clearly in Figure 7.7, where the solid line shows the stepped tube input impulse response spectrum, $IIR(\omega)$, calculated from the spectra shown in Figures 7.5 and 7.6 and the dotted line shows the theoretical input impulse response spectrum calculated in the previous section. Above 8 kHz, the agreement between the measured and theoretical input impulse response is much poorer than it is below 8 kHz. The bore reconstruction which results from applying the layer peeling algorithm to the measured input impulse response is shown in Figure 7.8. The basic shape of the stepped tube is reconstructed correctly but a rapidly fluctuating component is superimposed. Indeed it is not uncommon for this fluctuation to become unstable and cause the reconstruction algorithm to break down completely.

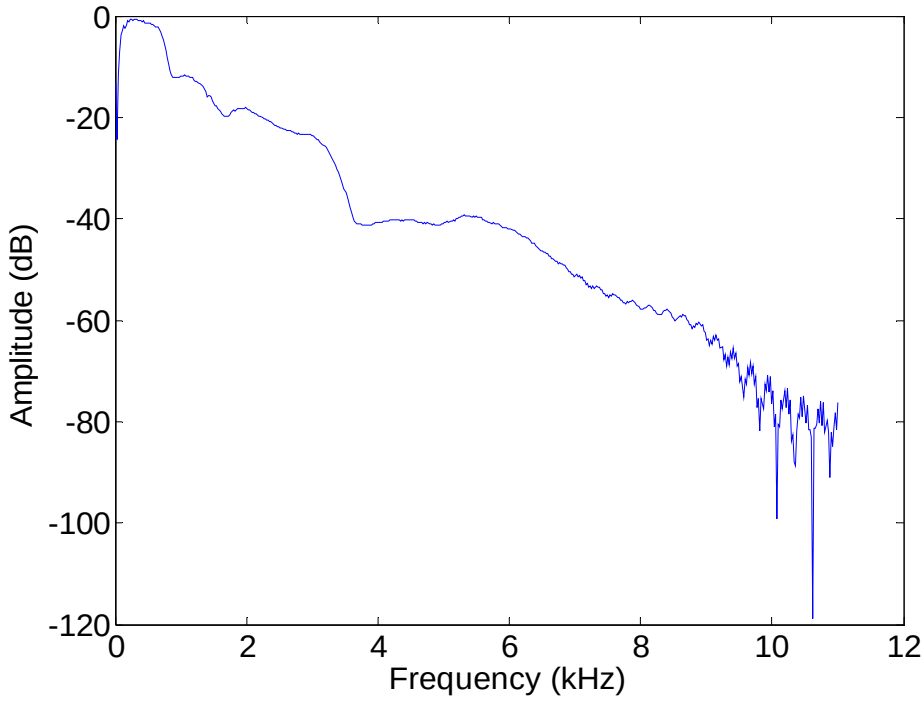

Figure 7.5: Typical input pulse spectrum

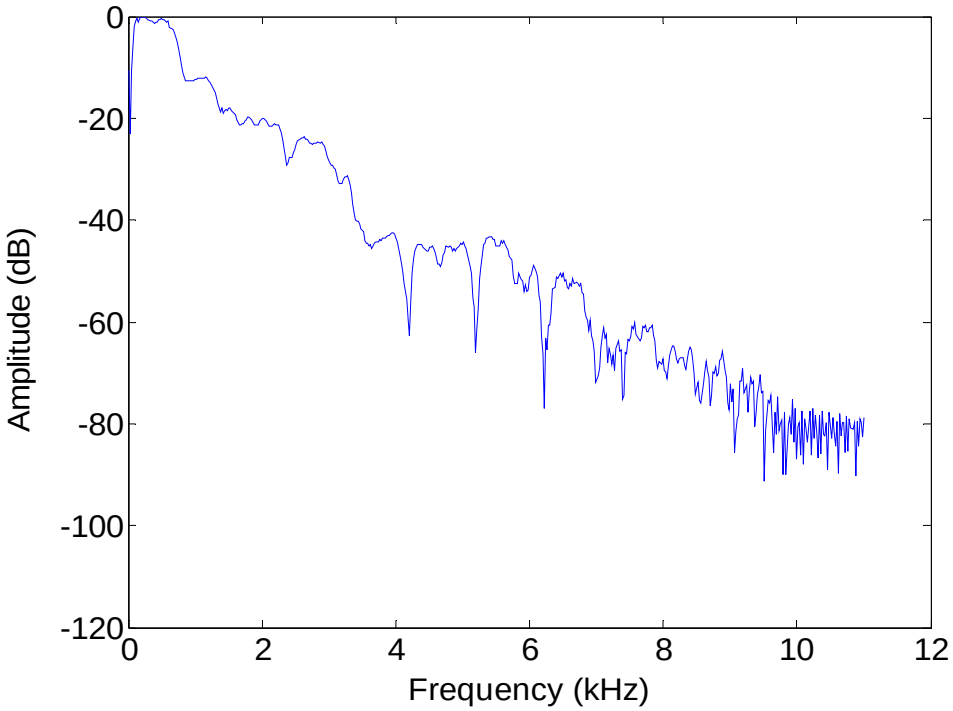

Figure 7.6: The spectrum of reflections from the stepped tube

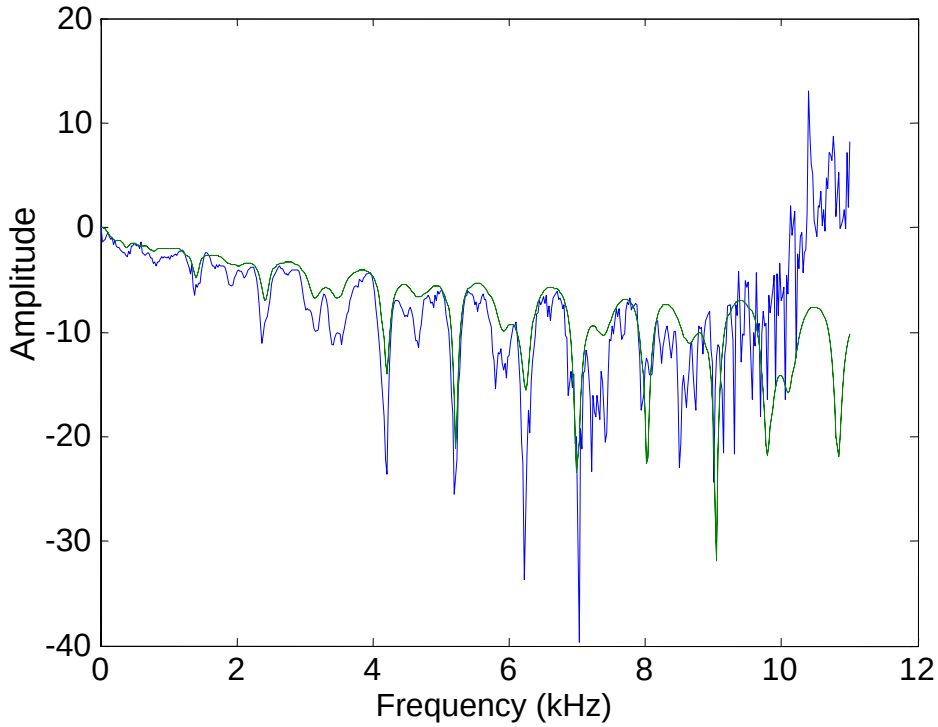

Figure 7.7: The input impulse response spectrum

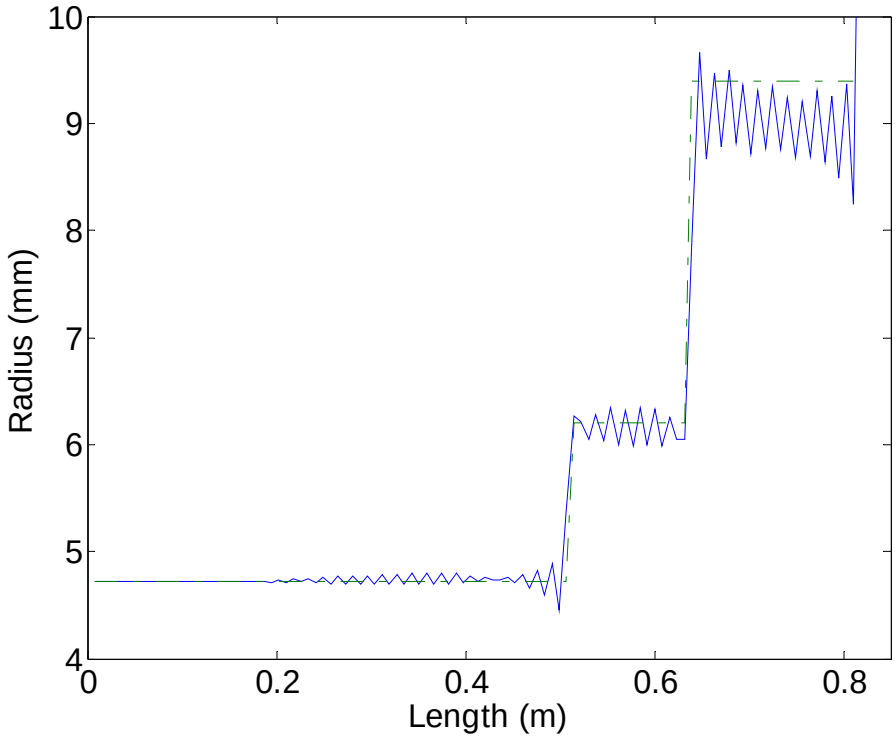

Figure 7.8: The reconstruction of the stepped tube

Previously, to overcome the "division by noise" problem when evaluating $IIR(\omega)$, either the sampling frequency had to be set such that the Nyquist frequency was equal to the bandwidth of the input pulse, or, as described previously in chapter 4, a constraining factor was introduced into the denominator of the deconvolution equation (see equation (4.1b)). This constraining factor has a low pass filter effect, preventing the "division by noise" error above 8 kHz. However, it also gives a small but unwanted modification of the input impulse response at low frequencies which can affect the accuracy of any subsequent bore reconstruction.

7.4 Sine wave packet technique

In order to solve the "division by noise" problem, a new method has been developed to improve the high frequency content of the input signal.

A standard reflectometry measurement is carried out as described in chapter 4 and the input impulse response spectrum $IIR(\omega)$, is calculated up to 8 kHz using equation (4.1a). Then, at frequencies between 8 kHz and 11.025 kHz, sinusoidal wave packets of 10 ms duration are used to probe the duct. Figure 7.9 shows one such sinusoidal wave packet (comprising a sine wave with Gaussian window function). $I(\omega)$ and $R(\omega)$ are recorded at each discrete frequency and equation (4.1 a) is used to calculate the higher frequency contribution to the input impulse response.

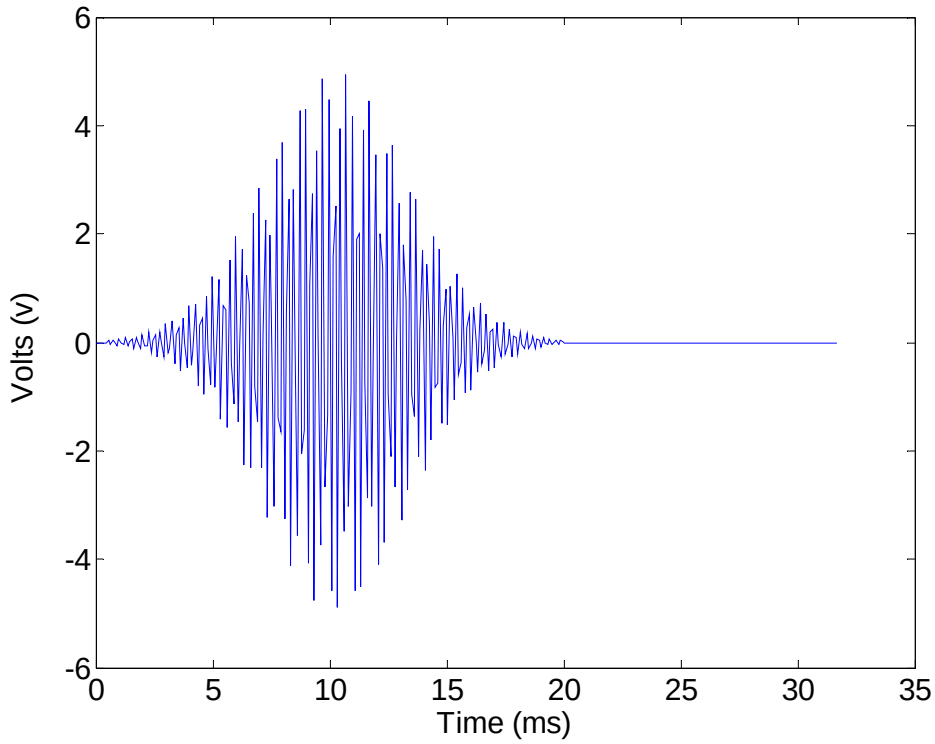

Figure 7.9: Sinusoidal wave packet used in reflectometer measurement

By combining the results of pulse and sine wave packet measurements, the input impulse response, $IIR(\omega)$, is found between 0 Hz and 11.025 kHz. The input impulse response $iir(t)$ is then obtained, as before, by inverse Fourier Transforming $IIR(\omega)$. (This method also allows the extra bass measurement for preventing low frequency offset, described in chapter 5, to be made).

Figure 7.10 shows the input impulse response spectrum for the stepped tube (shown by the solid line) obtained when the sine wave packet technique was used to supplement the standard reflectometry measurement. The agreement with the theoretical input impulse response spectrum (dotted line) is now good up to the Nyquist frequency of 11.025 kHz. There is a degree of background noise present. However, at a further computational cost, this can be reduced by averaging to improve the signal-to-noise ratio.

Figure 7.11 shows the bore reconstruction of the stepped tube calculated from the input impulse response of Figure 7.9. The fluctuating component observed in Figure 7.8 has been suppressed and therefore a better reconstruction is obtained. The underprediction of the radius of the second section of the stepped tube is a consequence of the poor low frequency content of the input impulse response (as described in chapter 5). By carrying out the extra bass measurement, the improved impulse response leads to the bore reconstruction shown in Figure 7.12. The underprediction in radius is now largely corrected and the reconstruction is found to be in good agreement with direct measurement.

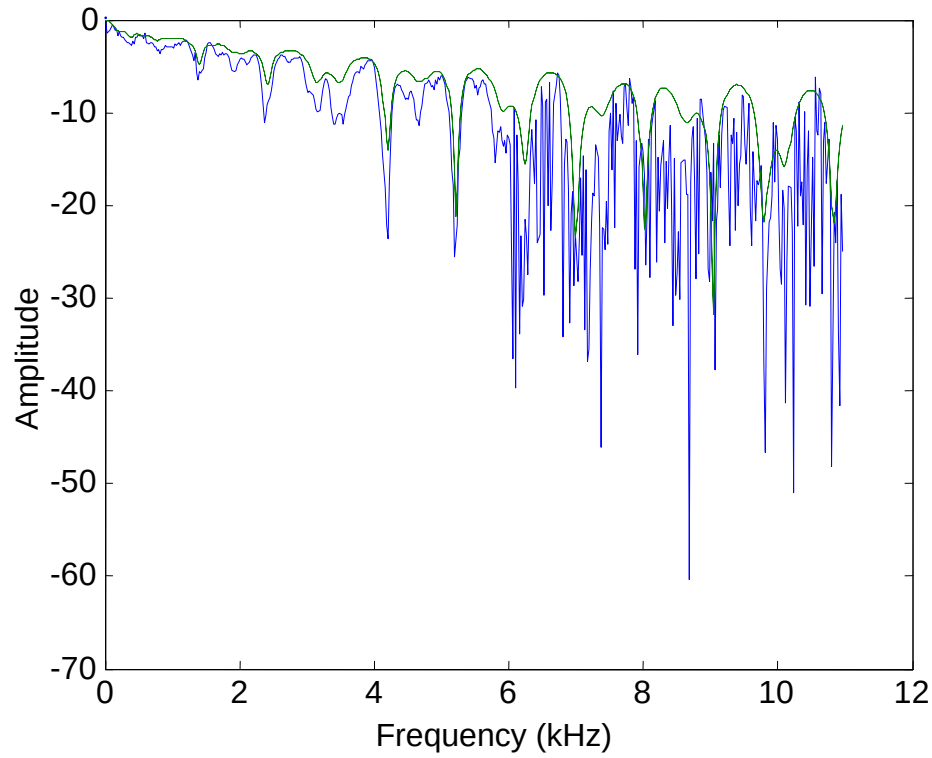

Figure 7.10: The combined input impulse response spectrum

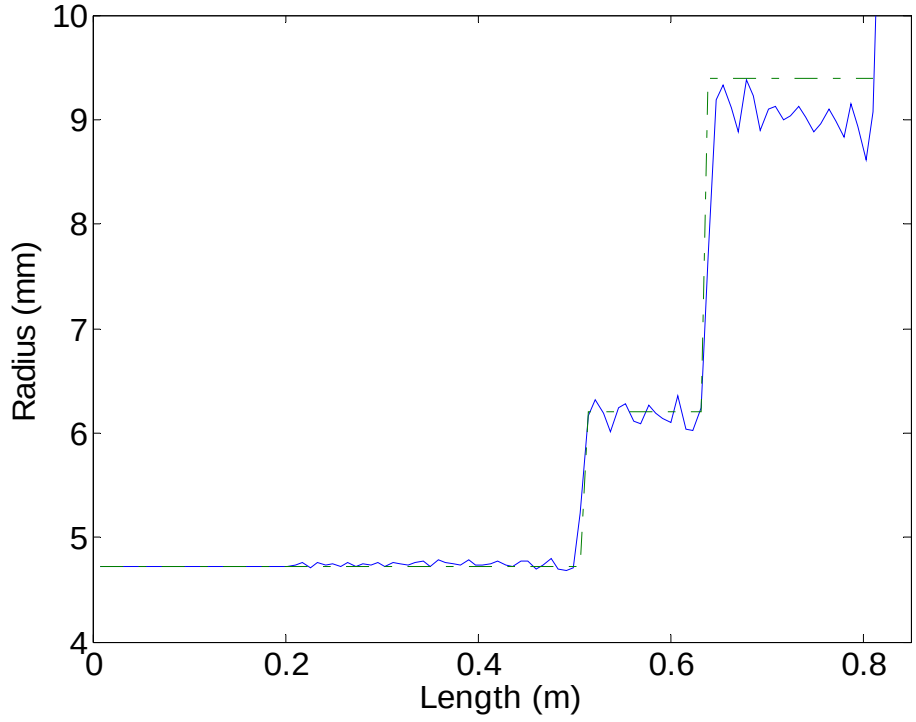

Figure 7.11: Reconstruction using the combined input impulse response

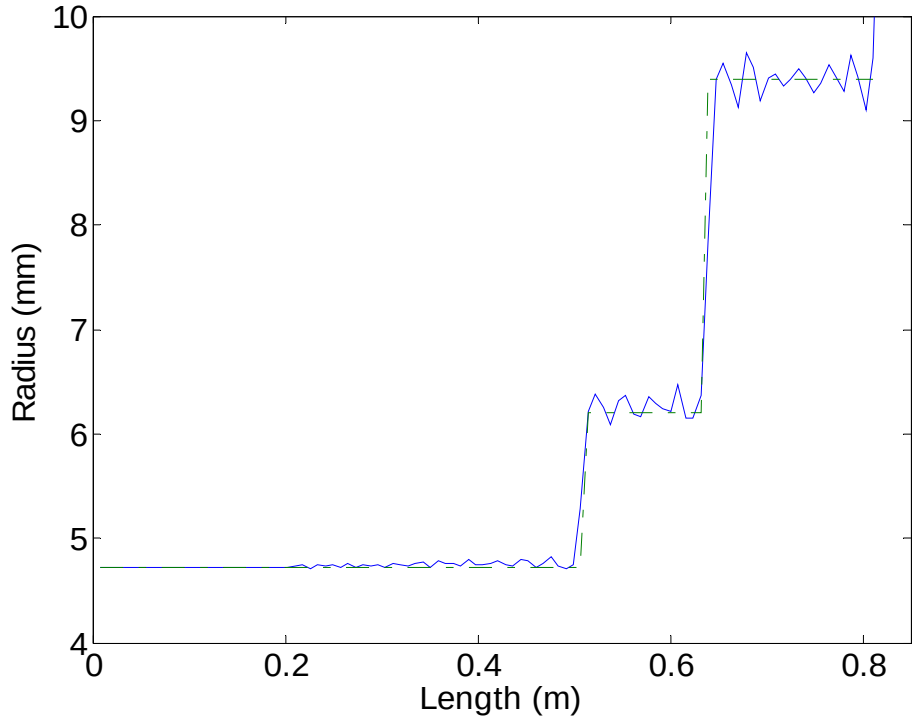

Figure 7.12: Bore reconstruction of stepped tube once low frequency content of input impulse response has been improved

7.5 Conclusions

A method of supplementing the standard acoustic pulse reflectometry technique by probing further with bursts of high frequency (greater than 8 kHz) sinusoidal pressure waves has been proposed and discussed. From the measurements, it is clearly shown that this new method has increased the high frequency energy injected into the duct, resulting in a more stable and accurate bore reconstruction. The bore profile is reconstructed from digital data sampled and converted from continuous sound waves. The axial resolution of the duct profile reconstruction is dependent on the data intervals and thereby the sampling frequency used to record the input pulse and reflections. When a sampling frequency of 22.05 kHz is used, the standard reflectometry technique only provides radius measurements at 8mm intervals along the axial of the duct. Using a higher sampling

frequency to record the reflections will improve the axial resolution provided that the input signal contains significant energy up to the new Nyquist frequency. In the standard reflectometry technique, the energy at higher frequencies is normally too small to contribute to the reconstruction. The method of sine wave packets has been shown to be effective in increasing the high frequency content. However, it is currently impossible to extend the sine wave packet method beyond 11.025 kHz, due to the very rapid attenuation of high frequencies. A method to overcome this problem will be discussed in next chapter. This should further improve the axial resolution and accuracy of reconstruction, particularly in regions of rapidly changing cross-section.

Chapter 8

Reducing source tube to improve bandwidth of input impulse response

8.1 Introduction

The design of the reflectometer described in chapter 4 includes a source tube to separate the forward and backward travelling waves. Although this provides an effective means of isolating the input pulse and the test object reflections, the attenuation of the signal while travelling in the source tube can be large, resulting in poor bandwidth input impulse response measurements. For a test object with rapid expansions and contractions this can lead to significant errors in the bore reconstruction.

In this chapter, a reflectometer with a shorter source tube is presented. The reduction in source tube length ensures less attenuation of the measured signals, leading to an improvement in the bandwidth of the experimentally determined input impulse response and more accurate bore reconstruction. However, the shorter source tube also means that a new way of separating the input pulse and test object reflections is required. Alternative calibration methods designed to achieve this separation are described. These methods are evaluated by comparing measurements of a stepped tube carried out using the original design of reflectometer and using the shorter source tube model[Li and Sharp 2003].

8.2 Reflectometer with shorter source tube

The reflectometer described in chapter 4 (Figure 4.1) has a total length of 10 m. Such a length of source tube is necessary to separate the forward and backward travelling pressure waves. The section l_2, of length 3 m, ensures that the input pulse has fully passed the microphone before the first reflection returning from the test object reaches the microphone. The section l_1, of length 7 m, ensures that further reflections from the speaker are not recorded. Therefore the reflections from the test object can be recorded for up to $2*l_1/c$ = 0.041 seconds (the time taken to travel the distance from the microphone to the loudspeaker and back, where c is the speed of sound in air) before the loudspeaker reflections return and contaminate the signal. The longer the section l_1 of the source tube, the longer the time period over which the test object reflections can be recorded.

Figure 8.1 shows a schematic diagram of an acoustic pulse reflectometer with a shortened source tube. The source tube length l_2 has been reduced to 0.5 m. However, the source tube length l_1 is left unchanged at 7 m so the time over which the test object reflections can be sampled is still 0.041 seconds. Consequently the maximum length of test object that can be measured using this shorter source tube reflectometer is the same as that using the original design of reflectometer. The reduction in source tube length results in a decrease in signal attenuation and, thus, an increase in the bandwidth of the input pulse and test object reflections. An improved input impulse response bandwidth and more accurate bore reconstruction can therefore be obtained.

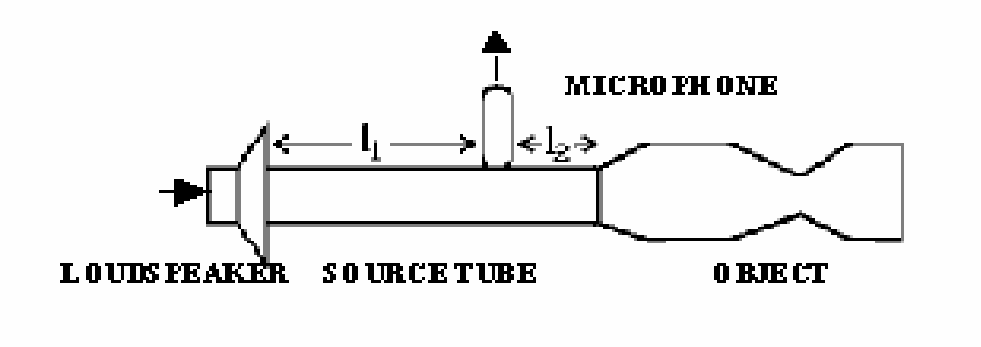

Figure 8.1: Reflectometer with shorter source tube

The shorter source tube reflectometer operates in much the same way as the original reflectometer, with a loudspeaker producing a sound pulse which travels through the source tube into the test object. The returning reflections from the test object are again captured by a microphone, amplified and stored on a PC. However, because of the shortened section l_2, the forward travelling pressure wave does not completely pass the microphone before the first reflection from the test object reaches it. Figure 8.2 shows the signal recorded by the microphone when the source tube is rigidly terminated. The signal is displayed from 2 ms before the pulse first passes the microphone so the first peak in Figure 8.2 is the forward travelling pulse and the second peak is the backward travelling reflected pulse. The two signals overlap. Figure 8.3 shows the signal captured by the microphone when a stepped tube is coupled to the source tube (to enable DC offset removal, a DC tube is positioned between the source tube and stepped tube). Again the forward travelling pulse and the reflections from the test object overlap. To be able to use this shorter source tube reflectometer for input impulse response and bore profile measurements, a new means of separating the forward and backward travelling signals is required. In the next section, two different methods of separating the overlapping signals are described and their merits discussed. To help evaluate the success of the methods, measurements made on one of the stepped tubes (Stepped tube A) described in chapter 6 are presented.

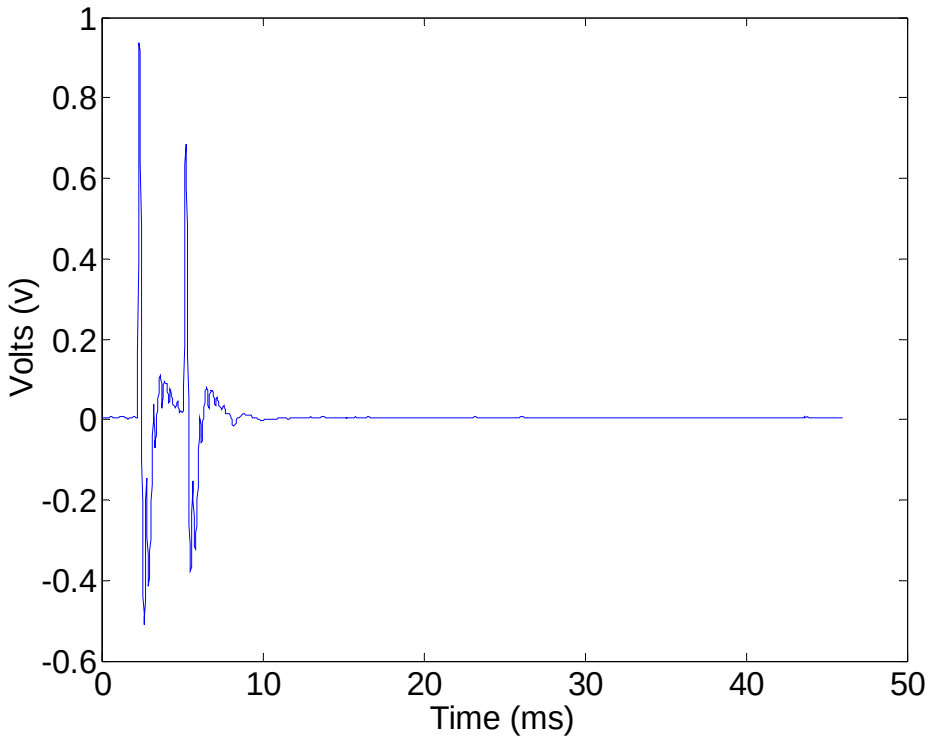

Figure 8.2: Overlapping forward and backward travelling pulses

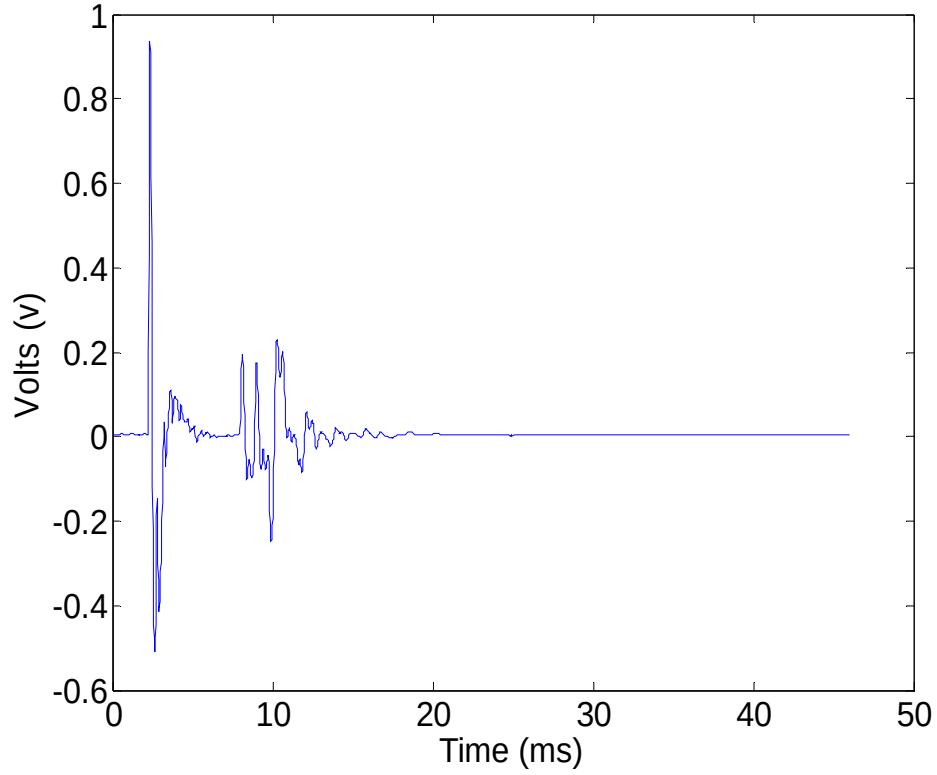

Figure 8.3: Overlapping forward travelling pulse and test object reflections

8.3 Signal separation methods

The two new methods for separating the forward and backward travelling signals both involve performing an extra calibration measurement in which the source tube is anechoically terminated. Consider the theoretical situation where an infinite length of cylindrical tubing of the same diameter as the source tube is attached to the end of the reflectometer. A forward travelling pulse would never undergo reflection and so wouldn't return to the microphone. In principle, therefore, it would be possible to measure the forward travelling pulse in isolation. In practice, such a measurement can be made using a 7 m length of copper tubing as an approximation to an infinite tube. This 7 m length is attached to the end of the source tube and a reflectometry measurement is carried out in a similar manner to that described in chapter 4. A sound pulse is generated by the loudspeaker and travels down the source tube. Two milliseconds before the forward traveling sound pulse reaches the microphone, the computer starts recording the signal from the microphone (2300 sample points are stored at a sample rate of 50 kHz). Once the sound pulse reaches the end of the source tube it enters the 7 m coil of copper tubing where it propagates without reflection. Figure 8.4 shows an isolated forward travelling pressure pulse which has been measured in this manner. Such a calibration measurement forms the basis of the two signal separation methods described over the next two subsections. The methods are named as 'one subtraction 'method and 'two subtractions' method respectively. 'One subtraction 'method is considered to achieve the better results.

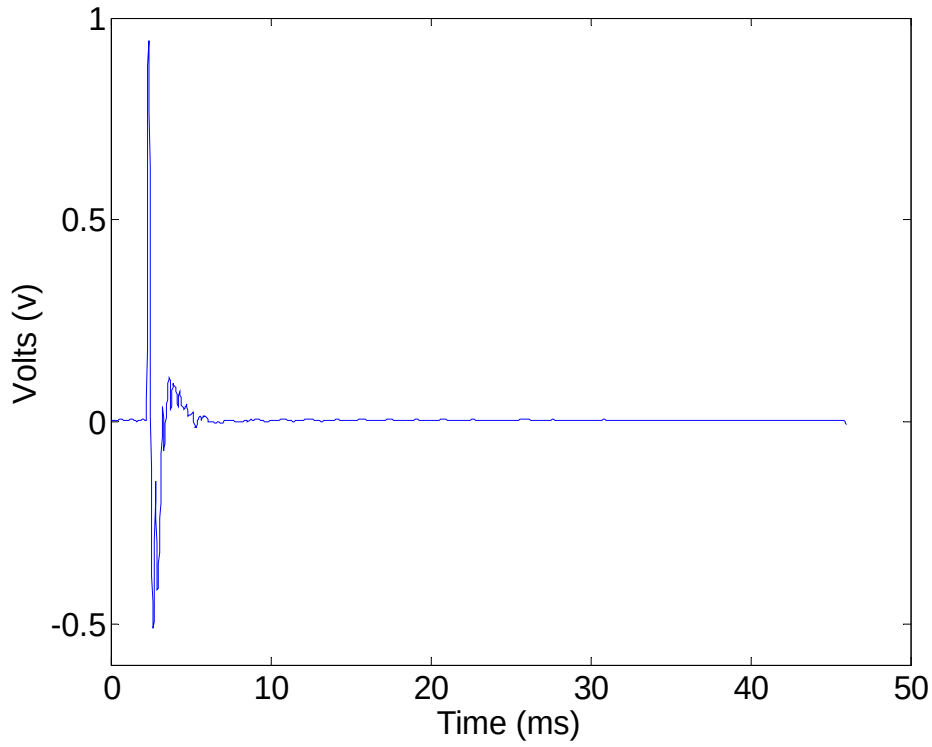

Figure 8.4: Isolated forward travelling pulse

8.3.1 'Two subtractions' method

In the 'two subtractions' method, the anechoic termination calibration measurement is used to subtract the forward travelling pulse from both rigid termination reflection and test object reflection measurements (where, in both cases, due to the shorter source tube, the forward travelling pulse overlaps with the desired signals). For example, Figure 8.5 shows a separated input pulse obtained by subtracting the isolated forward travelling pulse of Figure 8.4 from the overlapped signals of Figure 8.2 and then extracting the last 2048 points of the resulting signal. Similarly, Figure 8.6 shows the separated stepped tube reflections obtained by subtracting the isolated forward travelling pulse of Figure 8.4 from the overlapped signals of Figure 8.3 and then extracting the last 2048 points of the resulting signal. The input impulse response of the test object (or, more precisely, the DC

tube and the test object) can then be determined in the usual manner by deconvolving the separated test object reflections with the separated input pulse. Figure 8.7 shows the input impulse response spectrum for the DC tube and stepped tube A calculated from the input pulse and reflection data of Figures 8.5 and 8.6. The bandwidth of the input impulse response measurement is approximately 13 kHz. This is a distinct improvement over measurements made using the original design of reflectometer. This is apparent through examination of Figure 8.8 which shows the input impulse response spectrum for the same stepped tube A (with DC tube) measured during the experiments of chapter 6 using the original reflectometer. Here, the input impulse response becomes dominated by noise above approximately 8 kHz.

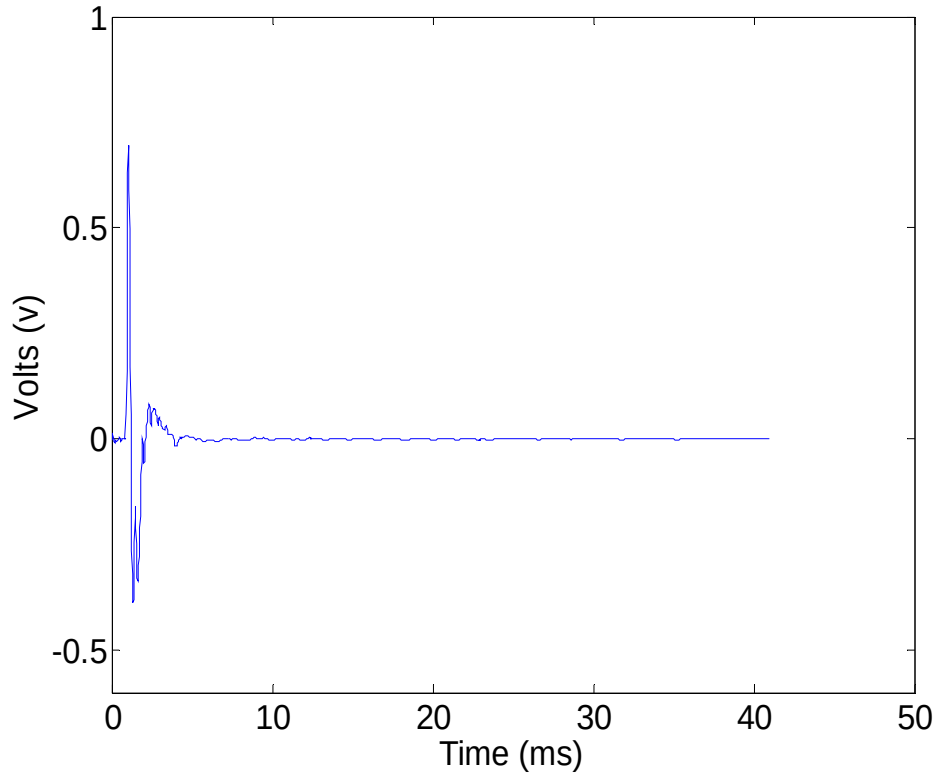

Figure 8.5: Input pulse

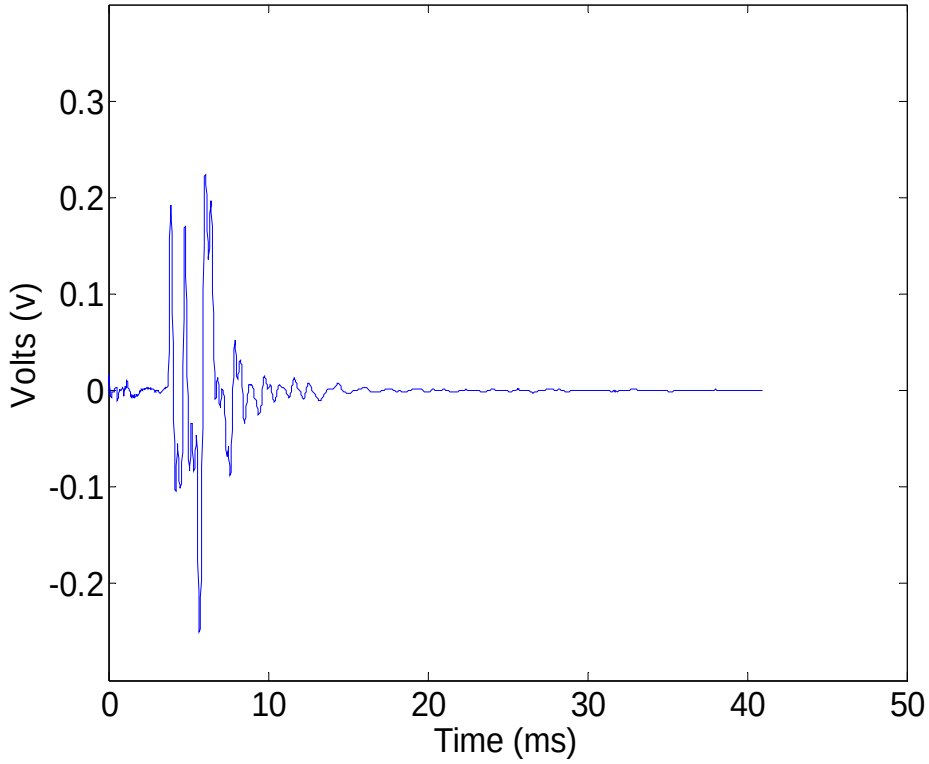

Figure 8.6: Reflections of DC tube and stepped tube

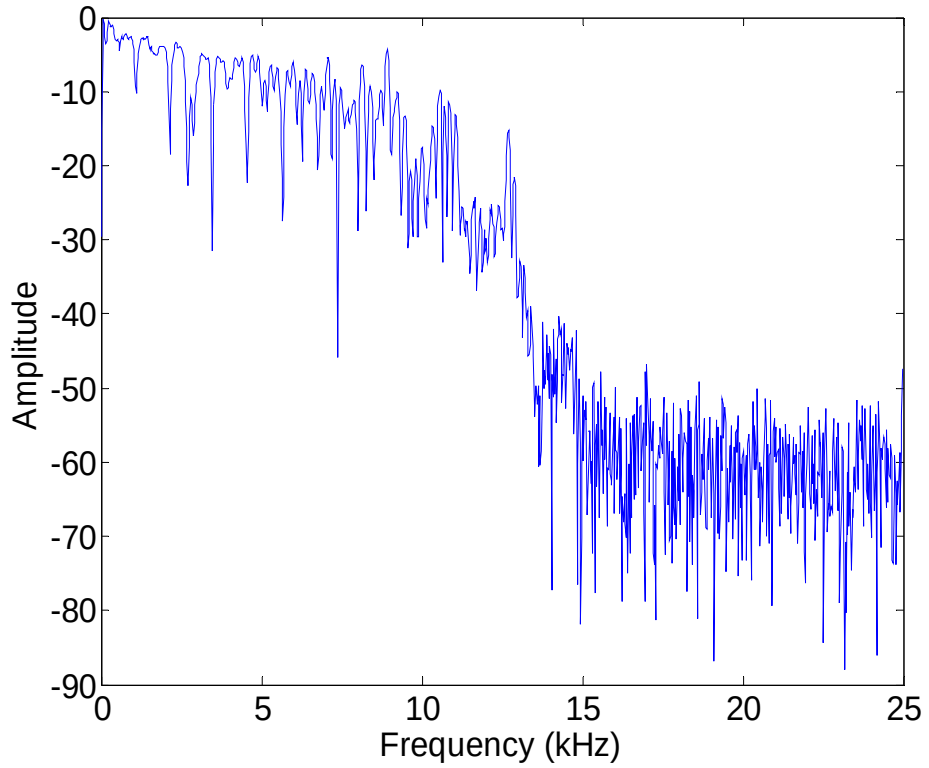

Figure 8.7: Input impulse response spectrum of DC tube and stepped tube measured using short source tube reflectometer

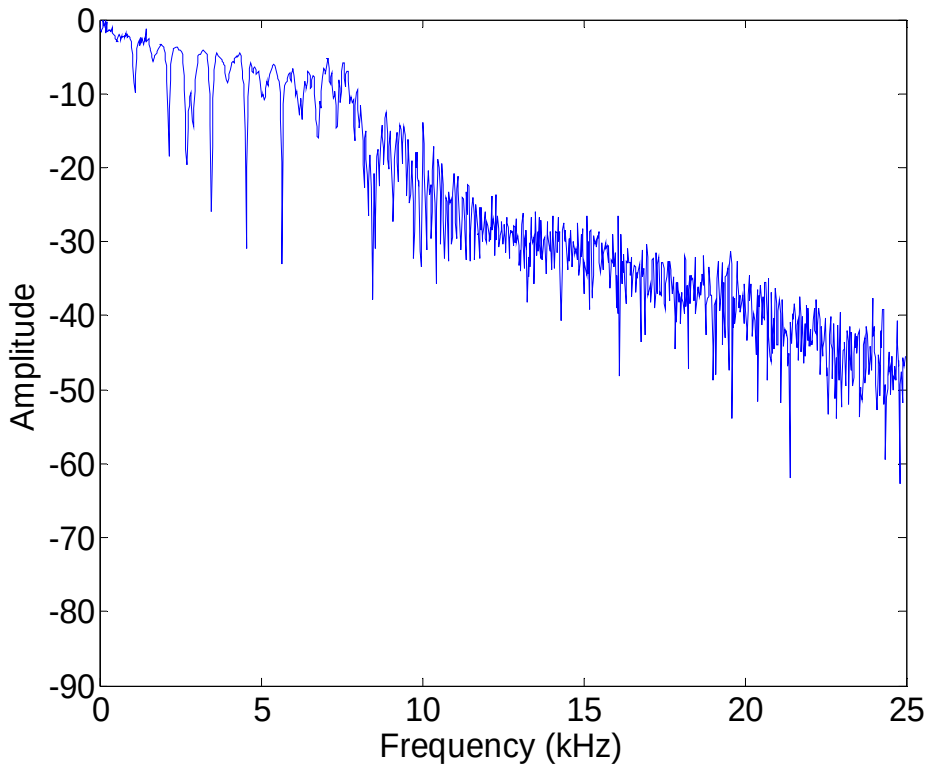

Figure 8.8: Input impulse response spectrum of DC tube and the stepped tube measured using original design of reflectometer

The improved input impulse response bandwidth obtained through use of the shorter source tube reflectometer results in the more accurate reconstruction of regions of rapidly changing cross-sectional area. This can be seen clearly by comparing the two reconstructions of the DC tube and stepped tube shown in Figures 8.9 and 8.10. The reconstruction of 8.9 was calculated from the input impulse response spectrum of Figure 8.8, measured using the original design of reflectometer. Although the calculated radii of the stepped tube sections are in good agreement with direct measurement, regions of rapidly changing cross-section are poorly reconstructed. For example, the step down from 3.55 mm radius to 2.25 mm radius is spread over an axial distance of approximately 20 mm. In the reconstruction of Figure 8.10, calculated from the input impulse response spectrum of Figure 8.7, measured using the shorter source tube reflectometer, the regions of rapid cross-sectional change are better reconstructed. This is due to the increased high

frequency content of the input impulse response measurement. The step down from 3.55 mm radius to 2.25 mm radius is now reconstructed as occurring over an axial distance of approximately 12 mm.

As an aside, it is worth noting that using the 'two subtractions' method has the additional benefit of removing any DC offset introduced by slight mis-calibration of the D/A and A/D converters. The removal of offset of this type was discussed previously in section 5.4.2. The two subtractions of one signal by another means that any DC offset in those signals is also subtracted out. Therefore, for example, the input pulse and stepped tube reflections of Figures 8.5 and 8.6 have no DC offset.

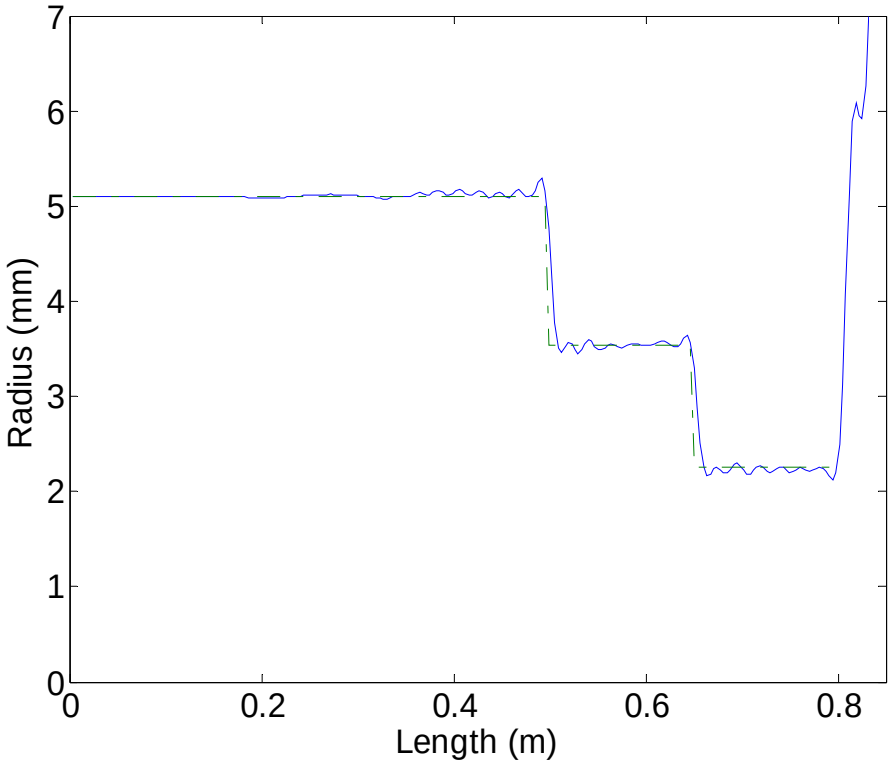

Figure 8.9: Bore reconstruction of stepped tube from measurements made using the original design of reflectometer

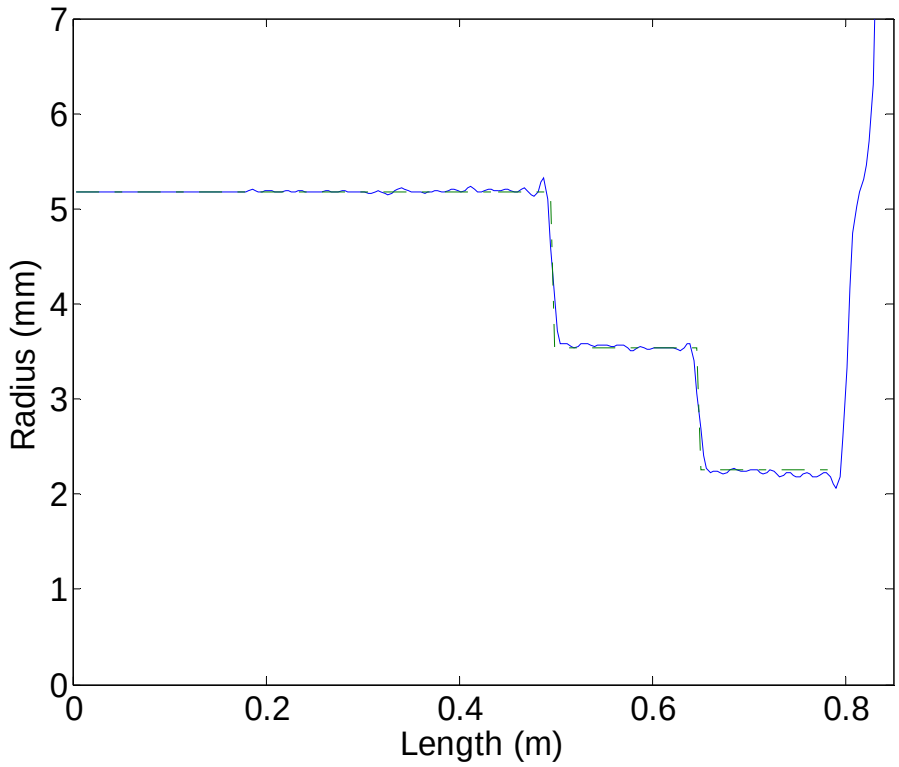

Figure 8.10: Bore reconstruction of stepped tube from measurements made using the shorter source tube reflectometer and the 'two subtractions' method

8.3.2 'One subtraction' method

The 'one subtraction' method is similar to the 'two subtractions' method in that it too uses the anechoic termination calibration measurement to subtract the forward travelling pulse from the test object reflections measurement (resulting in a separated test object reflections signal). However, with this method, the input pulse is not separated in the same way. Instead, the isolated forward travelling pulse, measured when the source tube was anechoically terminated, is itself used as the input pulse signal (extracting the first 2048 sample points of Figure 8.4). As this measured input pulse does not travel along source tube section l_2 and back, the losses it experiences are less than in the 'two subtractions' method, ensuring further improvement in the bandwidth of the input impulse response.

Another difference from the ‘two subtractions’ method is that, when employing the ‘one subtraction’ method, no DC tube is required and the test object must be coupled directly to the source tube. For example, Figure 8.11 shows the signal recorded by the microphone when stepped tube A is coupled directly to the shorter source tube reflectometer and measured in the usual way. As previously, the signal comprises 2300 sample points and is displayed from 2 ms before the forward travelling pulse reaches the microphone. By subtracting the isolated forward travelling pulse of Figure 8.4 from the overlapped signals of Figure 8.11 (and then extracting the last 2048 sample points) the separated stepped tube reflections of Figure 8.12 are obtained. Deconvolving the separated test object reflections with the isolated forward travelling pulse then yields the input impulse response of the test object (or, more precisely, of the section l_2 of the source tube and the test object). Any DC offset present in the input impulse response is then removed in a similar manner to that described in section 5.4.4. However, in this case the source tube section l_2 acts as the DC tube. Figure 8.13 shows the input impulse response spectrum for the section l_2 of source tube and stepped tube A, calculated from the input pulse and reflection data of Figures 8.4 and 8.12. The bandwidth of the input impulse response has been extended to 15 kHz, which is an improvement over that achieved with the ‘two subtractions’ method. The improved high frequency content again leads to a more accurate bore reconstruction. Figure 8.14 shows the bore reconstruction of the stepped tube calculated from this input impulse response measurement. The change in radius from 3.55 mm to 2.25 mm is now reconstructed as occurring over an axial distance of 10 mm.

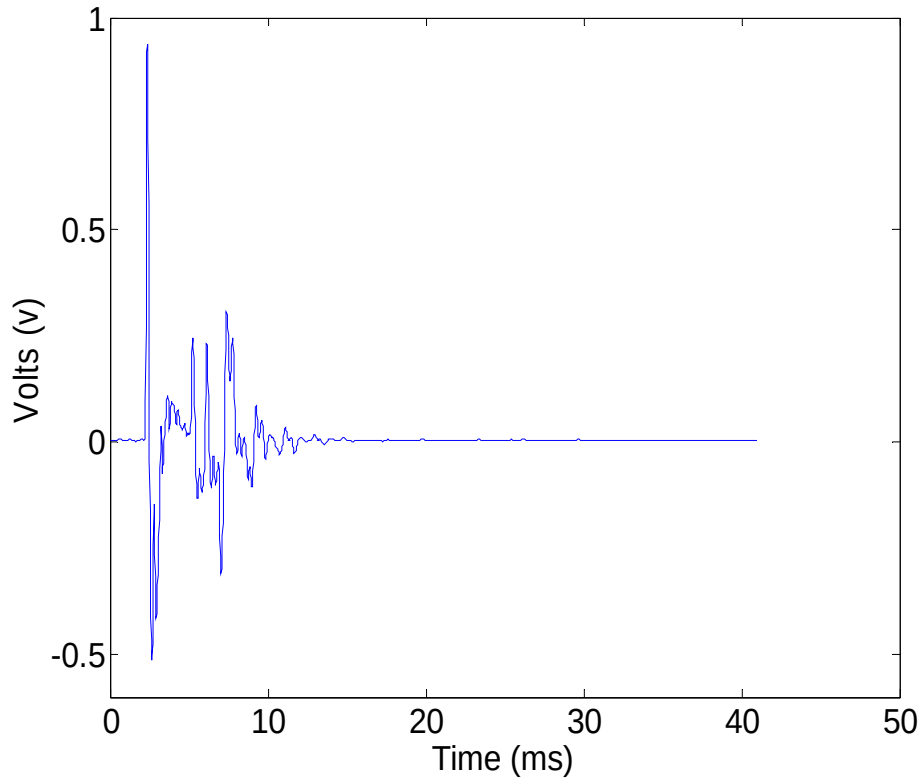

Figure 8.11: Overlapping input pulse and stepped tube reflections

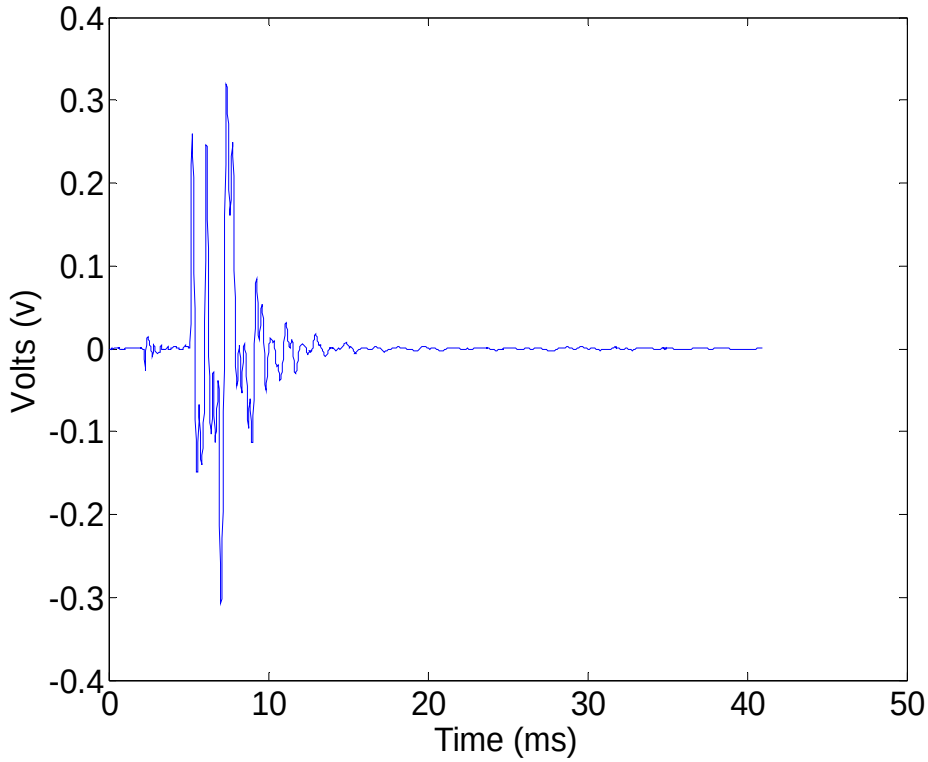

Figure 8.12: Separated reflections from the section l_2 *of source tube and the stepped tube*

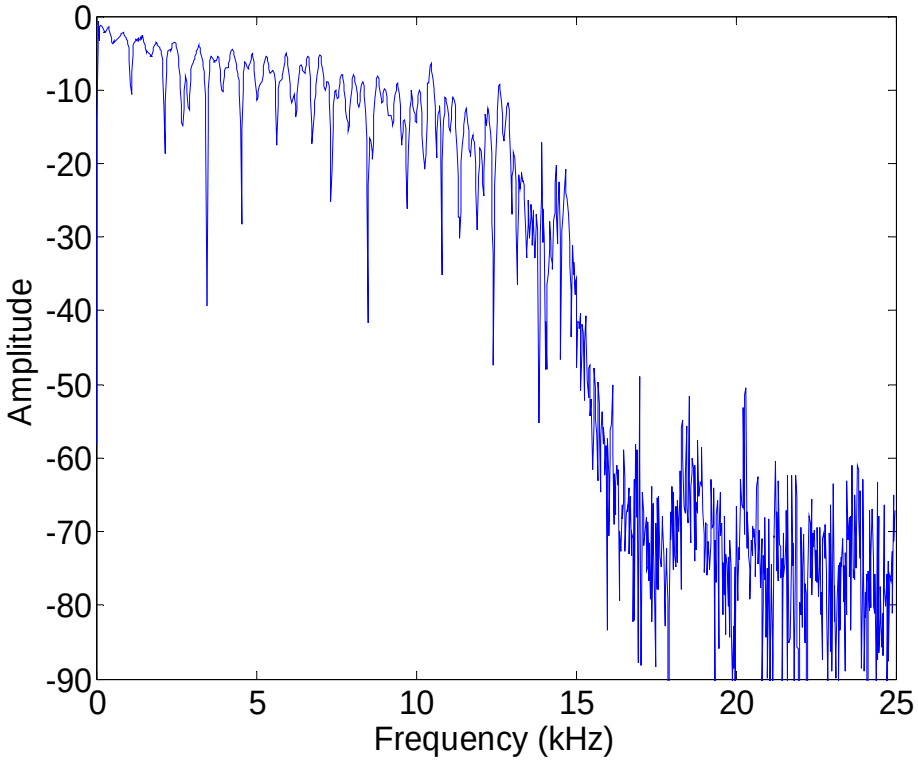

Figure 8.13:Input impulse response spectrum of source tube section l_2 *and the stepped tube*

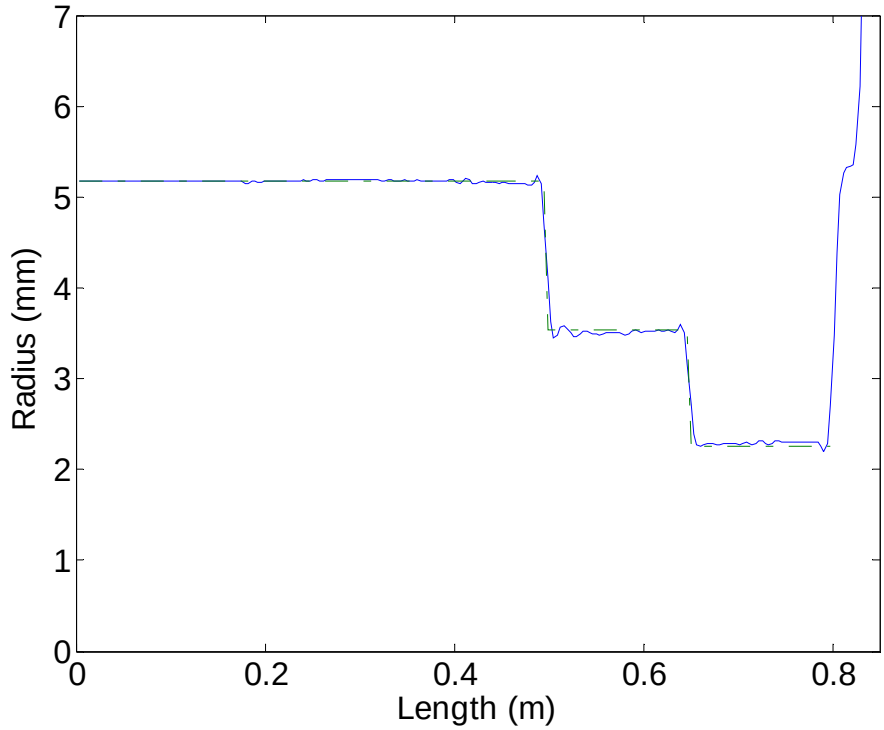

Figure 8.14: Bore reconstruction of stepped tube from measurements made using shorter source tube reflectometer and the 'one subtraction' method

8.4 Conclusions

The length of source tube in an acoustic pulse reflectometer is necessary to separate forward and backward travelling pressure signals, enabling them to be recorded in isolation. However, the losses experienced by the signals when travelling through the source tube limit the bandwidth of the input impulse response measurement and, consequently, the axial resolution of the bore reconstruction. Reducing the source tube length therefore results in bore reconstructions of greater accuracy but requires a new means of recording the input pulse and test object reflections in isolation.

In this chapter, a reflectometer with shortened source tube was described and two methods for separating the input pulse and reflections data were presented. Through measurements on a stepped tube test object, the ‘two subtractions’ method was shown to increase the bandwidth of input impulse response measurements from approximately 8 kHz to 13 kHz. This, in turn, resulted in a significant improvement in the reconstruction of sharp changes in cross-section in bore profile calculations. Using the same test object, the ‘one subtraction’ method was found to give an even greater increase in the high frequency content of the input impulse response measurement, with a bandwidth of approximately 15 kHz achieved. Again, the resultant improvement in the resolution of bore reconstructions was clearly demonstrated.

One additional benefit of using a shorter source tube reflectometer is the improvement it provides at low frequencies to the input impulse response measurements. Indeed, when using the shorter source tube, the supplementary bass loudspeaker measurements (described in chapter 5) used to prevent low frequency offsets are no longer needed.

Chapter 9

Concluding remarks

9.1 Achievement of aims

9.1.1 Objective 1

The first aim of this study was to identify any sources of inconsistency and inaccuracy in measurements made using the standard pulse reflectometry technique.

Previous studies on acoustic pulse reflectometry have shown that a DC offset is introduced into the input impulse response during the measurement process. In this study, it was demonstrated that the source of this DC offset is most likely a lack of polarity in the input pulse. Removing the DC offset from the measured input impulse response is vital for accurate bore reconstruction. This has usually been achieved by introducing a cylindrical tube of known dimensions (the so-called 'DC tube') between the source tube and object under test for calibration purposes. In this study, it was demonstrated that, providing the end conditions of the object being measured are known, the DC offset can be eliminated by replacing the 0 Hz component of the input impulse response with a corresponding theoretical value. The present research also revealed that, as well as a DC offset, reflectometry input impulse response measurements also contain a low frequency offset. Even if the DC offset is removed, unless the low frequency offset is also removed or prevented from occurring, reconstructed bore profiles will still expand or contract spuriously and unpredictably. Through examination of the spectra of input pulse, object

reflections and input impulse response measurements, the cause of the low frequency offset was found to be a lack of low frequency energy in the input pulse.

9.1.2 Objective 2

The second aim of the study was to find ways of improving the accuracy of the pulse reflectometry technique.

To this end, a method of increasing the amount of low frequency energy injected into the object under test was devised. This method involves performing a supplementary set of measurements using a bass loudspeaker with a good response in the low frequency range. The values of the input impulse response calculated at low frequencies from the bass loudspeaker measurements are then combined with the input impulse response calculated at higher frequencies from the standard measurements. The result is an input impulse response with improved low frequency content which, in turn, yields a more accurate bore reconstruction. When this method is employed, the consistency of the technique is also greatly improved. These improvements were demonstrated through measurements on a number of stepped tubes. With the increased low frequency content, the reconstructed stepped tube bore profiles have radii which agree well with directly measured values.

9.1.3 Objective 3

The third aim of the study was to increase the high frequency energy injected by the reflectometer and thereby improve the axial resolution of bore reconstructions. A greater axial resolution also ensures that regions of rapidly changing cross-sectional area are more accurately reconstructed.

To achieve this, a method of supplementing the standard pulse reflectometry measurement by probing further with bursts of high frequency (greater than 8 kHz) sinusoidal pressure waves was developed. This method enables the bandwidth of input impulse response measurements to be increased to 11.025 kHz (the Nyquist frequency when a sampling frequency of 22.05 kHz is used). Through measurements using stepped tubes as test object, the improved high frequency content of the input impulse response was shown to lead to a more accurate, sharper reconstruction of the step change in radius. Extending the sine wave packet method beyond 11.025 kHz proved impossible due to the rapid attenuation of such high frequencies within the source tube.

To overcome the problem of attenuation within the source tube, a reflectometer with a shortened source tube was produced. The reduction in source tube required a new method for separating forward and backward travelling waves to be developed. This method involves an extra calibration measurement, using a pseudo semi-infinite length of tubing, to enable the input pulse to be measured in isolation. The reduction in attenuation provided by the shorter source tube leads to input impulse response measurements with frequency content up to 15 kHz. Again, through measurements on stepped tubes, the improvement in the accuracy of bore reconstruction, particularly at regions where the cross-section changes rapidly, was demonstrated.

9.2 Limitation of present reflectometry technique

By supplementing the standard pulse reflectometry measurement with bursts of high frequency sinusoidal pressure waves, or by shortening the source tube, bore reconstructions with a higher axial resolution are obtained. This is due to the improved bandwidth of the input signal and, hence, the input impulse response measurement. However, if the bandwidth is increased beyond the first cut off frequency of the duct under

test, the assumption of plane wave propagation ceases to be valid. The effect of higher order modes on reflectometry measurements is demonstrated in this section.

9.2.1 Demonstration of the effect of higher order modes

In order to investigate the effect of increasing the bandwidth of the input pulse beyond the first cut off frequency of the duct under test, measurements have been made of a stepped tube consisting of two 0.15 m long cylindrical sections of wide radius (9.4 mm and 13.45 mm respectively).

The stepped tube was first measured using the original design of reflectometer (shown in Figure 4.1). Both a standard pulse measurement using a compression driver and a supplementary measurement using a bass loudspeaker were made. The results were then combined, as described in chapter 5, to yield an input impulse response measurement. Figure 9.1 shows the input impulse response spectrum of the DC tube and the stepped tube. The bandwidth of the input impulse response is approximately 10 kHz. Figure 9.2 shows the bore reconstruction of the DC tube and stepped tube calculated by applying the layer peeling algorithm to the input impulse response of Figure 9.1. The reconstruction of the first cylindrical section of the stepped tube is in good agreement with the directly measured radius of 9.4 mm. However, the reconstruction of the second cylindrical section is slightly narrower than the directly measured radius of 13.45 mm.

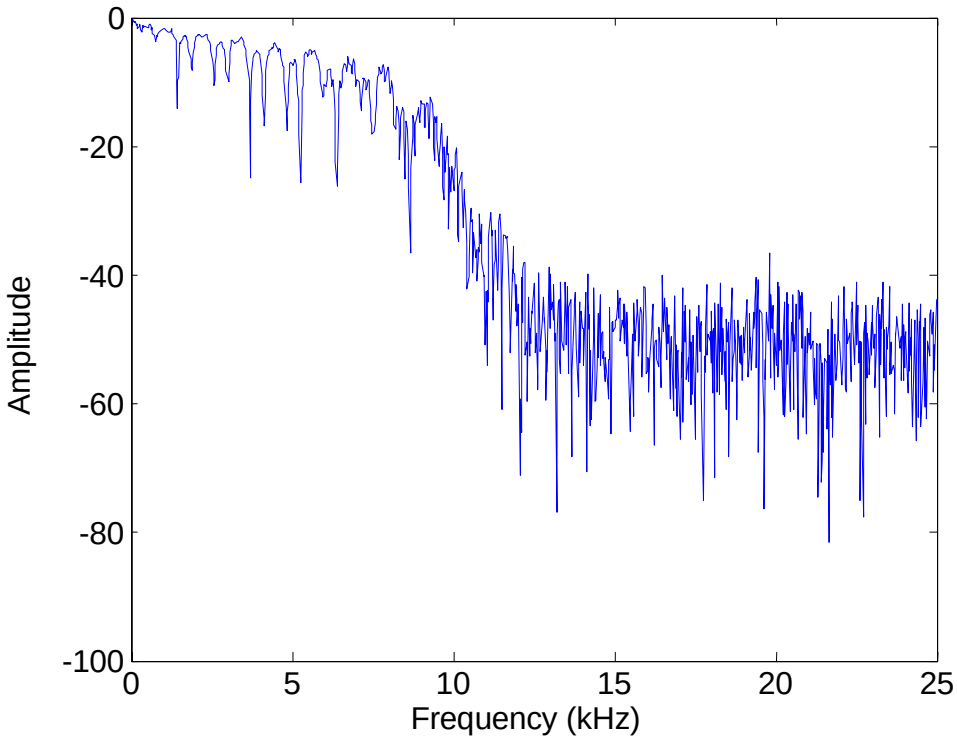

Figure 9.1: Input impulse response spectrum for wide radius stepped tube measured on original design of reflectoemter

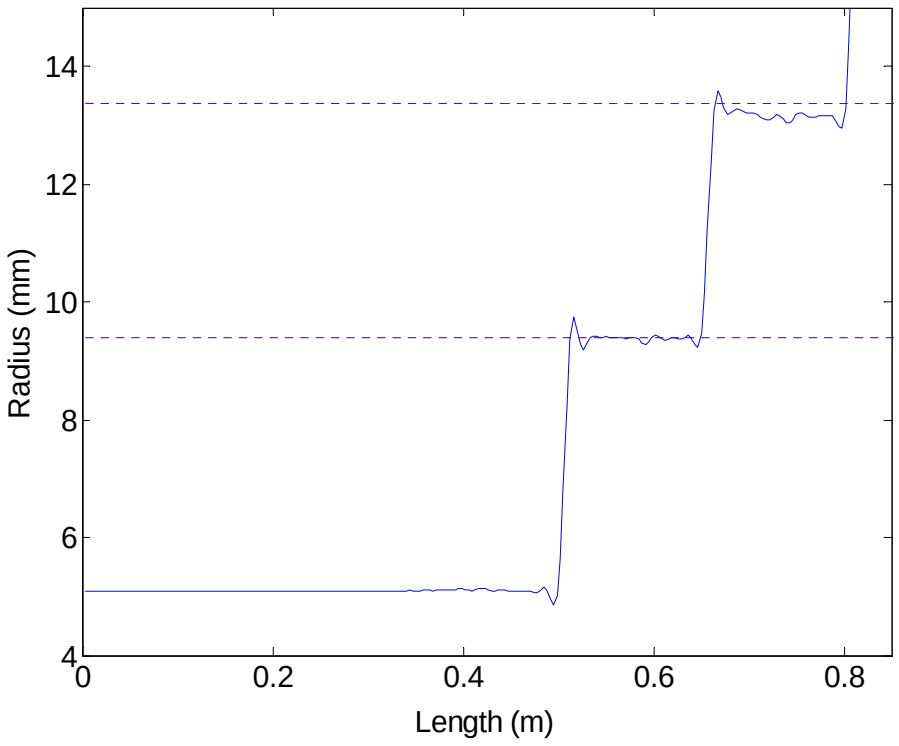

Figure 9.2: Bore reconstruction of wide radius stepped tube measured on original design of reflectometer

The same stepped tube was then coupled to the shorter source tube reflectometer (shown in Figure 8.1). The 'one subtraction' method was used to measure the input impulse response of the stepped tube, as described in chapter 8. Figure 9.3 shows the spectrum of the input impulse response of source tube section l_2 and the stepped tube. The bandwidth has now been expanded to approximately 15 kHz. Figure 9.4 shows the bore reconstruction which results when the layer peeling algorithm is applied to the input impulse response of Figure 9.3. In comparison with the directly measured values, the reconstruction seriously underpredicts the radii of both cylindrical sections.

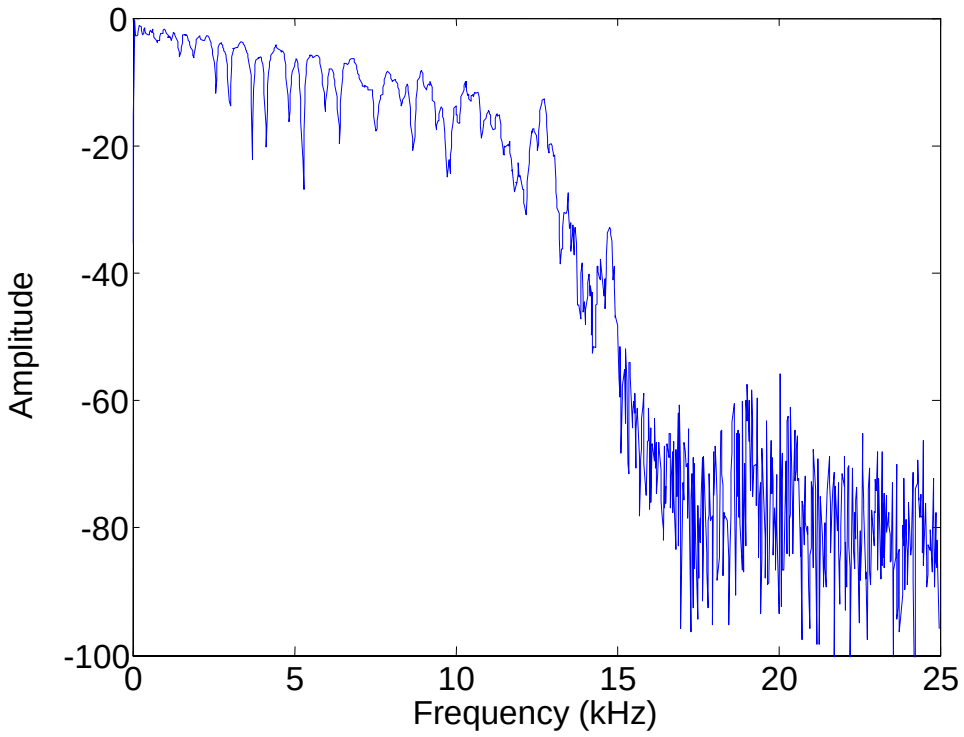

Figure 9.3: Input impulse response spectrum of wide radius stepped tube measured on shorter source tube reflectometer

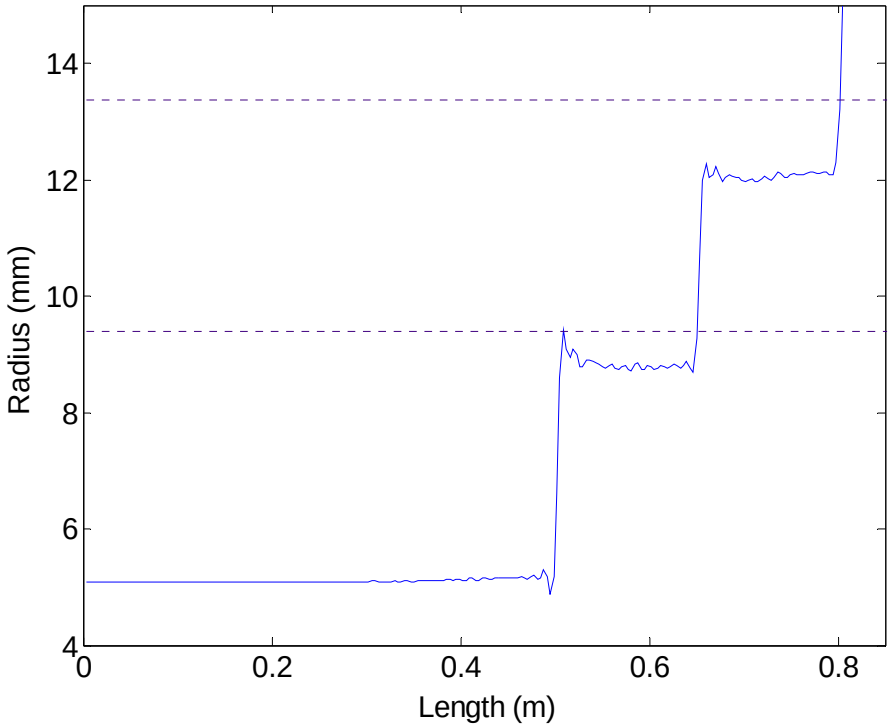

Figure 9.4: Bore reconstruction of wide radius stepped tube measured on shorter source tube reflectometer

9.2.2 Discussions

The reconstructions shown in Figures 9.2 and 9.4 both exhibit a lower degree of accuracy than the reconstructions presented in chapter 6 and 8 measured using the same techniques. In particular, the reconstruction of Figure 9.4 underpredicts the radius by over 1 mm in places. The reason for the observed underprediction is that the assumption of plane wave propagation that is integral to the layer peeling algorithm is no longer valid. That is, as well as plane waves, higher order modes were also propagating within the wide radius stepped tube during the two sets of measurements.

The issue of higher order modes was first discussed in chapter 2. To recap, wave propagation in a duct can be described in terms of a sum of modes. The fundamental (plane wave) mode travels in an axial direction and has wavefronts that are uniform across the duct cross-section. Higher order modes reflect off the duct walls as they travel along its

length and consequently have non-uniform pressure distributions across the duct. Associated with each mode is a cut off frequency [Kinsler et al. 2000]:

$$\omega_c = \alpha_{mn} c / a \tag{9.1}$$

where c is the speed of sound, a is the duct radius and α_{mn} is the extrema of mth order Bessel function, which is determined by the boundary condition. At frequencies below its cut off frequency, a mode is evanescent. That is, it is rapidly attenuated so does not propagate. Above its cut off frequency, however, a mode will propagate.

The fundamental (plane wave) mode propagates at all frequencies. This mode is often described as the (0, 0) mode, with $m = 0$ and $n = 0$, and it follows that $\alpha_{00} = 0$. The first of the higher order modes to become propagational is the (1,0) mode. For this mode, $\alpha_{10} = 1.84$ so its cut off frequency (as given by [Kinsler et al. 2000] is

$$\omega_c = 1.84 c / a \tag{9.2}$$

Using equation 9.2, the lowest cut off frequency for the first cylindrical section of the stepped tube (of radius 9.4 mm) can be calculated as being 10.6 kHz. Similarly, the lowest cut off frequency for the section of radius 13.45 mm is found to be 7.4 kHz.

Examination of Figure 9.1 reveals that this input impulse response measurement has a bandwidth of approximately 10 kHz, implying that the input signal must also have contained significant energy up to 10 kHz. As this is below the 10.6 kHz lowest cut off frequency of the first cylindrical section of the stepped tube, the assumption that only plane waves propagated in this section is valid. The consequence of this can be seen in Figure 9.2 where the 9.4 mm radius section of the stepped tube is accurately reconstructed. However, the 10 kHz bandwidth of the input signal is greater that the 7.4 kHz lowest cut off frequency of the second section of the stepped tube. In this section, those frequencies

higher than the cut off frequency would have propagated as a mixture of both plane waves and wavefronts associated with the (1, 0) mode. This loss of energy to the first higher order mode is the reason why, in the reconstruction shown in Figure 9.2, the radius of the second section of the stepped tube is slightly underpredicted in comparison with the directly measured value of 13.45 mm.

Examination of Figure 9.3 reveals that the input impulse response measurement made using the shorter source tube has a bandwidth of approximately 15 kHz. This implies that the input signal must also have contained significant energy up to 15 kHz. This is above the lowest cut off frequencies of both the 9.4 mm and 13.45 mm radius sections of the stepped tube. Therefore, a mixture of both plane waves and wavefronts associated with the first higher order mode would have propagated in both sections. This is manifested in the reconstruction of Figure 9.4 where, due to the loss of energy to the first higher order mode, the radii of both sections of the stepped tube are seriously underpredicted.

9.2.3 Conclusion

It was shown in chapters 7 and 8 that increasing the bandwidth of input impulse response measurements can result in more accurate, higher resolution bore reconstructions. However, this is only true provided that the frequencies present in the input signal remain below the lowest cut off frequency of the duct. If this is not the case then higher order modes begin to propagate within the duct and the assumption of plane wave propagation upon which the layer peeling algorithm is based becomes invalid. The result is a lowering of the accuracy of the bore reconstruction with underprediction of the radius of the duct under investigation. This has been clearly demonstrated in this section and was also reported by [Kemp 2003] to be the reason why the bell sections of musical wind instruments are poorly reconstructed.

To overcome this situation, the layer peeling algorithm must be adapted to take into account the effects of higher order modes. Several researchers have published work which describes the direct problem of calculating the input impedance of a duct, including the contributions of higher order modes, given the duct's internal dimensions. An early example of such work is given by [Oie et al. 1980]. Meanwhile, more recently, [Kemp et al. 2001] calculated the input impedance of the horn sections of wind instruments, using the [Pagneux et al. 1996] [Amir et al. 1997] model to take into account of higher order mode contributions. However, despite the successful incorporation of higher order modes into the direct problem, at present the problem of including their effects in the inverse problem (of calculating a duct's dimensions from its measured input impulse response or input impedance) remains unsolved.

9.3 Future work

Over the course of this thesis, modifications to the acoustic pulse reflectomery technique have been described which have led to great improvements in the accuracy and reproducibility of measurements of input impulse response and bore profile. However, there are still several practical limitations in the geometries of objects that can be measured using acoustic pulse reflectometry. Possible future work to overcome those limitations is discussed in this section.

One of the main future areas of study is the inclusion of the effects of higher order modes in the layer peeling reconstruction algorithm. Until this is achieved, the accurate reconstruction of ducts with large cross-sectional areas will not be possible. In addition, further improvements to the axial resolution of bore reconstructions (necessary for the accurate reconstruction of step changes in cross-sectional area), while still maintaining their overall accuracy, will be prevented.

At present, the length of duct that can be measured on a reflectometer depends on the length of source tube l_1 between the loudspeaker and microphone (necessary to separate the duct reflections from unwanted source reflections). The greater the length l_1, the longer the object that can be measured. However, increasing l_1 has the effect of increasing the losses experienced by the input signal, resulting in lower bandwidth input impulse response measurements and bore reconstructions of lower axial resolution and poorer accuracy. This could, to some extent, be counteracted by using a shorter source tube section l_2 together with one of the calibration methods described in chapter 8. An alternative approach to increasing the length of duct that can be measured using reflectometry would be to eliminate source reflections completely. This would remove the need for a source tube and thus lift the restriction on duct length. It would also have the benefit of increasing the bandwidth of the input signal and consequently, the axial resolution of bore reconstructions. Several methods for eliminating source reflections have been suggested [Marshall 1992] [Louis *et* al. 1993] [Sharp 1998] [Kemp *et al.* 2001] but none have so far been successfully implemented.

Finally, another potential area for further research involves ducts with sideholes (e.g. woodwind instruments or pipes containing holes). Acoustic pulse reflectometry has been used previously to detect leaks in short pipes [Sharp and Campbell 1997]. The leak presents a reduction in impedance to the probing pulse. This manifests itself in the reconstruction as a sudden widening in duct profile, allowing the leak position to be identified. However, the region of the duct after the leak is then incorrectly reconstructed. Future work could focus on, once a leak has been detected, adapting the reconstruction algorithm so that it compensates for the leak, enabling later sections of the duct to be reconstructed correctly.

Bibliography

- Amir N., Shimony U. and Rosenhouse G (1995). A Discrete Model for Tubular Acoustic Systems with Varying Cross-Section - the Direct and Inverse Problems. Part 1 and Part 2: Theory and Experiment. *Acustica* **81**(5): 450-474.

- Amir N., Shimony U. and Rosenhouse G (1996). Losses in tubular acoustic systems - Theory and experiment in the sampled time and frequency domains. *Acustica* **82**(1): 1-8.

- Amir N., Pagneux, V. and Kergomard, J. (1997). A study of wave propagation in varying cross-section waveguides by modal decomposition. 2. Results. *J. Acoust. Soc. Am.*, **101**(5): 2504-2517.

- Ayers R. D., Eliason L. J. and Salem M. N. B (1985a). An acoustic pulse generator for wind instrument bores. *J. Acoust. Soc. Am.* **77**(S89).1985

- Ayers R. D., Eliason L. J. and Salem M. N. B (1985b). Multiple reflections in simple bore shapes. *J. Acoustic. Soc. Am.* **77**(S90).1985

- Benade, A. H. and Smith J. H. (1981). Brass wind instrument impulse response measurements. *J. Acoustic. Soc. Am.* **70**(S22).

- Deane A. M. (1986). Time domain work on brass instruments. *PhD Thesis*, University of Surrey.

- Duffield A. (1984). Problems encountered when making simple impulse measurements. In *Proc. of the Institute of Acoustics*.

- Fincham L. R. (1985). Refinements in the impulse testing of loudspeakers. *J.Audio Eng. Soc.* **33**(No.3): 133 -140.

- Forbes B. J., Sharp D. B. Kemp J.A. and Li A. (2003). Singular system methods in acoustic pulse reflectometry. *Acustica* **89**: 743-753.

- Fredberg J. J., Wohl M. E. B. Glass G. M. and Dorkin H. L. (1980). Airway area by acoustic reflections measured at the mouth. *J. Appl. Physol.* **48**(5): 749-758.

- Goodwin J. C. (1981). Relations between the geometry and acoustics of brass instruments. *PhD Thesis*, University of Surrey.

- Jackson A. C., Butler J. P. Millet E. J. Hoppin F. G. and Dawson S. V. (1977). Airway geometry by analysis of acoustic pulse response measurements. *J. Appl. Physol.* **43**(3): 523-536.

- Jackson A. C. and Olsen D. E. (1980). Comparison of direct and acoustical area measurements in physical models of human central airways. *J. Appl. Physol.* **48**(5): 896-902.

- Kausel, W. (2003). Bore reconstruction of tubular from its acoustic input impedance curve. *IEEE Instrumentation and Measurement Technology Conference*, Vail, Co, USA.

- Keefe, D. H. (1984). Acoustical Wave-Propagation in Cylindrical Ducts - Transmission-Line Parameter Approximations for Isothermal and Non-Isothermal Boundary-Conditions. *J. Acoust. Soc. Am.* **75**(1): 58-62.

- Kemp J. A., Amir N. and Campbell D. M. (2001). *Multimodal propagation in acoustic horns.* In *Proc. International Symposium on Musical Acoustics (ISMA 2001), Perugia, Italy*: 521-524.

- Kemp J. A., Buick J. K. and Campbell D. M. (2001). Practical improvements to acoustic pulse reflectometry: the virtual DC tube method and source reflection cancellation. In *Proc. International Symposium on Musical Acoustics (ISMA 2001), Preugia, Italy*: 387-390.

- Kemp J. A. (2003). Theoretical and experimental study of wave propagation in brass musical instruments. *PhD Thesis*, University of Edinburgh.

- Kinsler L. E., Frey A. R. Coppens A. B. and Sanders J. V. (2000). Fundamentals of Acoustics. *John Wiley & Sons, 4th edition,* 2000.

- Li A., Sharp D. B and Forbes B. J. (2001). Improving the high frequency content of the input signal in acoustic pulse reflectometry. In *Proc. International Symposium on Musical Acoustics (ISMA 2001), Perugia, Italy:* 391-394.

- Li A., Sharp, D. B. and Forbes B. J (2002). Improving the measurement of the low frequency response of the impulse response using acoustic pulse reflectometry. In *Proc. Forum Acusticum 2002, Seville, Spain.*

- Li A., Sharp D. B., Forbes B. J. and Kemp J. A. (2002). The problem of DC offset in the measurement of impulse response using acoustic pulse reflectometry. In *Proc. Institute of Acoustics Spring Conference 2002, Salford, UK.*

- Li A., and Sharp D. B. (2003). Shortening the source tube to improve the bandwidth of acoustic pulse reflectometry measurements. In *Proc. Stockholm Music Acoustics Conference (SMAC 03), Stockholm, Sweden.*

- Louis B., Glass, G. M., Kresen B. and Fredberg. J. (1993). Airway area by acoustic reflection: the two-microphone method. *J. Biomech. Eng.* **115**: 278-285.

- Marshall I. (1990). The production of acoustic impulse in air. *Meas.t Sci. Technol.* (1): 413-418.

- Marshall I., Rogers M. and Drummond G. (1991). Acoustic Reflectometry for Airway Measurement - Principles, Limitations and Previous Work. *Clin. Phys. Physiol. Meas.* **12**(2): 131-141.

- Marshall I. (1992a). Acoustic reflectometry for airway measurement. *PhD Thesis*, 1992, University of Edinburgh.

- Marshall I. (1992b). Acoustic Reflectometry with an Arbitrarily Short Source Tube. *J Acoust. Soc. Am.* **91**(6): 3558-3564.1992.

- Mermelstein P. (1967). Determination of the vocal-tract shape from measured formant frequencies. *J. Acoustic. Soc. Am.* **41**(5): 1283-1294.

- Morse, P. M. and Ingard K. U. (2000). Theoretical Acoustics. *Princeton University Press*, 2000

- Oie S., Takeuchi R. and Shindo T. (1980). Sound radiation from a concave radiator in an infinite baffle. *Acustica* **46**: 268-275.

- Pagneux V., Amir N. and Kergomard J. (1996). A study of wave propagation in varying cross-section waveguides by modal decomposition .1. Theory and validation. *J. Acoust. Soc. Am.* **100**(4): 2034-2048.

- Schroeder M. R. (1967). Determination of the geometry of the human vocal tract by acoustic measurements. *J. Acoustic. Soc. Am.* **41**(4): 1002-1010.

- Sharp D. B. (1996). Acoustic pulse reflectometry for the measurement of musical wind instruments. *PhD Thesis,* The University of Edinburgh.

- Sharp D. B. and Campbell D. M. (1997). Leak detection in pipes using acoustic pulse reflectometry. *Acustica* **83**(3): 560-566.

- Sharp D. B. and Campbell D. M. (1998). Measuring longer tubular objects using acoustic pulse reflectometry. In *Proc.16th International Congress on Acoustics, Seattle.*

- SharpD. B. (1998). Increasing the length of tubular objects that can be measured using acoustic pulse reflectometry. Meas.Sci. Technol. **9**(9): 1469-1479.

- Smith, R. A. (1988). It's all in the bore! *International Guild Journal* **12**(4).

- Sondhi M. M. and Gopinath B. (1971). Determination of vocal-tract shape from impulse response at the lips. *J. Acoust. Soc. Am.* **49**(6): 1867-1873.

- Sondhi, M. M. (1974). Model for wave propagation in a lossy vocal tract. *J. Acoust. Soc. Am.* **55**(5): 1070-1075.

- Sondhi, M. M. (1981). Acoustical Inverse Problem for the Cochlea. *J. Acoust. Soc. Am.* **69**(2): 500-504.

- Sondhi M. M. and Resnick J. R. (1983). The Inverse Problem for the Vocal-Tract - Numerical-Methods, Acoustical Experiments, and Speech Synthesis. *J. Acoust. Soc. Am.* **73**(3): 985-1002.

- Ware J. A. and Aki K. (1969). Continuous and discrete inverse-scattering problems in a stratified elastic medium. 1 plane waves at normal incidence. *J. Acoust. Soc. Am.* **45**(4): 911-921.

- Watson A. P. and Bowsher J. M. (1987). Recent progress in time domain work on brass instruments. In *Proc. Institute of Acoustics*, 1987.

- Watson, A. P. and Bowsher J. M. (1988). Impulse Measurements on Brass Musical-Instruments. *Acustica* **66**(3): 170-174.

- Watson, A. P. (1989). Impulse measurements on tubular acoustic system. *PhD Thesis*, University of Surrey.

- Wylie, C. R. and Barrett L. C. (1982). Advanced Engineering Mathematics. *McGraw-Hill*, 5th edition, 1982. 388

List of Publications

Conference papers

Li A., Sharp D. B and Forbes B. J. (2001). Improving the high frequency content of the input signal in acoustic pulse reflectometry. In *Proc. International Symposium on Musical Acoustics (ISMA 2001), Perugia, Italy:* 391-394.

Li A., Sharp, D. B. and Forbes B. J (2002). Improving the measurement of the low frequency response of the impulse response using acoustic pulse reflectometry. In *Proc. Forum Acusticum 2002, Seville, Spain.*

Li A., Sharp D. B., Forbes B. J. and Kemp J. A. (2002). The problem of DC offset in the measurement of impulse response using acoustic pulse reflectometry. In *Proc. Institute of Acoustics Spring Conference 2002, Salford, UK.*

Li A., and Sharp D. B. (2003). Shortening the source tube to improve the bandwidth of acoustic pulse reflectometry measurements. In *Proc. Stockholm Music Acoustics Conference (SMAC 03), Stockholm, Sweden.*

Journal papers

Forbes B. J., Sharp D. B. Kemp J.A. and Li A. (2003). Singular system methods in acoustic pulse reflectometry. *Acustica* **89**: 743-753.